
# CREEP-RUPTURE AND FATIGUE BEHAVIOR OF A NOTCHED OXIDE/OXIDE CERAMIC MATRIX COMPOSITE AT ELEVATED TEMPERATURE

THESIS

Barth H. Boyer, Lieutenant Commander, USN
AFIT/GAE/ENY/08-J01

**DEPARTMENT OF THE AIR FORCE**
**AIR UNIVERSITY**

## AIR FORCE INSTITUTE OF TECHNOLOGY

**Wright-Patterson Air Force Base, Ohio**

AFIT/GAE/ENY/08-J01

# CREEP-RUPTURE AND FATIGUE BEHAVIOR OF A NOTCHED OXIDE/OXIDE CERAMIC MATRIX COMPOSITE AT ELEVATED TEMPERATURE

THESIS

Presented to the Faculty

Department of Aeronautics and Astronautics

Graduate School of Engineering and Management

Air Force Institute of Technology

Air University

Air Education and Training Command

In Partial Fulfillment of the Requirements for the

Degree of Master of Science (Aeronautical Engineering)

Barth H. Boyer, BS

Lieutenant Commander, USN

June 2008

AFIT/GAE/ENY/08-J01

CREEP-RUPTURE AND FATIGUE BEHAVIOR OF A NOTCHED OXIDE/OXIDE CERAMIC MATRIX COMPOSITE AT ELEVATED TEMPERATURE

Barth H. Boyer, BS
Lieutenant Commander, USN

Approved:

| | |
|---|---|
| //signed// | 30 May 2008 |
| Dr. Shankar Mall (Chairman) | date |
| //signed// | 30 May 2008 |
| Dr. Vinod Jain (Member) | date |
| //signed// | 30 May 2008 |
| Dr. Som Soni (Member) | date |

## Abstract

The inherent resistance to oxidation of oxide/oxide ceramic matrix composites makes them ideal for aerospace applications that require high temperature and long life under corrosive environments. The ceramic matrix composite (CMC) of interest in the study is the Nextel™720/Alumina (N720/A) which is comprised of an 8-harness satin weave of Nextel™ fibers embedded in an alumina matrix. The N720/A CMC has displayed good fatigue and creep-rupture resistance in past studies at elevated temperatures under an air environment.

One of the top applications for N720/A is in the combustion section of a turbine engine. This will require mounting and shaping the material with rivets and possibly sharp edges thereby introducing geometry based stress concentration factors. Sullivan's research concentrated on the effects of central circular notches with a notch to width ratio (2a/w) of 0.33 (Sullivan, 2006:14). This study expands upon his research to include the creep and fatigue response to a double edge notch geometry with the same notch to width ratio of 0.33. In short, 12.0 mm wide rectangular specimens with two edge notches of 2 mm depth and 0.15 mm width were subjected to creep and fatigue loading conditions in 1200°C of air. All fracture surfaces were examined by an optical microscope and a scanning electron microscope.

Sullivan's research concluded that specimens with a central circular notch were insensitive to creep but slightly more sensitive to fatigue than unnotched specimens. In contrast, this study showed significant creep and fatigue life reductions for double edge notch specimens.

**Acknowledgments**

Most importantly, I would like to thank my wife and children for their encouragement and support during my tour at AFIT. Their sacrifices made all the educational efforts possible. Thanks are also due to Dr. Mall, for his faithful guidance and support throughout the course of this research. The roadmap for this research was carefully laid out by Captain Mark Sullivan whose efforts saved me a lot of setup time and whose approach to analysis in his thesis was repeated here. Final thanks go to Sean Miller, Barry Page, and Captain Chris Genelin for all their help in the lab.

# Table of Contents

Page

## List of Figures

Figure Page

## List of Tables

Table Page

CREEP-RUPTURE AND FATIGUE BEHAVIOR OF A NOTCHED OXIDE/OXIDE CERAMIC MATRIX COMPOSITE AT ELEVATED TEMPERATURE

## I. Introduction

The aeronautical industry is under intense pressure to continuously improve aircraft performance. This is especially true recently in light of the significant rise in fuel costs borne by the airline industry. Fox News recently reported crude oil at an all time high of $125 per barrel. Propulsive efficiency is dominated by a need to increase turbine inlet operating temperatures in order to squeeze all available chemical energy from the consumed fuel (Barnard, 2004:1755). Ceramic matrix composites (CMC's) present a credible technological bridge to higher fuel efficiency due to advantageous specific strength even at high operating temperatures. Figure 1 shows typical operating temperatures for polymers, metals and ceramics:

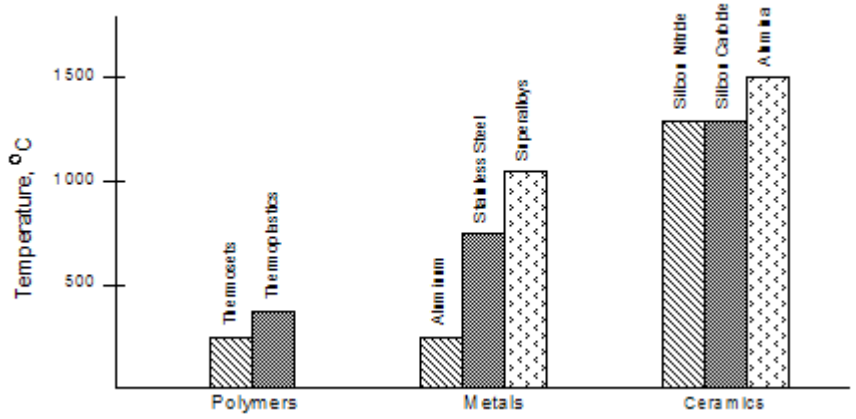


**Figure 1: Typical Operating Temperatures (Chawla, 1993:5)**

## 1.1 Propulsion Discussion

Current technology for increasing turbine inlet temperatures has resulted in operating temperatures increasing from 600°C in the 1930s to over 1000°C recently (Cantor, 2004:66). Although material advances in the usage of superalloys have helped this increase in operating temperatures, cooling air is also a main driver of these advances. Specifically, engine components require cooling air to be injected directly onto them or have effusion holes built into their surfaces to create a boundary layer of cooled air (Cantor, 2004:67). A downside to injecting cooling air is the inherent inefficiency this creates by having to draw the cooling air from the freestream flow resulting in an increased drag penalty. According to Oates, the most desirable option is to utilize the most heat resistant materials available (Oates, 1997:253). Thus CMCs hold the promise of desirable strength properties at high operating temperatures.

Yet CMCs have not been widely used (Cantor, 2004:66;Veitch, 2001:31). This is likely due to the time-tested properties of homogenous materials such as the superalloys. CMC properties are not as widely known or researched and the law of inertia leads to slow, incremental acceptance of new materials. Nevertheless, much research has taken place in the last decade to show potential CMC applications for combustion liners, turbine blades and vanes. Perhaps this thesis will add a small step to the body of knowledge in CMC properties and applications.

## 1.2 Ceramic Matrix Composite Design

One big design driver for CMCs is toughness. Because CMCs utilize fibers bonded to matrix material, they exhibit much better toughness than monolithic ceramics alone (Chawla, 1993). Yet improvement in toughness is needed for greater damage tolerance. This improved toughness comes from the property of reinforcing fibers which are able to either deflect a crack in an alternate direction or to act as a bridge across cracks while maintaining a load (Daniel, 2006:42; Lewinsohn, 2000:415). Another design driver to inhibit crack growth is fiber and matrix debonding (Chawla, 1993:315). When the fiber and matrix are allowed to debond, the strain produced by the crack opening can be exerted over a longer portion of the fiber. Otherwise, if the fiber and matrix were permanently affixed to each other, the crack opening would create a strain over a shorter portion of the fiber length - perhaps exceeding the critical design strain of the material much sooner than if the strain was spread out over a longer portion of the fiber. Figure 2 details a strong and weak interface between the fiber and its matrix.

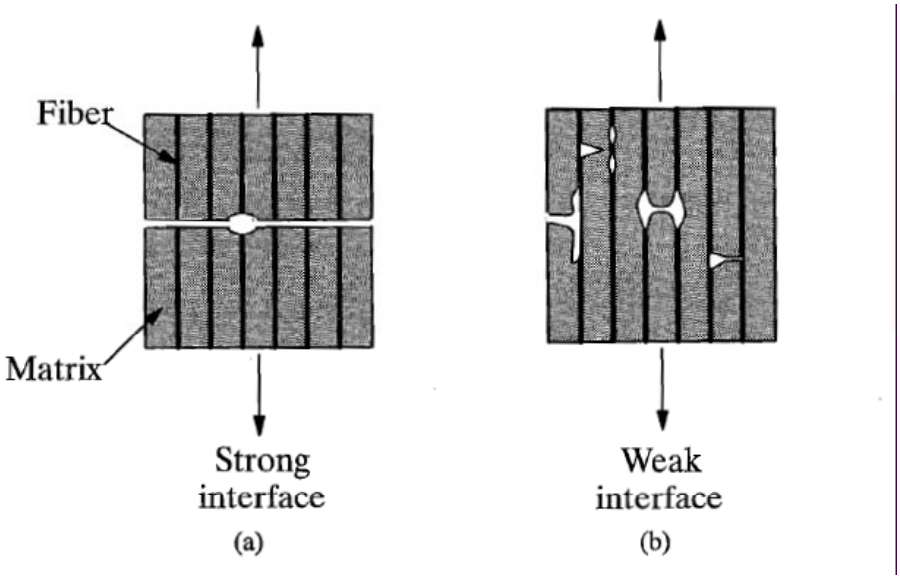


**Figure 2. Alternate crack propagation paths (Chawla, 148)**

There are currently two processes employed to allow fiber and matrix debonding. One process is to design the matrix porosity in such a way as to allow the matrix to break and let go of reinforcing fibers before the fiber failure load is reached. The second process uses a coating on the fibers to allow the fibers to shift more easily within the matrix. Figure 3 shows the different crack propagation paths for the two methods of fiber debonding:

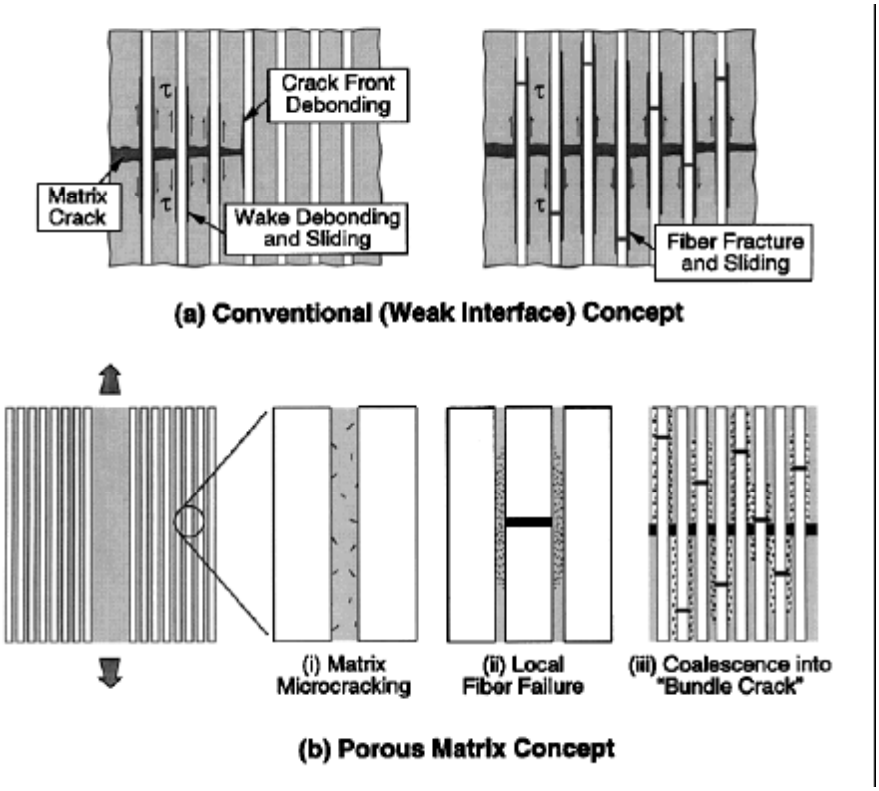


**Figure 3. Crack propagation with weak interface versus porous matrix (Zok)**

### 1.2.1 Corrosion

High temperature operating environments present significant corrosion challenges especially to materials containing carbon. Designers have typically employed two methods to combat corrosion. One method is to use inhibitors which retard the carbon oxidation rate. The second method is to coat the carbon fibers with a chemical barrier to prevent oxygen from reaching the carbon material. The method employed by the CMC under study in this thesis (Nextel™ 720/A oxide/oxide) is to utilize inherently corrosion resistant materials.

### 1.2.2 Nextel™ 720/Alumina (N720/A)

The CMC in this study consists of Nextel™ 720 fibers produced by the 3M™ Corporation. According to the corporate website, these fibers possess better strength retention at high temperature due to a reduced grain boundary. Note from Table 1 that this is a two phase alumina/mullite fiber. Also, the grain size is larger than other structural grade fibers such as N610. This serves to reduce grain boundary sliding and thus increasing creep resistance (Kaya, 2002:2333). Typical properties of these fibers from the 3M™ website are as follows:

**Table 1. Nextel 720 Properties (3M website)**

| Property | Units | Nextel 720 |
|---|---|---|
| Chemical composition | Wt/ % | 85 $Al_2O_3$<br>15 $SiO_2$ |
| Melting Point | °C<br>°F | 1800<br>3272 |
| Filament Diameter | µm | 10-12 |
| Crystal Phase | | α- $Al_2O_3$ +Mullite |
| Density | g/cc | 3.40 |
| Filament Tensile Strength | MPa | 2100 |
| Filament Tensile Modulus | GPa | 260 |
| Thermal Expansion (100-1100°C | ppm/°C | 6.0 |

A matrix performs several important functions. One function is to effectively transfer stress concentrations to the fibers. Another is to act as a "fail safe" between a failed fiber and an adjacent fiber. Finally, the matrix serves as a corrosive resistant barrier (Baker, 2004:7). The matrix material utilized by Composite Optics, Incorporated (COI, 2005) was pure alumina as opposed to aluminum oxide previously used (N720/A versus N720/AS**).** The N720/A relies on matrix porosity to encourage fiber and matrix debonding just as N720/AS does; however, the N720/A was formulated with another feature in mind (Antti, 2004:565; COI; Kramb, 2001:1561). Specifically, N720/A was utilized to reduce matrix sintering that was occurring between 1100°C and 1200°C with N720/AS (Steele, 2000:27). This sintering was reducing the ability of the matrix to crack and spread stress concentrations over a larger volume of matrix (COI website). The alumina matrix of N720/A is designed to remain stable at high temperatures of up to 1200°C. Both Eber and Harlan have demonstrated good creep and fatigue resistance properties for N720/A. Matrix properties are presented in Table 2.

**Table 2. Typical Properties for Alumina (Chawla, 1993)**

| Property | Unit | Alumina |
|---|---|---|
| Chemical composition | Wt/ % | 100 $Al_2O_3$ |
| Melting Point | °C | 2050 |
| Young's Modulus | GPa | 380 |
| Coefficient of Thermal Expansion | $10^{-6}$/°K | 7-8 |
| Fracture Toughness | $Mpam^{1/2}$ | 2-4 |

Figures 4 and 5 show N720/A with micro-cracking and demonstrate the inherent porosity designed into this CMC to allow crack dissipation.

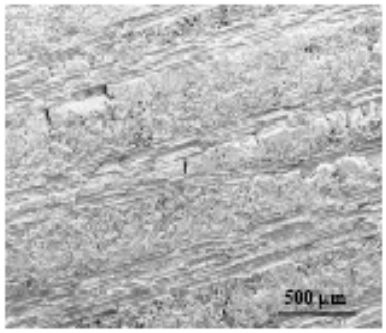


**Figure 4. Microcracking in N720/A (Merhman, 2006)**

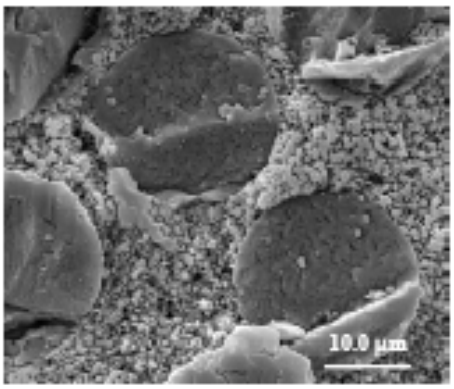


**Figure 5. Porosity of N720/A (Mehrman, 2006)**

### 1.3 Sharp Notch Sensitivity

Even though the ultimate goal of utilizing CMCs in high temperature engine environments is to reduce the amount of drag penalty due to cooling air, some bypass air will still be required. Also, the mounting of CMC products in a structural environment necessitates mounting hardware such as rivets or bolts. Both of the above situations require an understanding of the material's notch sensitivity. There are several ways this is characterized, one of which is the double notch specimen. The sharp double edge notched specimen in this thesis is shown schematically in Figure 6.

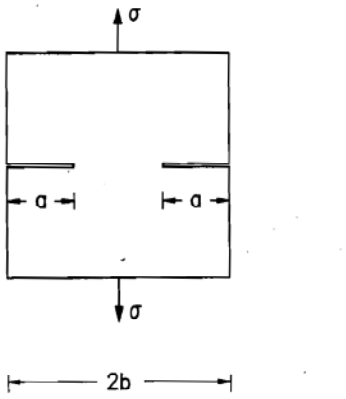


**Figure 6. Double edge notch geometry (Gdoutos, 2005:55)**

According to Gdoutos, the following equation represents the stress concentration factor, $K_t$:

$$K_t = \sqrt{\pi} \left( 1.12 - 0.23 \left( \frac{a}{b} \right) + 10.56 \left( \frac{a}{b} \right)^2 \right) \qquad (1)$$

In the present study, *a* and *b* are 2mm and 6mm respectively which implies a stress concentration factor of 2.64. This results in a 38% reduction in ultimate tensile strength (UTS) if the crack cannot redistribute the concentrated stresses at the notch tip. Typically, ductile materials such as metals begin to deform plastically which spreads the stress concentration over a greater region allowing the material to fail at a higher load (Dowling, 1999:289). Ceramic materials; however, cannot redistribute stresses via plastic deformation but can spread stresses out through microcracks located at the notch tip region. This has been demonstrated in N720/AS (Heredia, 1994:2820-2821; Mackin, 1995:1724-1725; Kramb, 2001:1565-1567; Kramb, 1999:3091). Monolithic ceramics tend to fail catastrophically from a single crack because they cannot redistribute stresses (Chawla, 1993:296; Dowling, 1999:290).

Previous research by Heredia et al. (Heredia) and Mackin et al. (Mackin) showed that brittle, notched CMCs were characterized by three types of damage indicated in Figure 7. When net section stress was reached, Class I behavior was observed but all other loading scenarios were characterized by Class II behavior. By utilizing C-scans, Kramb et al. noted that notched specimens of N610/AS loaded monotonically showed temperature dependent damage behavior. Specifically, Class I behavior was noted at room temperature while Class II behavior was observed at 950°C (Kramb, 2001:1565-1568).

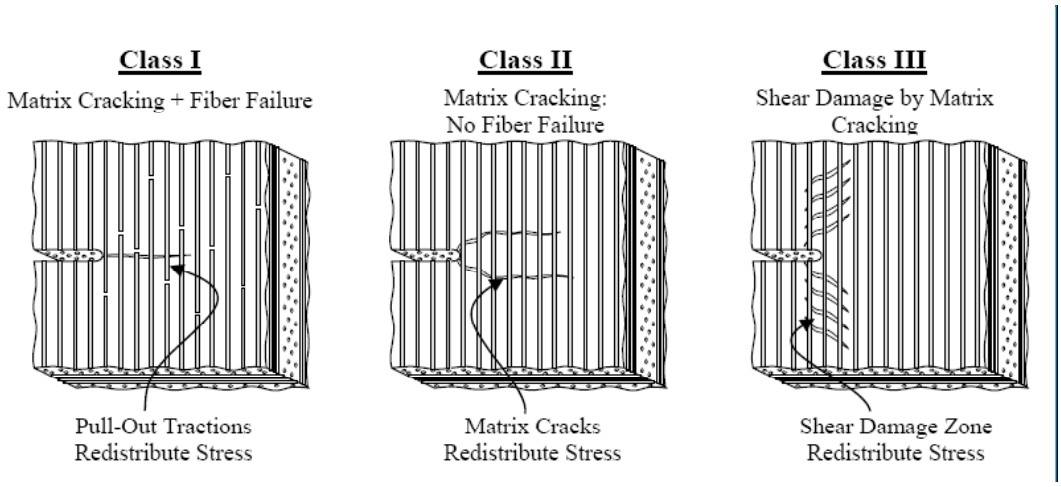


**Figure 7. Damage classes observed in CMCs (Heredia, Mackin)**

## 1.4 Creep and Fatigue Loading

Turbo machinery components experience a harsh loading environment of cyclic, constant and high temperatures loads – all these necessitate a thorough investigation of creep and fatigue properties at elevated temperature. According to Dowling, creep becomes a dominant variable in a temperature range of 30% to 60% of the material's melting point (Dowling, 1999:706). In this case, the test temperature of 1200°C is 66% of the melting point temperature reported by 3M™ (see Table 1). A previous thesis by Harlan indicated that at temperatures above this point (tests at 1330°C), creep becomes unacceptable. Specifically, Mattingly states that design creep should be restricted to 1% over a 1000 hour lifecycle (Mattingly, 2002:289). Harlan calculated that this corresponding creep rate of 2.8E-9 (1/s) would correspond to creep stresses being limited to 30MPa or less for N720/A at 1200°C (Harlan, 2005:58). Another study by Musil indicated a 30 MPa creep load for N610/Alumina/Monzanite would limit temperatures to 1000°C or less to stay under the creep restraint (Musil, 2005:87). Wilson conducted a study which determined that the creep rate of N720 fibers are 250 times less than that of

N610 fiber when loaded to 170 MPa in 1100°C of air (Wilson, 1995:1011). N720 fibers thus possess the potential for dramatic creep performance.

Fatigue loading is another dominant factor when selecting materials for turbine engines. Multiple rotating parts lead to vibrations at high frequencies greater than 1000Hz. This can lead to flutter which can destroy engine components in a matter of minutes (Mattingly, 2002:285). Engine components experience both high and low cycle fatigue. One high cycle fatigue source is uneven airflow. The constantly changing flow over blade faces while they are rotating leads to high cycle fatigue. Low cycle fatigue sources include: constantly changing throttle settings, maneuvering, and environmental temperature variation. N720/A has typically demonstrated good fatigue resistance; however, fatigue resistance for notched specimens is lacking.

### 1.5 Previous Research

Several studies have been performed on the notch sensitivity of related CMCs such as N720/AS and N610/AS. Buchanan et al. reported marginal notch sensitivities to specimens of N720/AS with effusion holes subjected to creep loads at 1100°C. However, double notched specimens did impair the creep life versus unnotched specimens (Buchanan, 2000:581, 2001:659). Buchanan also performed monotonic tests of notched N720/AS specimens and reported only small impairment from the notches. Kramb's research indicated that notched specimens of N610/AS at 950°C possessed only 35% of their original unnotched strength (Kramb, 1999:3095). John et al. examined specimens of N720/AS at 1100°C under tensile test with both large and small holes and found little

notch sensitivity. However, the same specimens showed significant notch sensitivity to creep loading (John, 2002:627).

The only research of N720/A examining notch sensitivity was that of Sullivan. Sullivan tested N720/A specimens under creep and tension/tension fatigue regimes at 1200°C. His specimens were all center-circular notches with a notch ratio (2a/w) of .33. His research showed little notch sensitivity in either creep or fatigue loading (Sullivan, 2006:64-65). Thus, the aforementioned background and previous studies clearly demonstrate that there is currently no or very little information on the notched N720/A ceramic matrix composite at elevated temperature when subjected to creep or fatigue loading conditions. This study is a step in this direction.

## 1.6 Thesis Objective

Highly advanced CMCs like N720/A hold great promise for high temperature structural applications but only if they have thoroughly tested performance that design engineers can rely upon. With the exception of Sullivan's work, there is no notch sensitivity data for N720/A. The focus of this research was to characterize sharp double edge notch sensitivity under a similar testing regime as Sullivan so that a baseline of data can be established. With this end in mind, creep of a N720/A double edge notched specimen at 1200°C was tested. Also, the same notched geometry was tested under tension-tension 1Hz sinusoidal load with a .05 stress ratio ($R=\sigma_{min}/\sigma_{max}$).

## II. Material and Specimens

This chapter will concentrate on describing the N720/A CMC used in this research. The aim is to make follow-on research easy to replicate.

### 2.1 Description of Material

The N720/A CMC was manufactured by Composite Optics, Incorporated (now a division of ATK Space Systems) using a sol gel process. This consists of several steps. The fibers are initially woven into a fabric and then dipped in a slurry which infiltrates the fabric with alumina matrix and an organic binder (Jurf, 2004:204). Precipitate particles of alumina form a gel which penetrates the fabric while subject to a low temperature and pressure (Chawla, 23,125). Then the matrix is formed as the gel dries. Finally, the CMC is sintered. Figure 8 represents a sketch of this procedure.

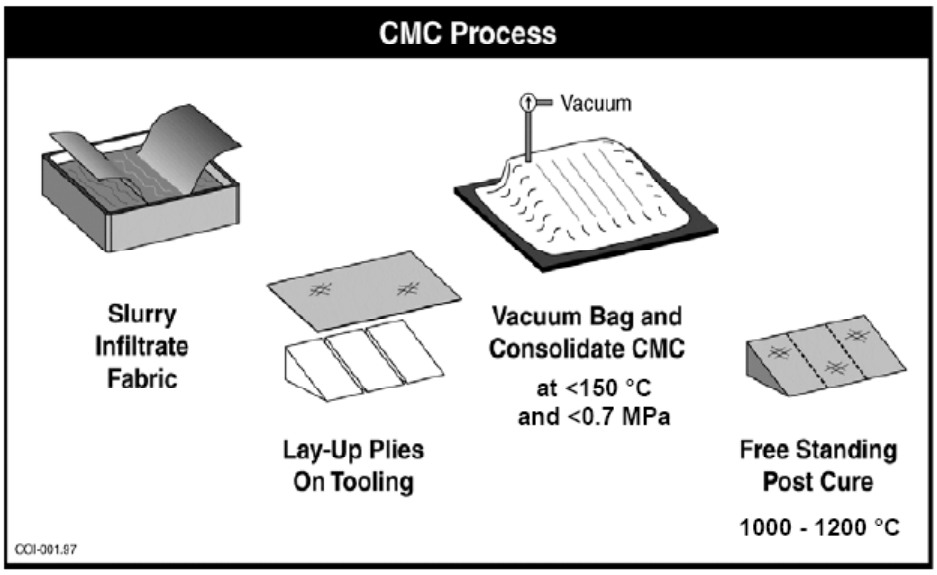


**Figure 8. N720A manufacturing process. (Jurf)**

This sol gel manufacturing process results in a porous matrix as well as microcracking. This was previously shown in Figures 4 and 5. Other characteristics of this material include: eight harness satin weave (8HSW) design, and [0°/90°] fiber orientation. The 12x12 $in^2$ panel used in this study was panel #4569-2. COI provided the following information on this panel:

**Table 3. Panel 4569 Data**

| Thickness (mm) | Fabric Vol % | Matrix Vol % | Porosity % | Density g/cc |
|---|---|---|---|---|
| 2.70 | 46.4 | 29.9 | 23.7 | 2.77 |

## 2.2 Specimen Geometry

All test specimens were cut with a water jet from panel #4569-2 of nominal thickness 2.7mm. Specimens were cut to a length of 150mm and width of 12mm. While cutting, a plexiglass sheet was used as a template to prevent edge round over from the water jets. Two double edge notches of depth 2mm and blade width of 0.15mm were cut with a high carbon steel blade which utilized water cooling. This notch width was intentionally cut to a diameter to width ratio of 0.33 for direct comparison to Sullivan's work. Next, the specimens were washed in an ultrasonic bath of deionized water to remove any excess debris and then dried in an oven at 90°C for 30 minutes.

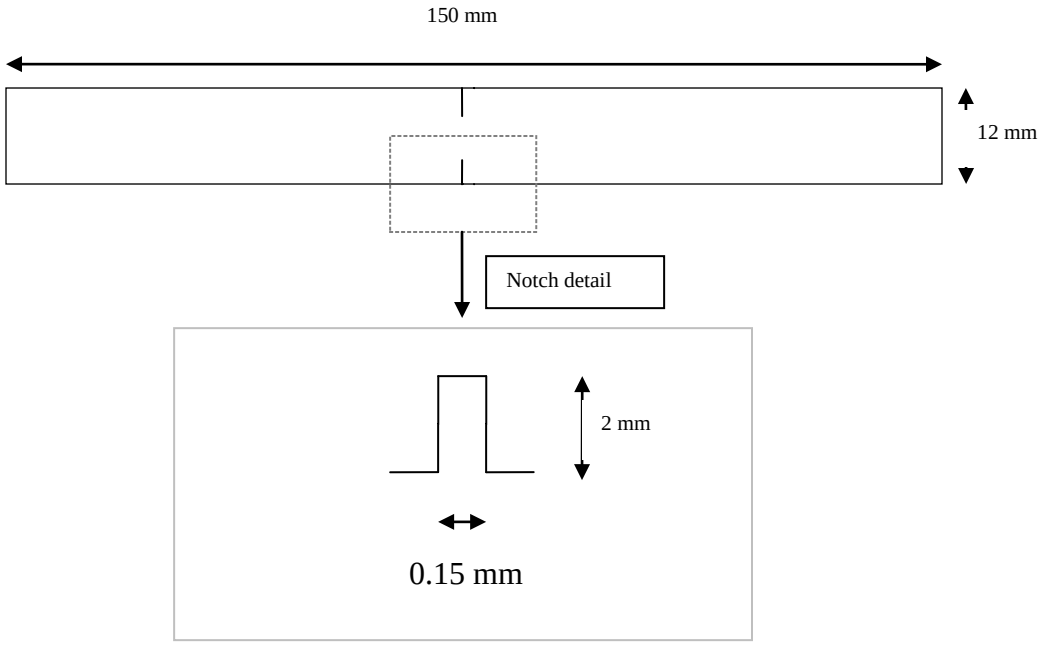


**Figure 9. Specimen dimensions**

Note: (not to scale)

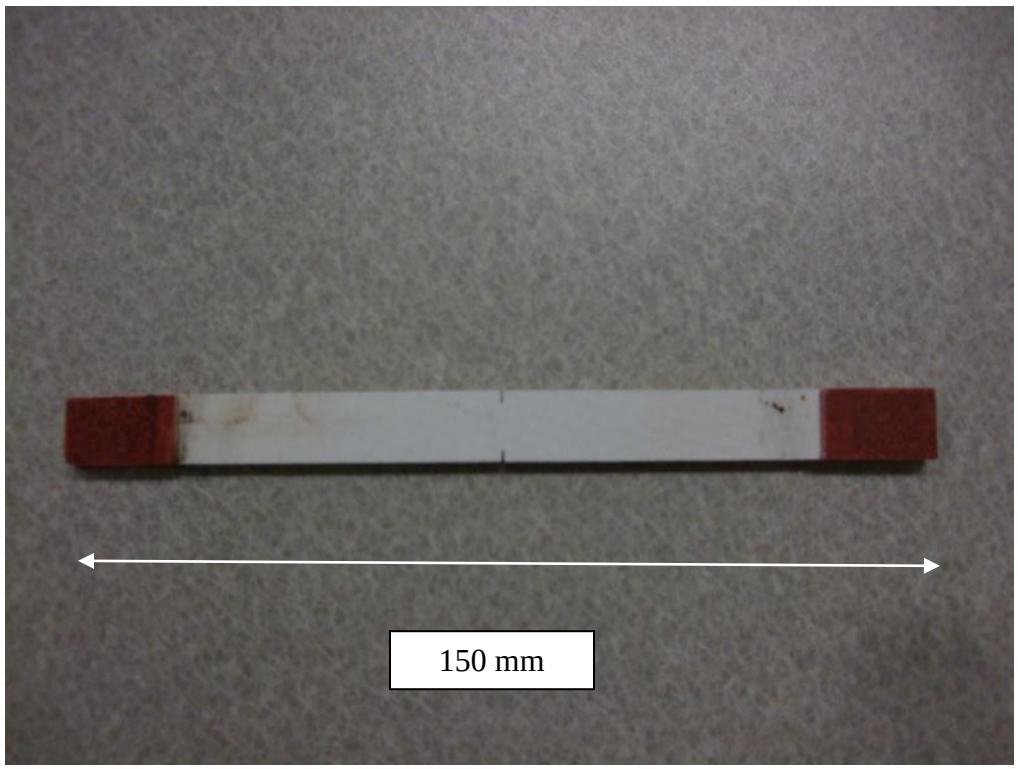


**Figure 10. Photo of specimen with notches and grip tabs.**

# III. Experimental Equipment and Procedures

The following chapter will detail the equipment used to test the N720/A specimens under creep and fatigue regimes.

## 3.1 Equipment

The test equipment includes: the Material Test Systems (MTS) apparatus, the high temperature oven, and the optical and scanning electron microscope (SEM) imaging devices.

### 3.1.1 Material Test Apparatus

All creep and fatigue tests were conducted on a vertically actuated, servo-hydraulic MTS 810 test stand. Although this machine is rated at 97 KN, actual testing never exceeded 3.8 KN due to the small specimen size. Additionally, an MTS Test Star II digital controller was used as the interface for both signal generation as well as data acquisition. *Multi-Purpose Testware* provided by MTS was the graphical user interface utilized to program all test instructions.

Specimens were gripped with a pair of MTS 647 Surfalloy surface grips. Both creep and fatigue specimens were gripped with 1.5 MPa of pressure. The grips were continuously cooled by a Neslab HX-75 chiller which constantly circulated 16°C deionized water through the wedge grips. Maximum temperature reached in the grips was 165°F – well below the 300°F published limit. In addition to grip cooling, the grips

were aligned via strain gauge technique to ensure no bending or torsional forces were exerted on the specimens.


**Figure 11. MTS 810 Test Apparatus**

Load and strain data were collected in all tests. Load data was collected by a MTS 661 Force Transducer and strain data was collected via a MTS 632.53E-14 high temperature extensometer. The extensometer consisted of two 3.5mm diameter ceramic rods with an overall gage length of 12.7mm. The extensometer was calibrated with an MTS 650.03 Extensometer Calibrator. The extensometer was held on the specimens with simple spring tension. The full extensometer assembly includes the following: heat shield, an air diffuser (for constant cooling air), and a three axis spring positioning system. Figure 12 shows the extensometer assembly.

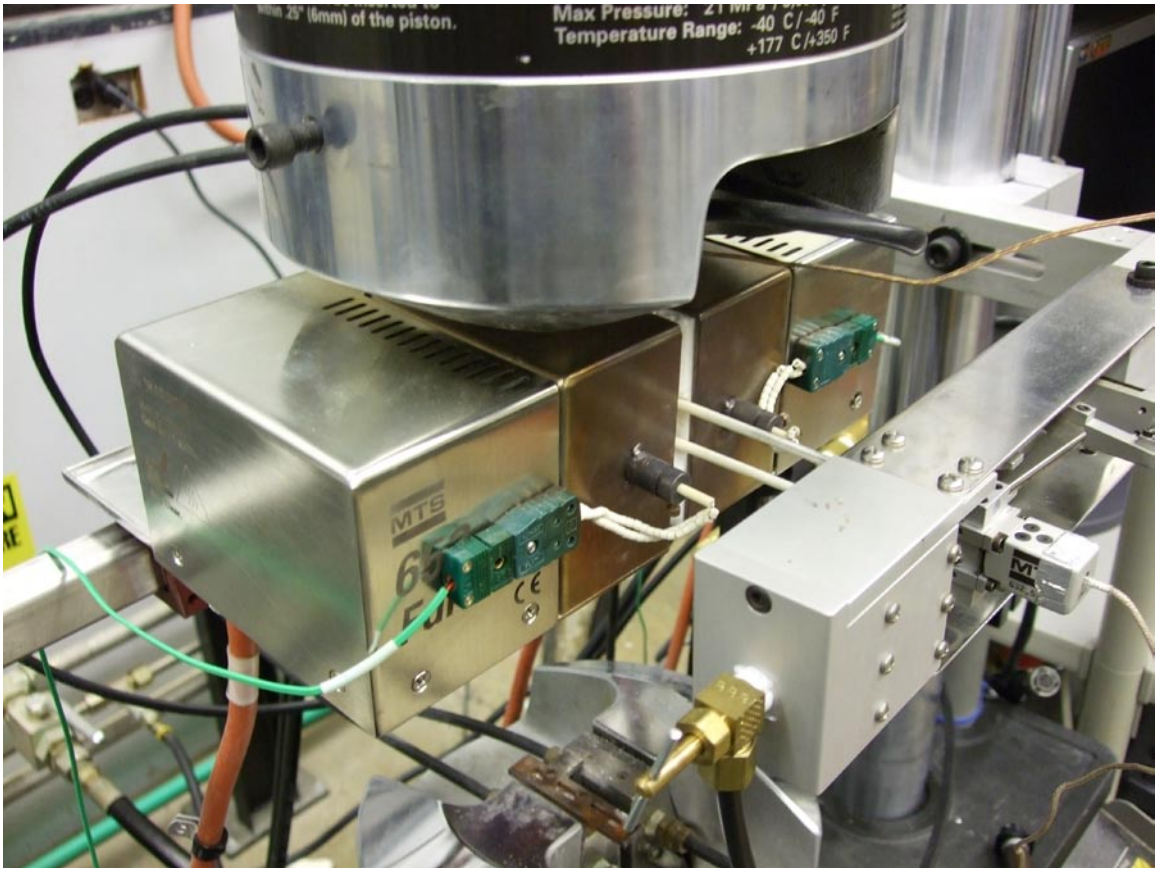


**Figure 12. Extensometer Assembly**

### 3.1.2 Environmental Equipment

The high temperature equipment included a furnace and an external temperature controller. The furnace used to heat the specimen was a two-zone MTS 653 Hot-Rail Furnace System. It was made up of two halves, each containing one silicon carbide heating element, mounted to either side of the specimen. Temperature feedback control was achieved using two R-type thermocouples, one for each half of the furnace. The furnace was protected with a fibrous alumina core of insulating material that was hand carved with gaps to allow the extensometer to reach the specimen inside . Furnace control was provided by two MTS model 409.83B temperature controllers, one for each element.

The test temperature set point was applied via a PID control algorithm to each furnace element using feedback from the control thermocouples. High temperature cloth insulation was used to protect the top of the furnace from the grips and to reduce air infiltration in the gap on top of the ovens. Note that the displayed temperature by the furnace controllers was not necessarily the actual specimen temperature. This was calculated separately as will be discussed later. Figure 13 below shows the temperature controller.


**Figure 13. MTW409 Temperature Controller**

In order to achieve a 1200°C actual specimen temperature, the temperature controller had to be calibrated. This was achieved by attaching two Omega Engineering P13R-015 .38mm diameter R-type thermocouples to a spare specimen. The thermocouples were sandwiched between plates of scrap N720/A material held together with high temperature wire. This ensured that any material touching the thermocouple had the same thermal properties of all tested specimens. The R-type leads were then plugged into an Omega HH202A digital thermometer.

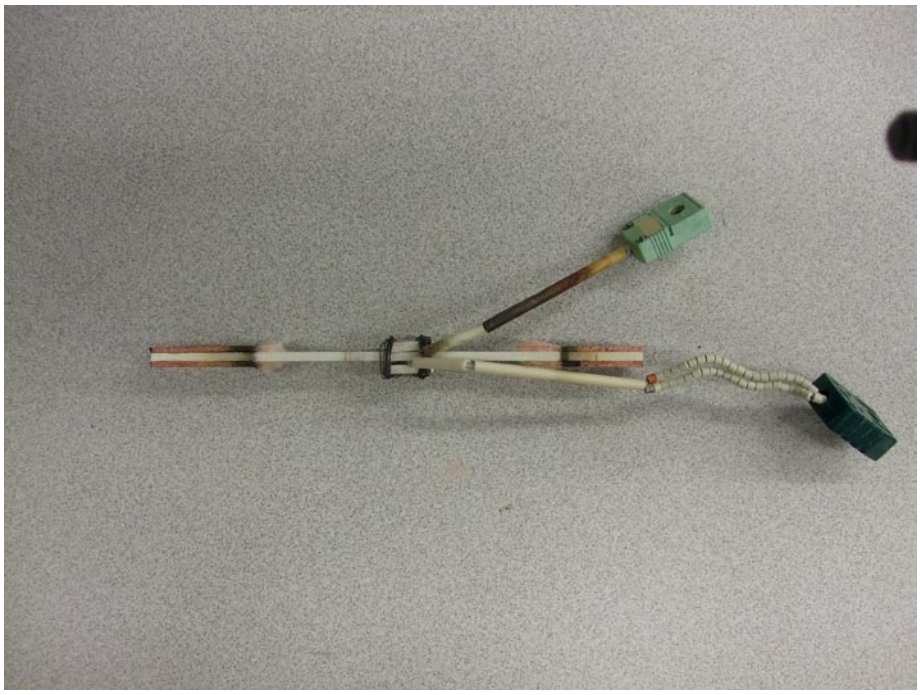

**Figure 14. Thermocouples sandwiched between N720/A specimen and scrap material**

During calibration, the temperature calibration specimen was placed in the MTS machine under zero load and oven temperature was raised by 1°C per second until 1200°C was reached. Next, the left and right oven temperature controllers were varied manually until the Omega digital thermometer displaying the temperature at the specimen center matched the target temperature of 1200°C. The following were the set points used in this study.

**Table 4. Temperature Controller settings**

| | |
|---|---|
| Specimen temperature | 1200°C (target) |
| Left oven temperature (air) | 1215°C |
| Right oven temperature (air) | 1201°C |

### 3.1.3 Equipment Used For Imaging

Specimen fracture regions were imaged using a Scanning Electron Microscope (SEM) as well as an optical microscope. The SEM employed in this research was the FEI Quanta 200 and the optical microscope was the Zeiss Discovery V12 with an attached Zeiss Axiocam HRc.

**Figure 15. Zeiss Discovery V12 optical microscope**


**Figure 16. Quanta 200 SEM**

Low magnification images utilized the Zeiss optical microscope. These post-fracture images provided a macro view to determine the dominant fracture mechanism or check for any specimen flaws. Higher magnification end views utilized the Quanta SEM. This SEM generates a primary electron beam in a raster fashion to excite secondary electrons off the specimen surface thus creating an optical image. The N720/A material used in this study is a poor conductor which makes grounding the primary electron beam difficult. Without proper grounding, the primary electron beam leaves areas of charge buildup which distort the final image.

The specimens used in this study were coated with a layer of gold to reduce surface charge buildup. This gold coating was applied via the SPI-Module 11428 coater. Specimens were first cut to a length of 1cm below the lowest fracture surface with an MTI EC400CNC saw with a water cooled 3.5 inch diamond impregnated blade. Next,

the specimens were mounted on metal tabs via carbon tape. The mounted specimens were then placed in an evacuated chamber and a current was allowed to pass thru the gold anode vaporizing it and forming a deposit over the specimen surface. This was repeated three more times at various angles to ensure a thorough coating. Finally, a bead of silver paste was applied to the sides of the mounted specimens to provide a consistent ground.

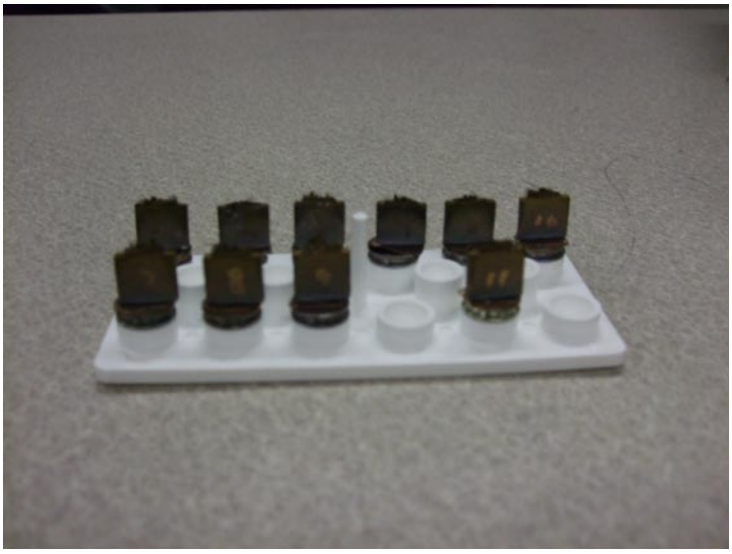

**Figure 17. Specimens after gold coating.**

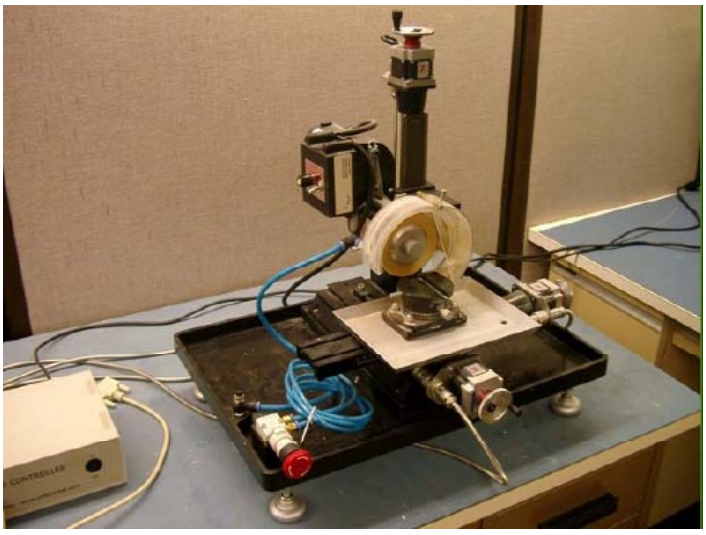

**Figure 18. CNC saw**

## 3.2 Test Procedures

This section discusses specific test procedures for creep and fatigue. Microsoft Excel 2003/2007 was used to plot and analyze all data collected.

### 3.2.1 Further Specimen Processing

Before actual creep and fatigue test, all potential specimens were examined for visible damage that occurred during processing and fabrication. Three specimens were rejected based upon fabrication damage. Cross-sectional measurements were taken across the width and thickness (minus notch length) using a Mitutoyo Corporation Digital Micrometer, model CD-S6 CT. Cross sectional area was calculated as follows:

$$A = t\,(w - 2d) \tag{2}$$

Where *t* is thickness, *w* is width, and *d* is notch width. The net section stress was formulated as:

$$\sigma_{net} = P/A \tag{3}$$

where *P* is the axial load. Note, that the net section stress does not include any stress concentration factor.

Next, fiberglass tabs were glued to each end of the specimen, on both sides. The tabs served to protect the specimens from damage by the MTS grip surface. The tabs consisted of a glass fabric/epoxy material. Three drops of M-bond catalyst were applied to each surface, and then pressure was applied for about a minute, to ensure good contact between the tab and the specimen.

### 3.2.2 Equipment Warm Up and Specimen Loading

Before all testing, the MTS hydraulic servos were allowed to warm up for 30 minutes utilizing the Basic Testware control software. A function generator was programmed to run in displacement mode with a magnitude of 0.0762 mm along a sinusoidal wave of frequency 1Hz.

The Neslab chiller was turned on during this warm up time to bring the grips to an initial temperature of 16°C. The temperature controller was checked on with no error codes present and the flow control valve was set to maximum flow. Additionally, the cooling air valve for the extensometer assembly was verified open and running.

MTS procedures for each specimen were written utilizing the MPT Procedure Editor Module. During warm up time, each procedure was verified for the test being given as well as destination formatting for the data acquisition, sampling rate, and file names.

After a thorough warm up, specimens were placed flush against the grip stops with the grips in an open position and then centered vertically so that the center of the specimen would be in the center of the oven enclosure. The top grip was closed first with the MTS set in displacement control mode. Next, the bottom grips were closed after switching the MTS back to force control mode and zeroing out the force setting. This would ensure the specimen would remain at zero load even during oven warm up time.

The extensometer was then positioned so that the rods were at an equal vertical distance centered on the edge notch of the specimen. Small adjustments to the extensometer were made until measured strain was as close as possible to .1% after

which the strain was zeroed in the Station Manager software. Next, the ovens were closed around the specimen as tightly as possible while taking care to not actually touch the specimen.

All procedures began with a 20 minute warm up time to the target temperature of 1200°C followed by a 15 minute dwell time to ensure the specimen had also reached the target temperature. Thermal strain was calculated for the last five minutes of dwell time. This thermal strain was then subtracted from strain under load conditions to calculate the actual load response strain.

### 3.2.3 Creep Rupture Tests

Six creep rupture tests were performed on the double edge notched specimens in laboratory air at 1200°C. Load was applied at a rate of 25 MPa/s after the specimen had warmed up to the target temperature. Load was held constant until machine runout of 500,000 seconds or specimen failure. During the initial ramp load, time, displacement, force, strain and oven temperature data were sampled every .05 seconds. After the load up, data sampling rates varied to keep data files to a sufficient yet manageable size. A representative creep test is presented below.

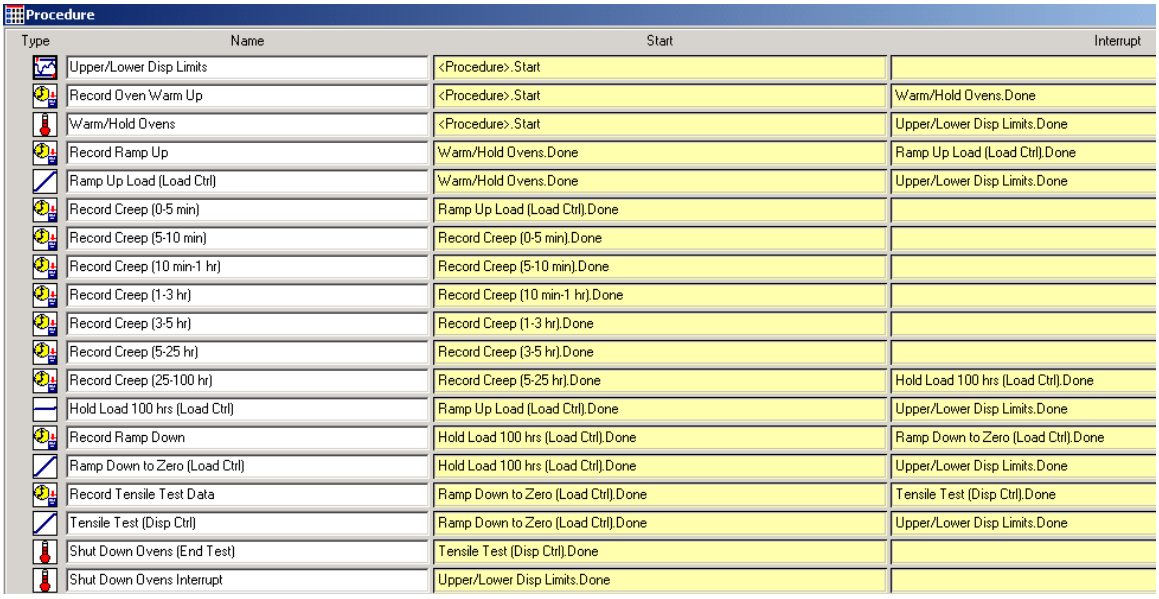

Procedure

| Type | Name | Start | Interrupt |
|---|---|---|---|
| | Upper/Lower Disp Limits | <Procedure>.Start | |
| | Record Oven Warm Up | <Procedure>.Start | Warm/Hold Ovens.Done |
| | Warm/Hold Ovens | <Procedure>.Start | Upper/Lower Disp Limits.Done |
| | Record Ramp Up | Warm/Hold Ovens.Done | Ramp Up Load (Load Ctrl).Done |
| | Ramp Up Load (Load Ctrl) | Warm/Hold Ovens.Done | Upper/Lower Disp Limits.Done |
| | Record Creep (0-5 min) | Ramp Up Load (Load Ctrl).Done | |
| | Record Creep (5-10 min) | Record Creep (0-5 min).Done | |
| | Record Creep (10 min-1 hr) | Record Creep (5-10 min).Done | |
| | Record Creep (1-3 hr) | Record Creep (10 min-1 hr).Done | |
| | Record Creep (3-5 hr) | Record Creep (1-3 hr).Done | |
| | Record Creep (5-25 hr) | Record Creep (3-5 hr).Done | |
| | Record Creep (25-100 hr) | Record Creep (5-25 hr).Done | Hold Load 100 hrs (Load Ctrl).Done |
| | Hold Load 100 hrs (Load Ctrl) | Ramp Up Load (Load Ctrl).Done | Upper/Lower Disp Limits.Done |
| | Record Ramp Down | Hold Load 100 hrs (Load Ctrl).Done | Ramp Down to Zero (Load Ctrl).Done |
| | Ramp Down to Zero (Load Ctrl) | Hold Load 100 hrs (Load Ctrl).Done | Upper/Lower Disp Limits.Done |
| | Record Tensile Test Data | Ramp Down to Zero (Load Ctrl).Done | Tensile Test (Disp Ctrl).Done |
| | Tensile Test (Disp Ctrl) | Ramp Down to Zero (Load Ctrl).Done | Upper/Lower Disp Limits.Done |
| | Shut Down Ovens (End Test) | Tensile Test (Disp Ctrl).Done | |
| | Shut Down Ovens Interrupt | Upper/Lower Disp Limits.Done | |

**Figure 19. Representative Creep Test**

### 3.2.4 Fatigue Tests

Four double edge notch specimens were loaded under a tension/tension fatigue regime in laboratory air at 1200°C. The fatigue loading was applied via a 1Hz sinusoidal wave with a stress ratio of .05 ($R=\sigma_{min}/\sigma_{max}$). PVC adaptive compensation was utilized to ensure that commanded loads matched the applied loads.

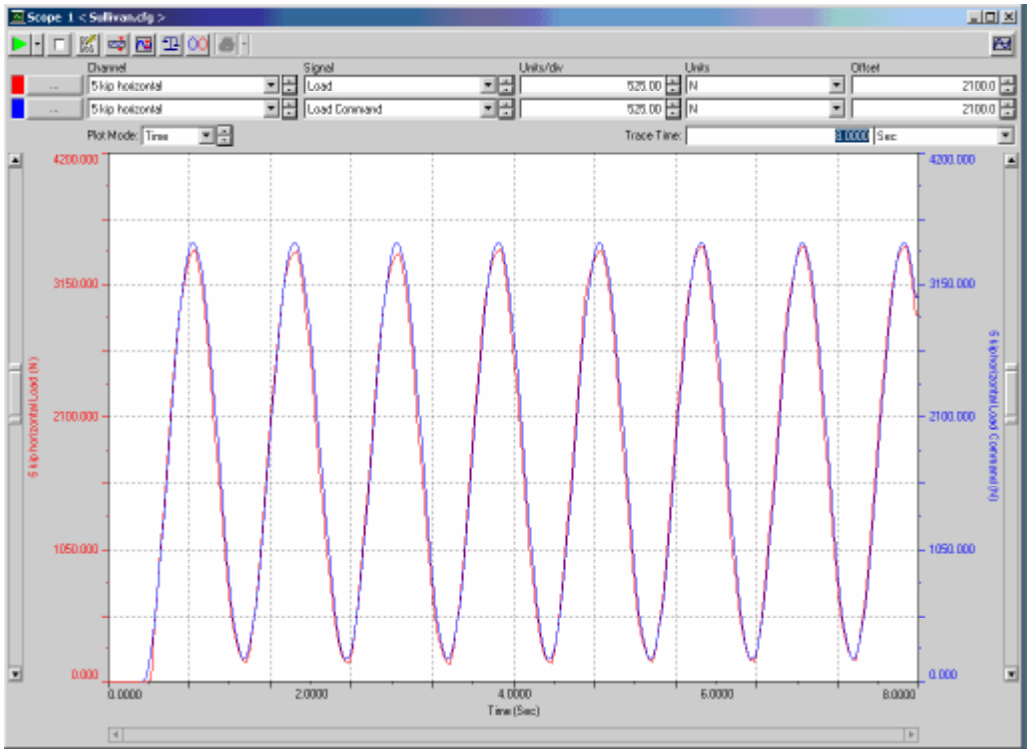


**Figure 20. PVC compensation matched commanded and applied loads**

In all fatigue tests, the following was recorded under various data collection modes: time, run-time, lower count, upper and lower force, oven temperatures, strain, and displacement. The data collection modes were circular, peak- valley, and hysteresis. The circular mode collected data every .05 seconds and constantly overwrote all of its data when the buffer size was filled up. Circular data collection ensured that failure data would be captured if one of the other two data collection modes was "off cycle." Peak-valley and hysteresis data were collected on log cycles at a rate of 200Hz (i.e. 1, 2, 5, 10, 20, 50…). Machine run out was limited to 10E5 cycles. A sample fatigue test is depicted below.

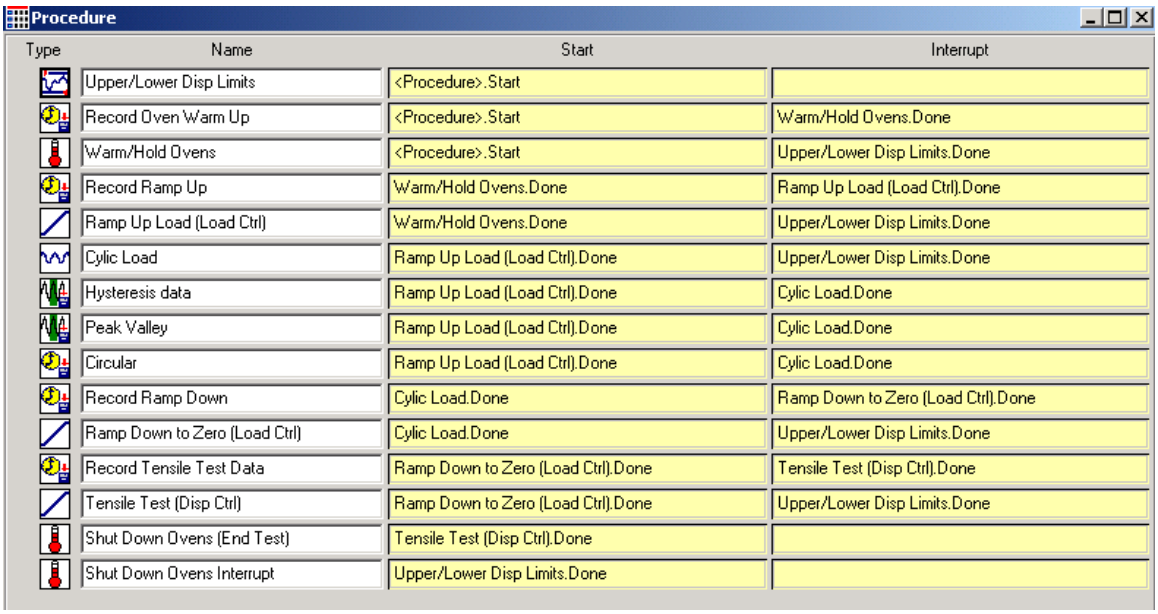


**Figure 21. Representative Fatigue Test**

### 3.3 Test Matrix

Table 5 shows all creep and fatigue tests performed in the course of this study on N720/A double edge notched specimens.

**Table 5. Test Matrix**

| Specimen | Loading Type | Temperature °C | Maximum Stress MPa |
|---|---|---|---|
| 1 | Creep | 1200 | 175 |
| 2 | Creep | 1200 | 120 |
| 3 | Creep | 1200 | 80 |
| 4 | Creep | 1200 | 100 |
| 5 | Creep | 1200 | 110 |
| 10 | Creep | 1200 | 140 |
| 7 | Fatigue | 1200 | 150 |
| 8 | Fatigue | 1200 | 155 |
| 9 | Fatigue | 1200 | 135 |
| 11 | Fatigue | 1200 | 152.5 |

# IV. Results and Analysis

The next chapter presents the results and analysis of double edge notch geometry specimen response under creep and fatigue loading conditions in 1200°C air. This data is compared to unnotched specimen response as reported in previous research efforts. Finally, micro structural characterization of the fracture surfaces as represented by optical and SEM images will be presented.

## 4.1 Monotonic Tensile Data

Although direct monotonic tensile data was not the purpose of this particular study, unnotched tensile strength data was needed in order to provide a baseline of comparison for the double edge notch specimen response. Dog bone specimens of N720/A at 1200°C were tested under displacement control at a rate of 0.05 mm/sec by Eber, Harlan, and Sullivan (Eber, 2005; Harlan, 2005; Sullivan, 2006). Additionally, COI reported tensile strength data on the corporate website. The average strength of these values was 203.7 MPa. This study will use 192 MPa as used by Sullivan for the baseline when comparing notched geometry impact on specimen strength.

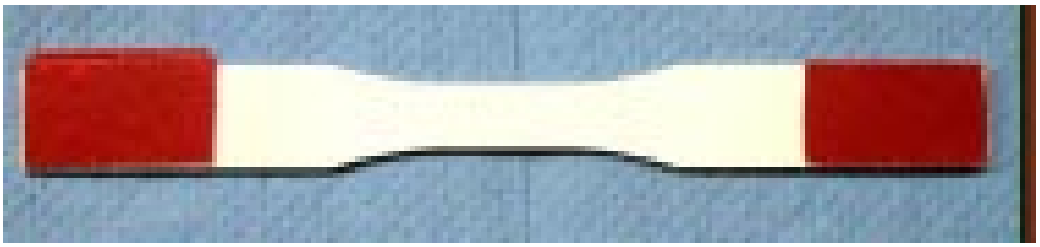

**Figure 22. Representative Dog bone Specimen (Braun)**

**Table 6. Summary of unnotched tensile Strengths**

| Source | Temperature °C | Elastic Modulus (GPa) | Ultimate Tensile Strength (MPa) | Failure Strain % |
|---|---|---|---|---|
| Sullivan | 1200 | 85 | 200.2 | .35 |
| COI | 1200 | 76.1 | 218.7 | .43 |
| Eber/Harlan | 1200 | 74.7 | 192.2 | .38 |
| Average | 1200 | 78.6 | 203.7 | .387 |

### 4.2 Thermal Strain

The thermal strain as measured by the extensometer was calculated in all creep and fatigue tests by averaging the strain during the last five minutes of dwell time. This thermal strain was then used to calculate the coefficients of thermal expansion using the equation $\alpha_t = \varepsilon_t/\Delta T$, where $\varepsilon_t$ is the thermal strain and $\Delta T$ is the temperature differential between room temperature and the as tested temperature.

**Table 7. Thermal Expansion of N720/A between 20°C and 1200°C**

| Specimen Number | Thermal Strain % | $\alpha_t$ ($10^{-6}$/°C) |
|---|---|---|
| 1 | .7097 | 6.01 |
| 2 | .7043 | 5.97 |
| 3 | .7264 | 6.16 |
| 4 | .7383 | 6.26 |
| 5 | .7341 | 6.22 |
| 10 | .7441 | 6.31 |
| 7 | .7443 | 6.31 |
| 8 | .7248 | 6.14 |
| 9 | .7368 | 6.24 |
| 11 | .7225 | 6.12 |
| Average | 0.7285 | 6.17 |
| Standard Deviation | 0.014 | 0.116 |

The average value of the coefficient of thermal expansion showed a small standard deviation and matched the value of $6x10^{-6}$/°C of a bare fiber as published by COI.

### 4.3 Creep Rupture Results

Six **c**reep rupture test were conducted at the target temperature of 1200°C at stress levels of 80, 100, 110, 120, 140, and 175 MPa. Time to rupture as well as strain at failure data are presented in Table 8 along with data from previous research conducted on unnotched specimens for comparison. Note that the present study uses 192 MPa as the baseline for calculating percent of ultimate tensile strength (UTS). This differs from Sullivan's technique which used notched UTS as well as unnotched UTS as baselines. Specimen 3, which achieved run-out was tested monotonically under displacement control at 0.05 mm/sec to check for the retained strength. This specimen achieved monotonic tensile strength of 166 MPa or 86% of the original UTS.

**Table 8. Summary Creep Data for 1200°C**

| Specimen | Creep Stress | | Failure Strain (%) | Time to Rupture (secs) | Location of failure |
|---|---|---|---|---|---|
| | (MPa) | (%) | | | |
| Boyer data | | | | | |
| 3 | 80 | 42 | 2.04 | >360,000 | Run-out |
| 4 | 100 | 52 | 3.14 | 157,081 | Notch |
| 5 | 110 | 57 | 1.83 | 20,585 | Notch |
| 2 | 120 | 63 | .934 | 2933 | Notch |
| 10 | 140 | 73 | 1.21 | 344 | Notch |
| 1 | 175 | 91 | .335 | ~0 | Notch |
| Sullivan data for center circular notched specimens | | | | | |
| CH3 | 100 | 52 | .54 | 847,585 | Run-out |
| CH1 | 125 | 65 | .43 | 69,750 | Hole |
| CH2 | 150 | 78 | .51 | 5,726 | Hole |
| CH5 | 175 | 91 | .31 | 106 | Hole |
| Harlan data for unnotched specimens | | | | | |
| 14-1 | 80 | 42 | 1.11 | 917,573 | Taper |
| 7-2 | 100 | 52 | 3.04 | 147,597 | Center |
| 9-2 | 125 | 65 | 3.40 | 15,295 | Center |
| 5-2 | 154 | 80 | .58 | 968 | Center |

Note: % Creep Stress is actual stress divided by 192 MPa.

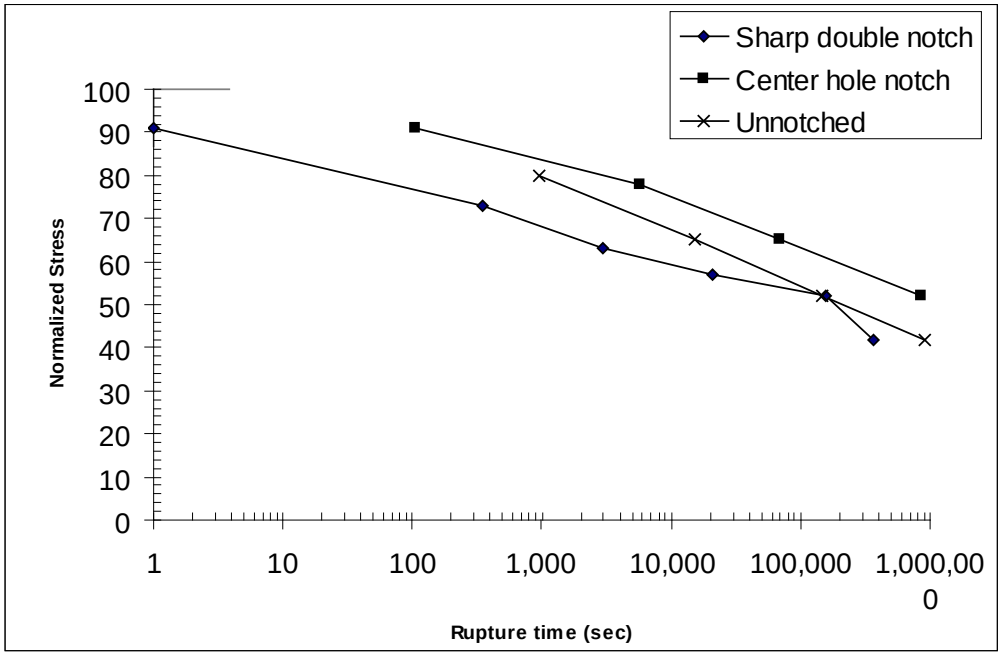


**Figure 23. Normalized Net Stress vs. Time**

Note: Circular Notch data from Sullivan and Unnotched data from Harlan

Figure 23 is a plot of the normalized stresses in Table 8 (i.e. % creep stress) versus a logarithmic scale of time. Figure 23 shows a mostly linear-logarithmic relationship between normalized net section stress and rupture time between values of 73% down to 52%. Except for the data point at 52% normalized net section stress, the rupture time for the double edge notch specimens were approximately three to five times less than an unnotched specimen. This implies that the double edge notch geometry has a sizable effect upon creep rupture time. One explanation is that the double edge notch geometry is not able to spread the stress concentrations across a greater volume of material as the unnotched or circular notched specimens so the defects reach critical strains much sooner. Interestingly, Sullivan's center notch data showed the opposite effect.

Creep strain versus time can show three different creep regimes. Figure 24 shows these three regimes of creep. Primary creep (stage 1) is characterized by a relatively high strain rate. Then as the material hardens, secondary creep (stage 2) results in a lower and steady creep rate. Finally, tertiary creep (stage 3) occurs when the material begins to behave in an unstable manner until rupture (Dowling, 1999:709).

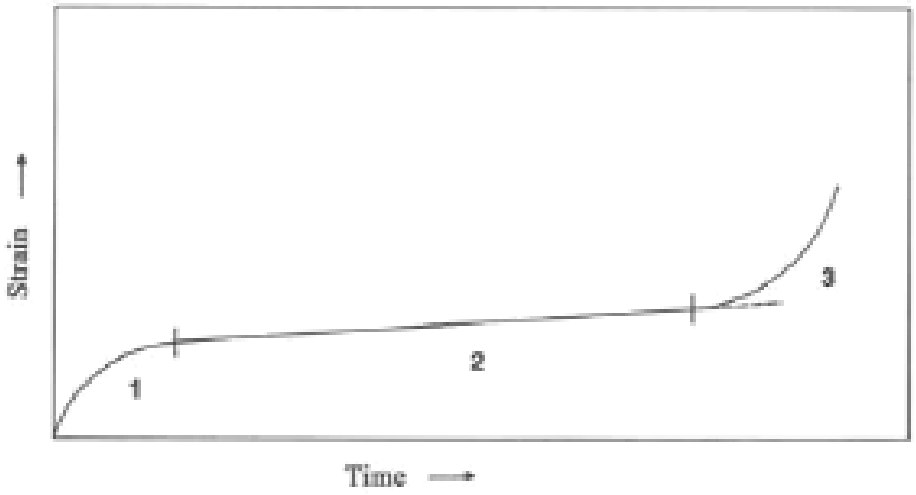


**Figure 24. Representative Creep Regimes (Chawla, 42)**

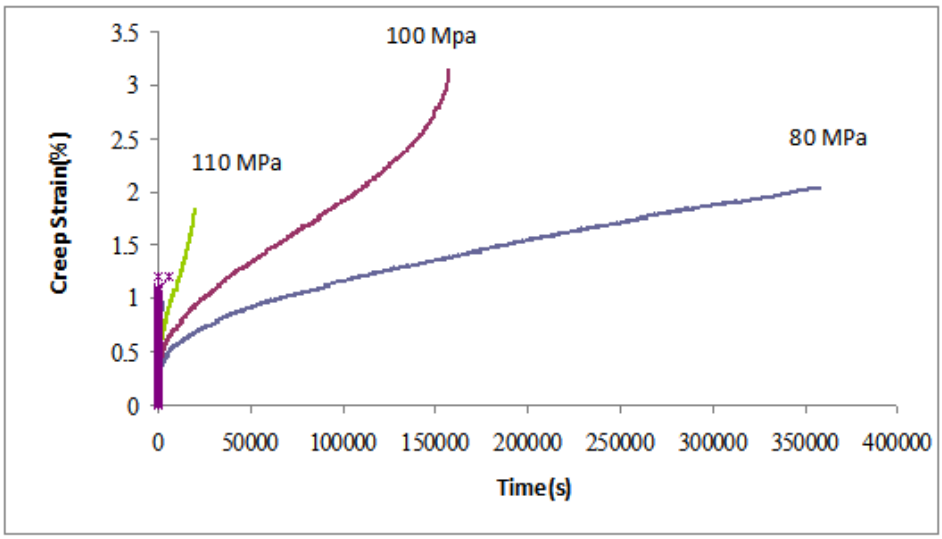


**Figure 25. Creep versus Time (full scale)**

Figure 25 primarily shows the various creep regimes experienced by the 80 MPa and 100 MPa double edge notch specimens. The 80 MPa sample lasted until the programmed machine limit of 100 hours was reached and shows both primary and steady state creep regions. The 100 MPa sample lasted approximately half as long but showed a higher final failure strain. This is likely due to the 100 MPa sample reaching the tertiary non-linear region of creep where the creep rate rapidly increased before failure at 3.14%.

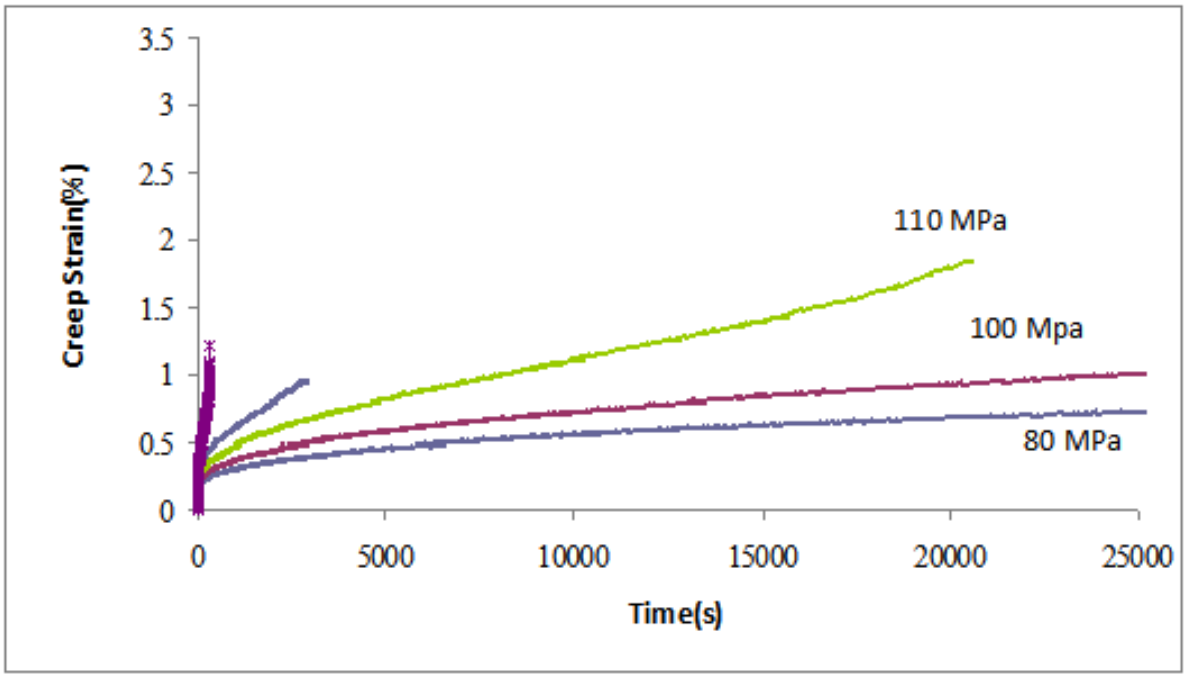


**Figure 26. Creep Strain versus Time (truncated scale)**

Figure 26 shows the same data as Figure 25 but with a truncated scale. This scale allows the identification of primary, secondary, and a small tertiary creep regime for the 110 MPa sample.

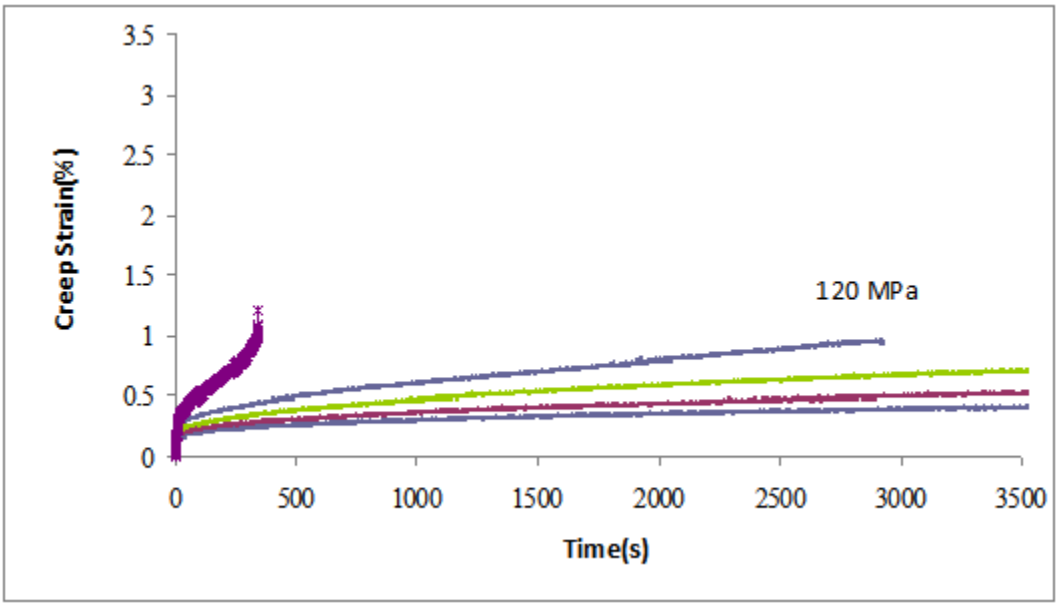


**Figure 27. Creep Strain versus Time (truncated scale)**

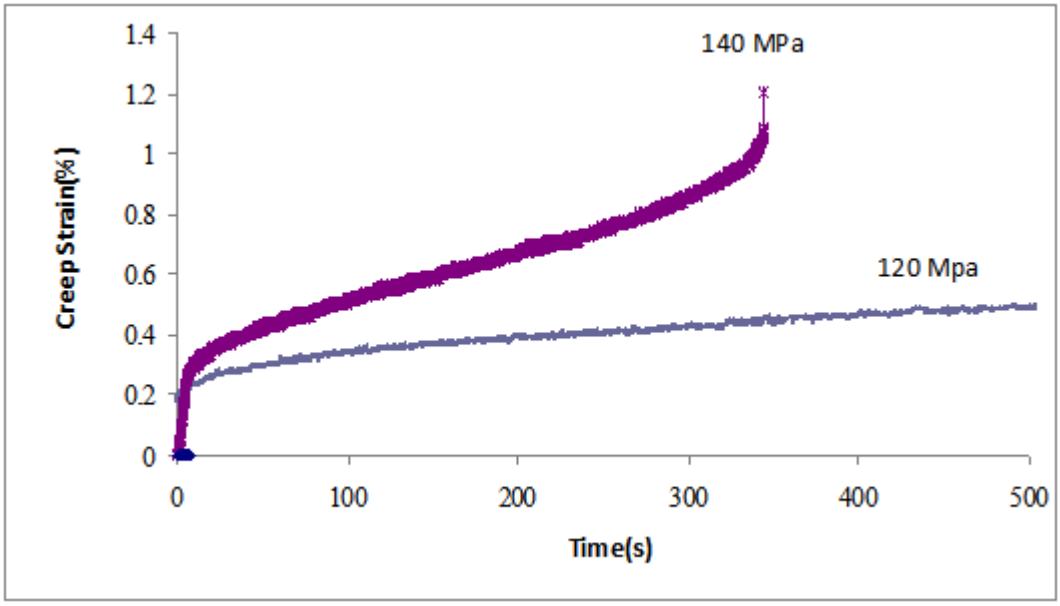


**Figure 28. Creep versus Time (truncated scale)**

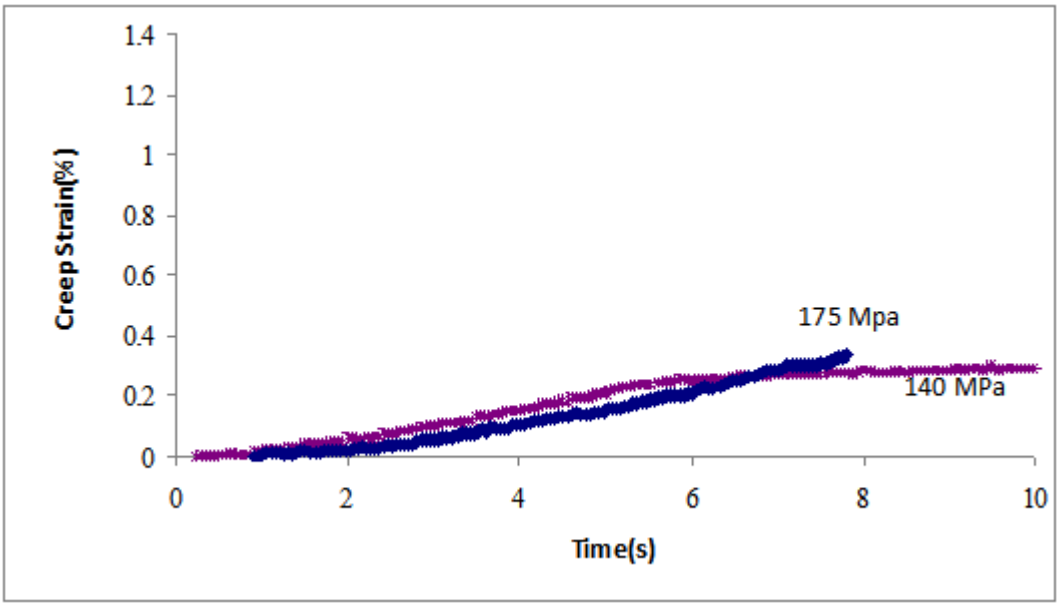


**Figure 29. Creep Strain versus Time (truncated scale)**

Figure 27 highlights the creep response of the 120 MPa double edge notch sample. Specifically, this sample shows only primary and secondary creep regimes. The 140 MPa notched specimen in Figure 28 shows primary, secondary and tertiary creep. Figure 29 shows the 175 MPa notched sample to possess only primary creep behavior before rupture. This failure strain of .335 % matches closely the published value of .43% monotonic failure strain (COI, 2005). This indicates that the damage mechanism in this creep test is similar to the damage mechanism in the monotonic loading. Also, since this test occurred so quickly, 175 MPa is a good approximation of the doubled edge notch adjusted UTS.

The previous creep data was used to calculate steady state strain rates from the secondary creep regions. Note that the 175 MPa specimen does not have a creep rate listed because it only demonstrated primary creep behavior. The Table below summarizes this data.

**Table 9. Summary Creep Rate Data**

| Specimen | Creep Stress (MPa) | Creep Rate (1/s) |
|---|---|---|
| Boyer data | | |
| 3 | 80 | 3.4E-08 |
| 4 | 100 | 1.7E-07 |
| 5 | 110 | 5.9E-07 |
| 2 | 120 | 3.0E-6 |
| 10 | 140 | 1.6E-05 |
| 1 | 175 | N/A |
| Sullivan data for center circular notched specimens | | |
| CH3 | 100 | 3.2E-09 |
| CH1 | 125 | 7.8E-09 |
| CH2 | 150 | 3.2E-07 |
| CH5 | 175 | 4.8E-06 |
| Harlan data for unnotched specimens | | |
| 14-1 | 80 | 1.5E-08 |
| 7-2 | 100 | 3.1E-07 |
| 9-2 | 125 | 5.1E-07 |
| 5-2 | 154 | 6.1E-06 |

The double edge notch specimens showed higher creep rates than either unnotched or center notched specimens except in the case of specimen 4 which showed a lower creep rate than the equivalent 100 MPa unnotched specimen.

When creep rates are plotted as a function of stress, a power regression can be used by Excel to generate the coefficients of the Norton-Bailey creep rate model. The Norton Bailey equation is as follows:

$$\frac{d\varepsilon}{dt} = A\sigma^{n} \qquad (4)$$

where $\frac{d\varepsilon}{dt}$ is the steady state creep rate, $A$ is a temperature related constant, $\sigma$ is the applied stress and $n$ is the stress exponent (Dowling, 1999:740). Figure 30 shows that the creep rate power regression for double edge notch specimens is higher across all stress levels.

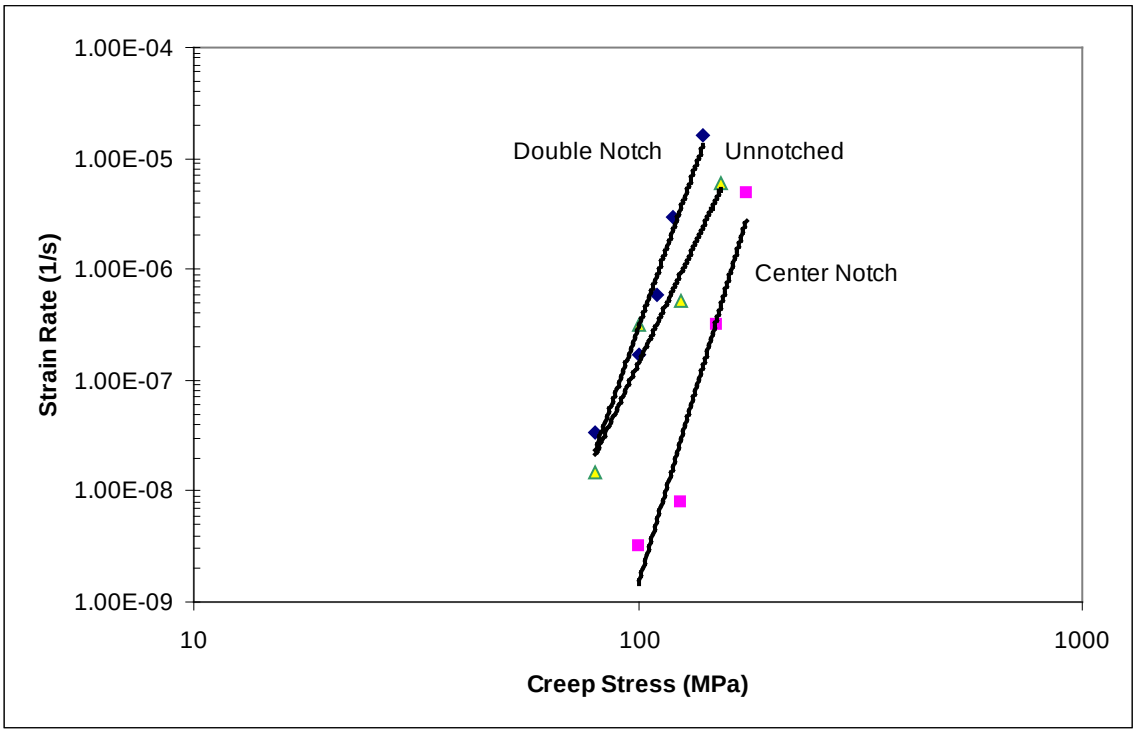


**Figure 30. Steady State Creep Rate versus Stress**

$\frac{d\varepsilon}{dt} = 6E\text{-}30\sigma^{11.324}$ is the creep rate for the double notch specimens

$\frac{d\varepsilon}{dt} = 2E\text{-}24\sigma^{8.4579}$ is the creep rate for the unnotched specimens

$\frac{d\varepsilon}{dt} = 1E\text{-}36\sigma^{13.495}$ is the creep rate for the center notch specimens

## 4.4 Digression

The creep results in the previous section present a dilemma. Specifically, the failure strain rates of some of the creep specimens are 5 to 10 times the monotonic failure strain. Interestingly, Harlan's work showed two unnotched creep specimens with failure strains at 3.04 and 3.40% at 1200°C. Nevertheless, after the initial failure creep strains were recorded in this particular study, they were viewed skeptically and so a short test of an aluminum dog bone sample was studied to verify the MTS machine and extensometer were recording data properly. The aluminum dog bone specimen was loaded within a known elastic region while strain data was collected for 5 tension/tension fatigue cycles. The fatigue cycle was utilized to ensure the extensometer was not slipping during machine loading and unloading. Also, the slope of the hysteresis loops which is Young's modulus could be used to verify the accuracy of the MTS machine and extensometer.

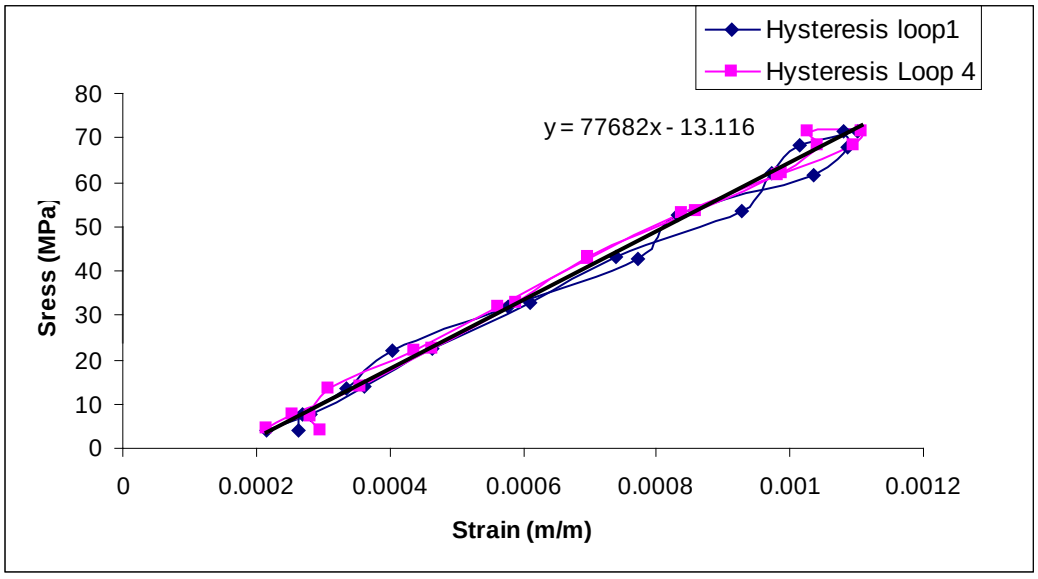


**Figure 31. Hysteresis Plots of Aluminum Specimen**

A linear curve fit of the hysteresis data shows a slope of 77 GPa which is very close to the published Young's modulus of 70 GPa (Dowling, 1999:50). This verifies the accuracy of the previous MTS and extensometer creep data and the following fatigue data.

### 4.5 Tension-Tension Fatigue Tests

Four double edge notch specimens were tested under a tension-tension fatigue regime at 1200°C with a sinusoidal load and .05 stress ratio ($R=\sigma_{min}/\sigma_{max}$). Table 10 summarizes the work performed in this research as well as the work by Sullivan and Eber. Note that *% UTS* is normalized by 192 MPa in all samples whether notched or notched. This was performed so that the baseline would be the same for all specimens and so that the following graphs would represent a fair comparison of normalized data.

**Table 10. Summary Fatigue Data**

| Specimen | Fatigue Stress | | Failure Strain (%) | Cycles to Failure | Location of failure |
|---|---|---|---|---|---|
| | (MPa) | (%) | | | |
| Boyer double edge notch data | | | | | |
| 9 | 135 | 70 | 2.5 | 500,000 | Run-out |
| 7 | 150 | 78 | 3.37 | 196,149 | Notch |
| 11 | 152.5 | 79 | 3.01 | 129,034 | Notch |
| 8 | 155 | 81 | .21 | 3 | Notch |
| Sullivan data for center circular notched specimens | | | | | |
| FH4 | 150 | 78 | .43 | 500,992 | Run-out |
| FH6 | 160 | 83 | .41 | 301,292 | Hole |
| FH5 | 175 | 91 | .28 | 8 | Hole |
| Eber data for unnotched specimens | | | | | |
| 6 | 100 | 52 | .43[1] | >120,199 | Run-out |
| 7 | 125 | 65 | .45[1] | >146,392 | Run-out |
| 8 | 150 | 78 | .53[1] | >167,473 | Run-out |
| 9 | 170 | 89 | .51[1] | >109,436 | Run-out |

Note: [1]Failure strain found by monotonically testing run-out specimens.

Whereas Sullivan's data showed the center notched specimens to have greater fatigue resistance, the double edge notch specimens here showed lower fatigue life than the center notch specimens and similar fatigue life to the unnotched specimens. Maximum fatigue life, which was defined as 500,000 cycles, was achieved at fatigue loads ≤70% UTS. Interestingly, failure strains for the double edge notch specimens were six to eight times those of either center notched or unnotched specimens except for the double edge notch specimen at 81% UTS which had a failure strains of .30%. The highest stressed specimen at 81% UTS failed in only 3 cycles. This indicates that the stress concentration at the notch likely exceeded the tensile strength of the specimen and that more and more fibers failed during each successive cycle as the crack propagated very quickly. Specimen 9 which achieved machine run-out was monotonically tested under displacement control at a rate of 0.05 mm/sec at 1200°C in order to check retained strength. Under monotonic testing, this specimen failed at 161 MPa or 84% of original UTS.

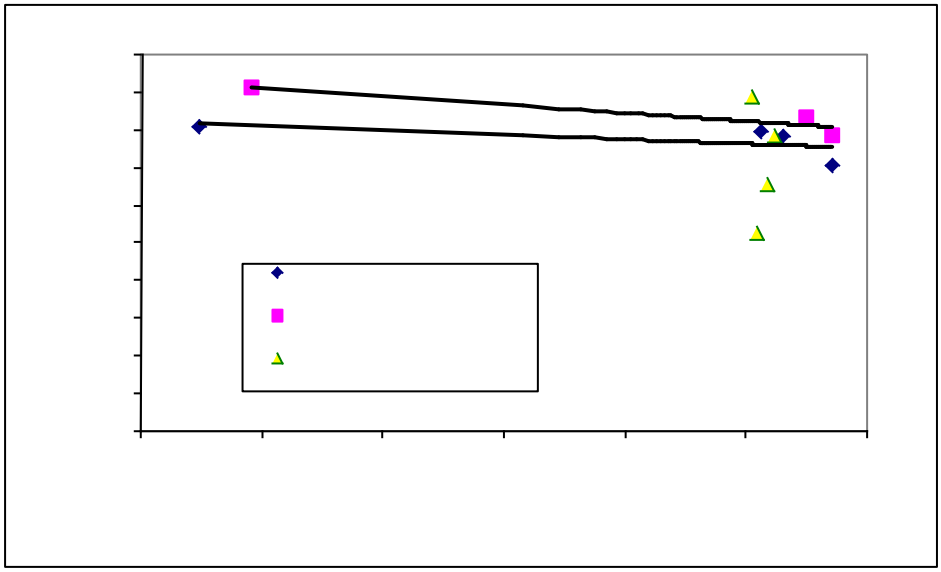

**Figure 32. Fatigue Stress versus Cycles to Failure**

Figure 32 is a plot of normalized net section stress (i.e. % Fatigue Stress) versus logarithmic cycles (data taken from Table 10). The data above suggest that the double edge notch geometry contributes to greater fatigue sensitivity. For example, Sullivan's center notch trend line in Figure 32 has a slight negative slope implying that as long as stresses remain below 80%, then fatigue resistance is good. The double edge notch trend line slope is nearly flat, implying that a slight increases in stress leads to a disproportionately reduced fatigue life. Specifically, increasing the stress from 152.5 MPa to 155 MPa reduces the fatigue life from 190,054 cycles down to 3 cycles. Furthermore, the unnotched geometry showed the most fatigue stability with all data points >100,000 cycles. In short, the flat trend line curve and comparison with unnotched data suggest that the double edge notch geometry causes a sensitive fatigue life response.

Fatigue damage accumulation can be pictured by plotting the maximum and minimum strains for each cycle. Increasing damage can then be seen by the minimum and maximum strains increasing over time.

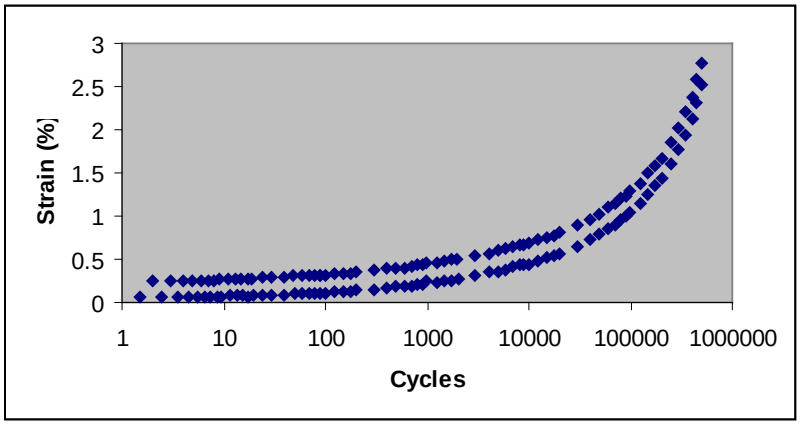


**Figure 33. 135 MPa Fatigue Maximum and Minimum Strain**

The 135 MPa specimen held a fairly stable fatigue damage rate but after 10,000 cycles fatigue damage started to accumulate rapidly. Another way to picture this accumulated damage is to subtract minimum strain from maximum (i.e. strain range) and note that it has a positive slope over time.

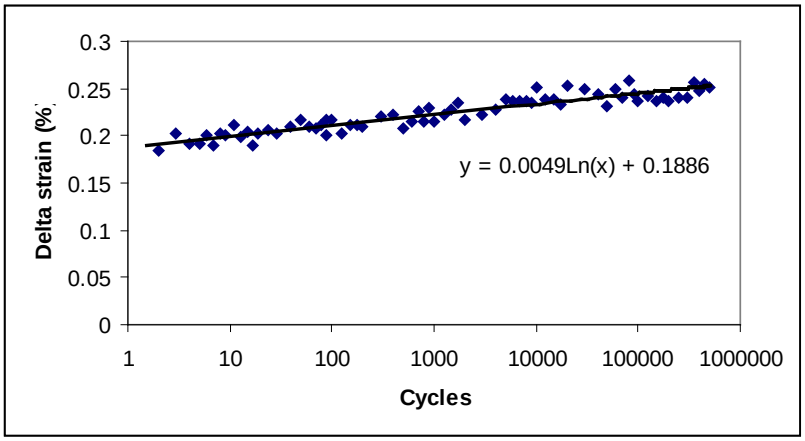


**Figure 34. 135 MPa Delta Strain versus Cycles**

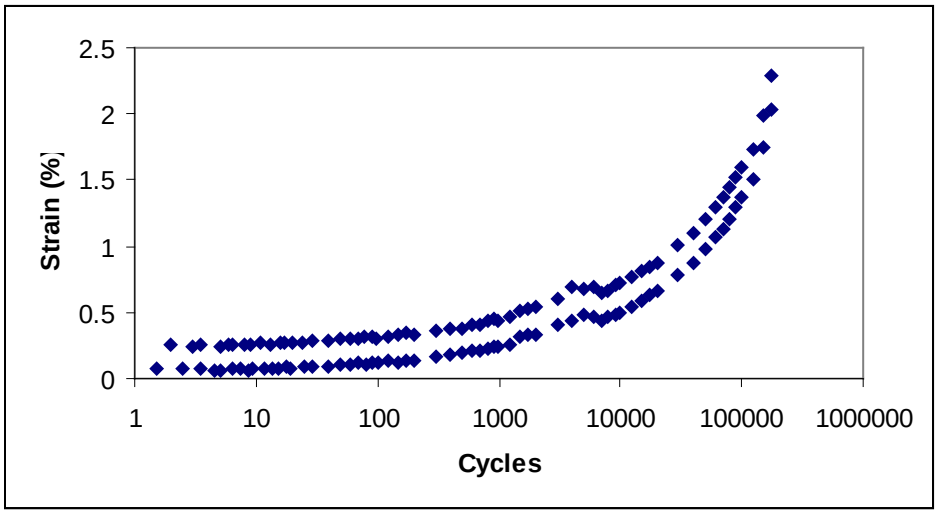


**Figure 35. 150 MPa Maximum and Minimum Strain**

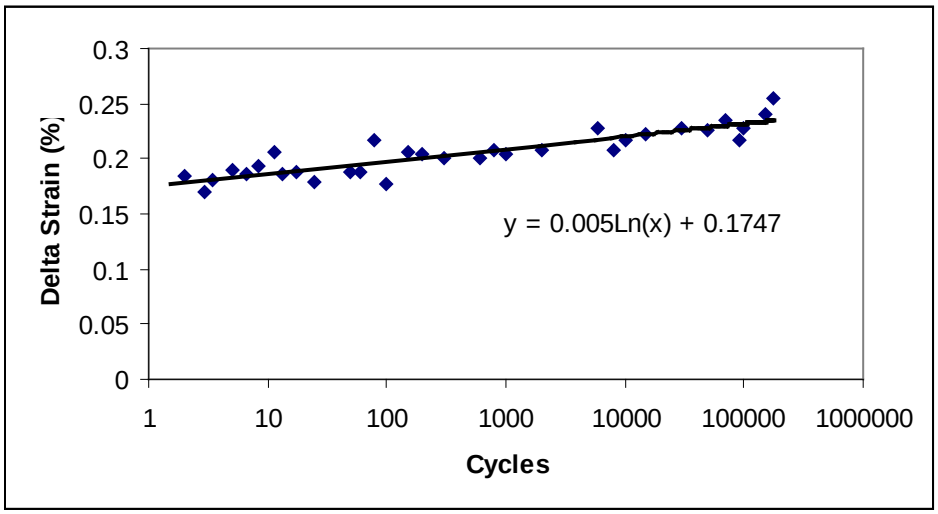


**Figure 36. 150 MPa Delta Strain versus Cycles**

Figure 35 shows the 150 MPa damage specimen accumulating fatigue damage in a linear fashion only until 1,000 cycles after which there is a rapid increase in damage. Interestingly, the trend line in Figure 36 closely matches the 135 MPa trend line in Figure 34. Also, Figures 34 and 36 suggest that the maximum delta strain achievable is .25 % after which material failure will occur. Note that this value is close to the monotonic failure strain.

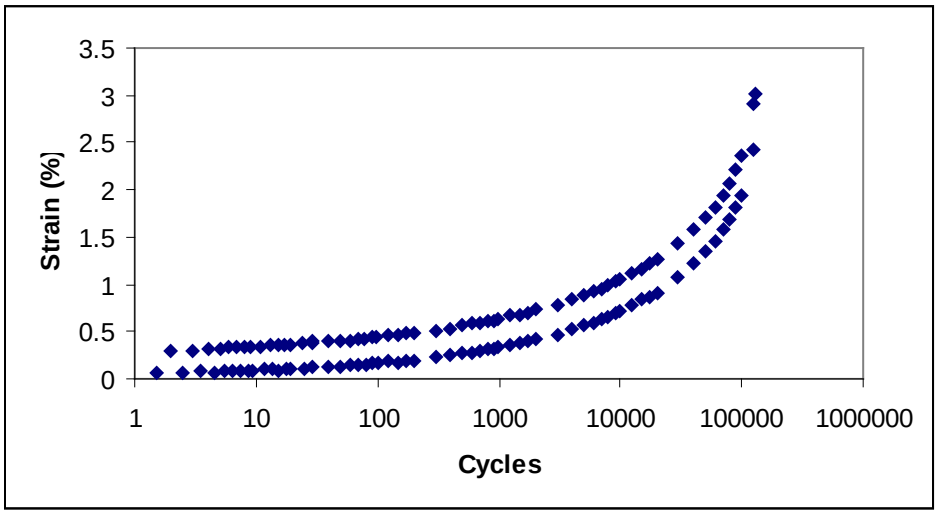


**Figure 37. 152.5 MPa Maximum and Minimum Strain**

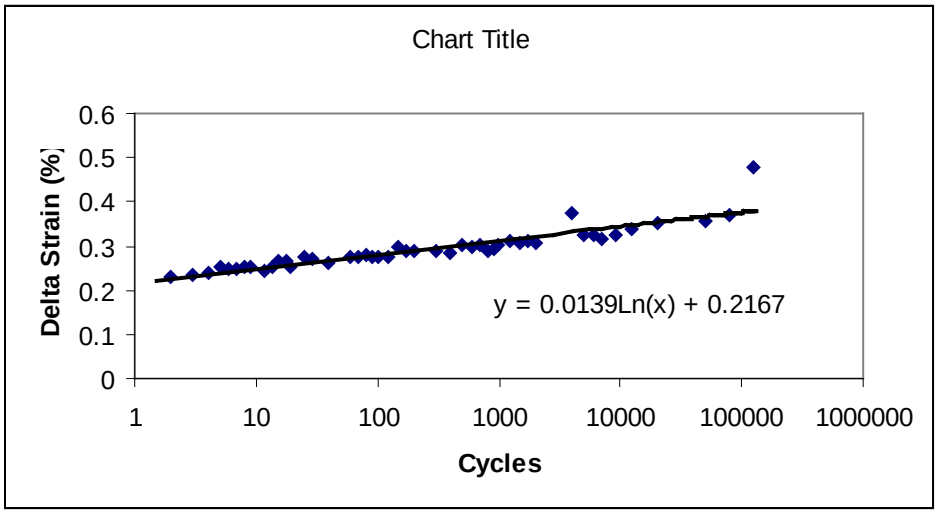


**Figure 38. 152.5 MPa Delta Strain versus Cycles**

Figure 37 shows a linear maximum and minimum strain growth until 700 cycles after which growth becomes rapid. The slope of the strain range versus cycles trend line is nearly 3 times that of the 135 and 150 MPa specimens. Also, the highest delta strain measured is nearly twice as large as the 135 and 150 MPa specimens indicating greater fiber pullout was achieved.

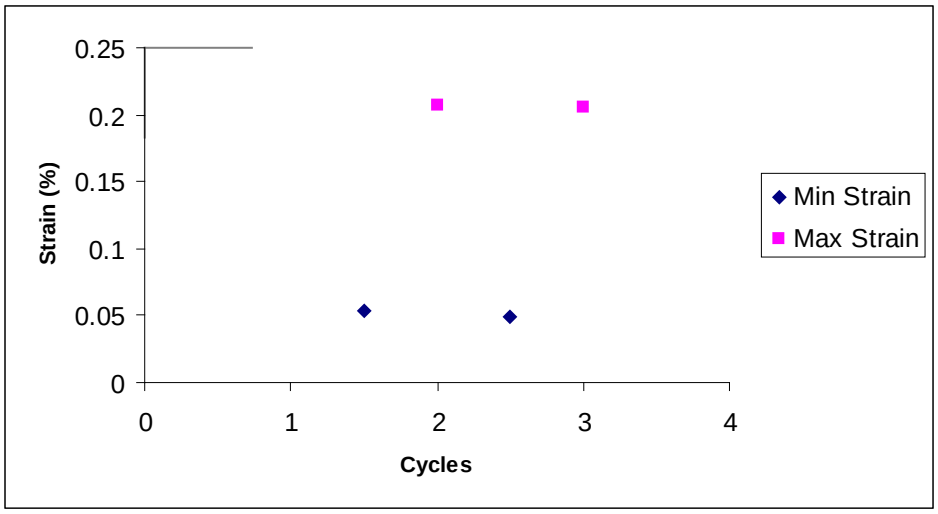


**Figure 39. 155 MPa Maximum and Minimum Strain**

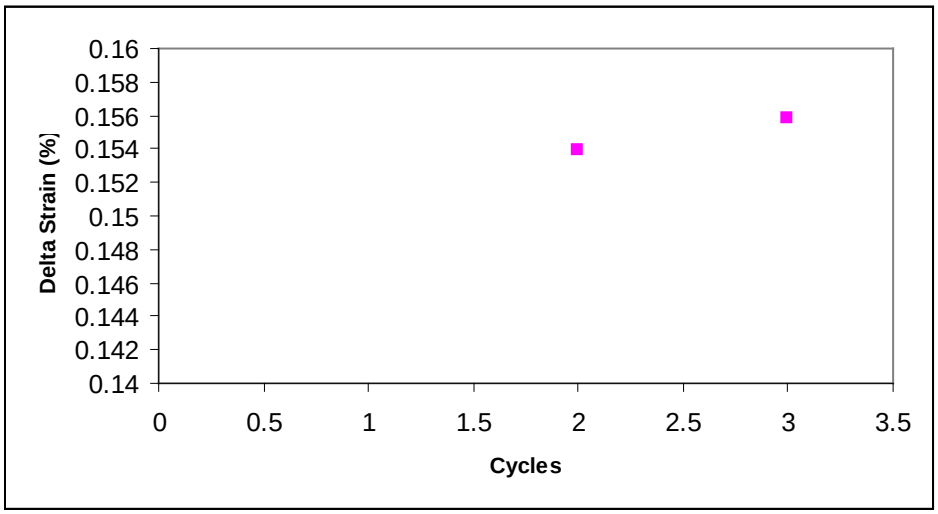


**Figure 40. 155 MPa Delta Strain versus Cycles**

The 155 MPa maximum and minimum strains stayed constant as evidenced by Figures 39 and 40; however, the specimen failed so quickly (on the third cycle) that any conclusions as to material response to fatigue would be premature.

Hysteresis data is presented next. The area contained within a hysteresis loop is analogous to the energy dissipated per unit volume of a fatigue load cycle (Stephen, 2001:99). Ductile materials like metal dissipate this energy in the form of plastic work; however, brittle materials like CMCs dissipate this energy through microcrack formation and internal friction.

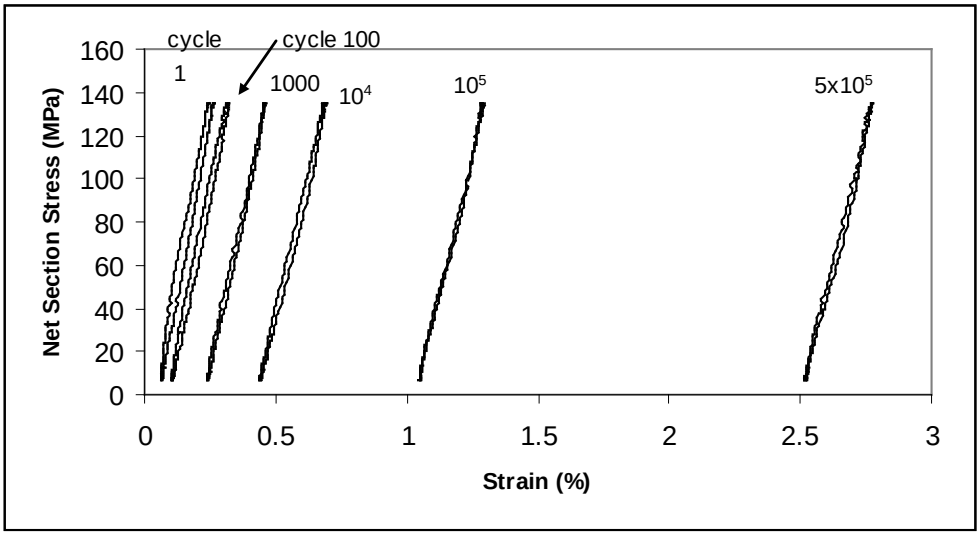


**Figure 41. 135 MPa Hysteresis Data**

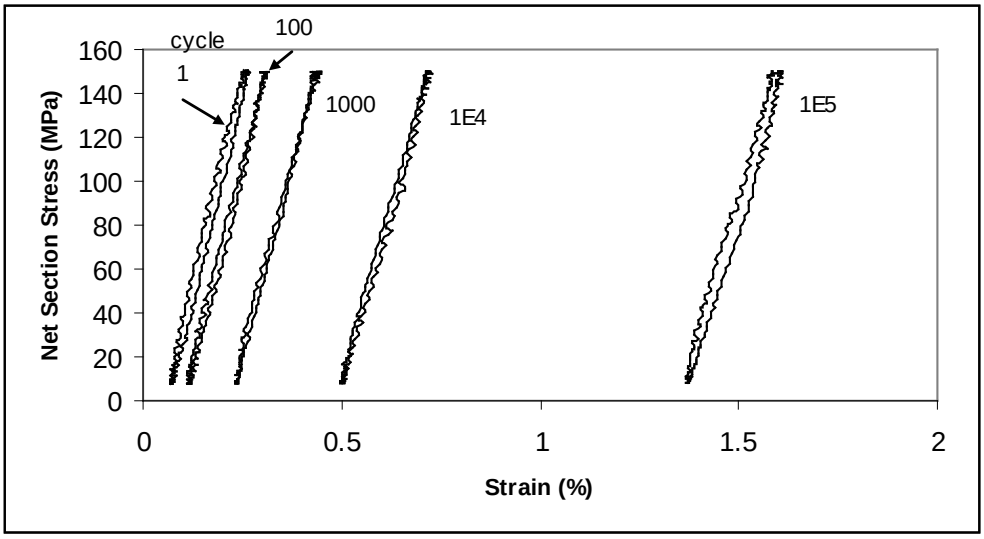


**Figure 42. 150 MPa Hysteresis Data**

Figures 39 and 40 both indicate that the specimens exhibited linear elastic loading and unloading with most of the energy being dissipated during the first cycle – the exception being cycle 100,000 for the 150 MPa specimen which is larger than the first cycle and shows a slight nonlinear response. The small size of the hysteresis loops suggest that the fatigue loading regime is causing only small damage; however, creep is the likely culprit for the increasing strain as cycles increase.

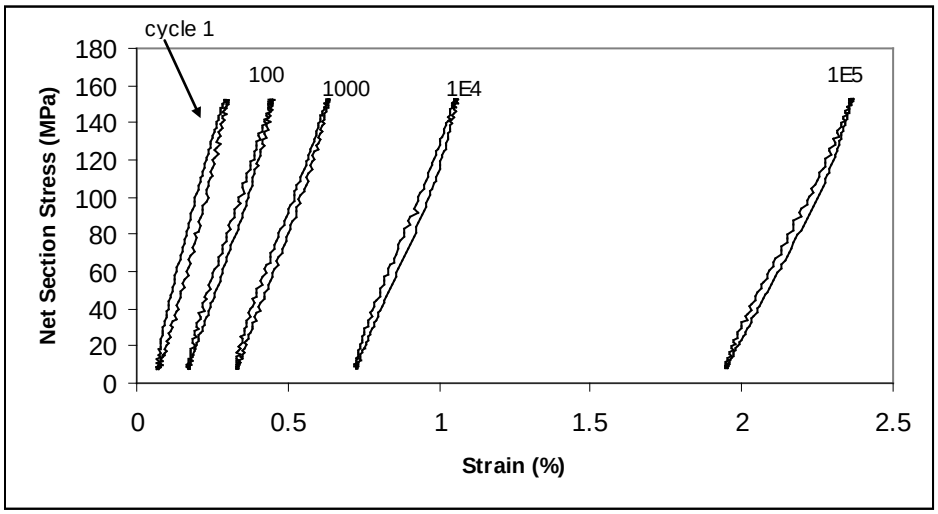


**Figure 43. 152.5 MPa Hysteresis Data**

The slope of the hysteresis loops in Figure 41 show a nonlinear response as early as cycle 1000 which indicate inelastic damage occurring much earlier than the previous 150 MPa specimen.

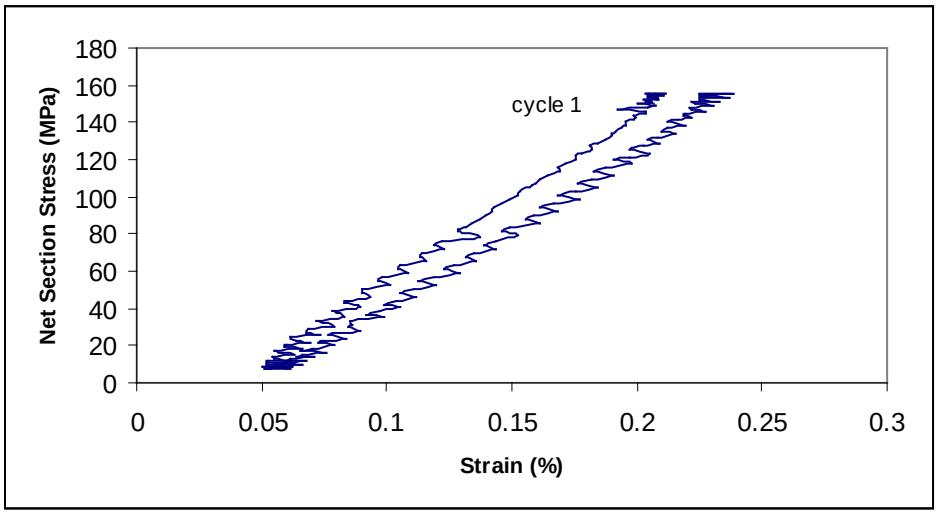


**Figure 44. 155 MPa Hysteresis Data**

Only one cycle of the 155 MPa specimen was recorded for hysteresis data as the specimen failed on the third cycle. Although the resolution is high - and thus the response shows the sensitivity based noise of the extensometer - it can be seen that the overall response is linear.

Another way to picture increasing damage as fatigue progresses is to plot how stiffness versus fatigue cycle varies. Because all the specimens exhibited mostly linear elastic response in their hysteresis behavior, the slope between the low and high points can be approximated by the secant modulus as follows:

$$S_{\sec} = \frac{\sigma_{\max} - \sigma_{\min}}{\varepsilon_{\max} - \varepsilon_{\min}} \tag{5}$$

Also, since the stress ratio does not change for each fatigue cycle and these values can be normalized by the $\Delta\varepsilon$of the first cycle, the normalized stiffness can be expressed as :

$$S_{\sec_{norm}} = \frac{(\varepsilon_{\max} - \varepsilon_{\min})^{cycle1}}{\varepsilon_{\max} - \varepsilon_{\min}} \tag{6}$$

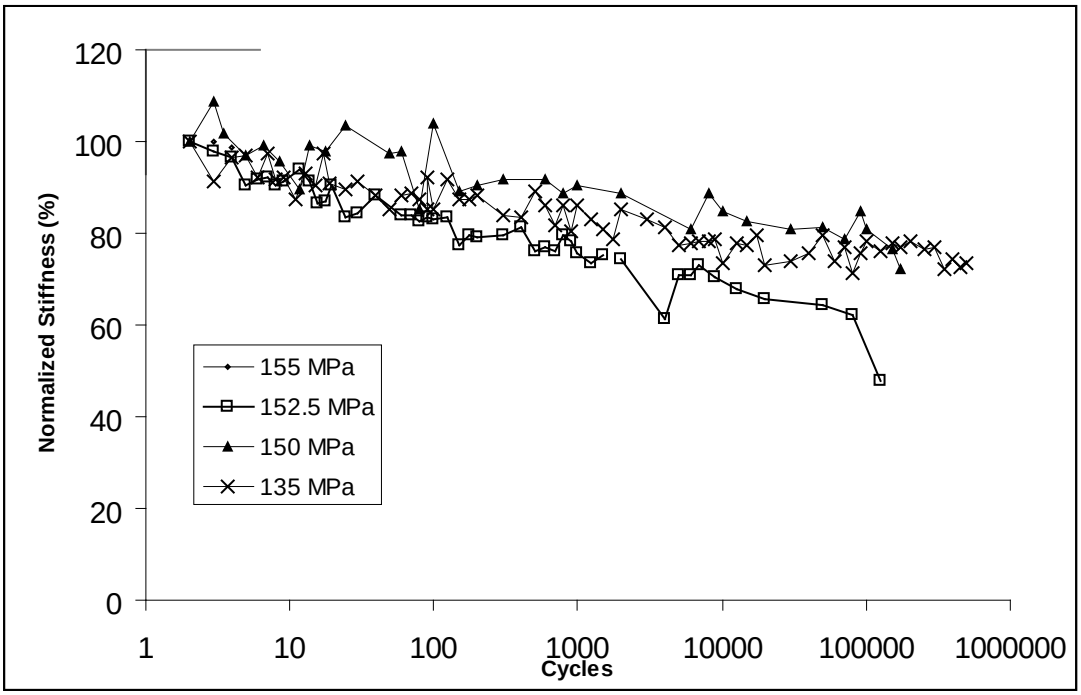


**Figure 45. Normalized Stiffness versus Fatigue Cycle**

Figure 45 is a plot of the normalized stiffness versus a logarithmic scale of cycles. The normalized stiffnesses generally follow a linear downward trend when plotted against a logarithmic scale of cycles. This reduction in stiffness over time is due to the strain range (i.e.$\Delta\varepsilon$) increasing – which is representative of ideal fatigue damage. However, minimum strain is also increasing over time as evidenced by the hysteresis data – which suggests a creep damage mechanism is present. In short, specimens loaded under fatigue conditions showed damage due to both fatigue and creep mechanisms.

## 4.6 Comparison of Creep and Fatigue Tests

From the previous section, it can be seen that creep is the likely damage agent in either creep or fatigue loading. This was evidenced by small increases in $\Delta\varepsilon$over time. Figure 46 shows a comparison of creep strains and mean fatigue strains ((strain$_{max}$-strain$_{min}$)/2).

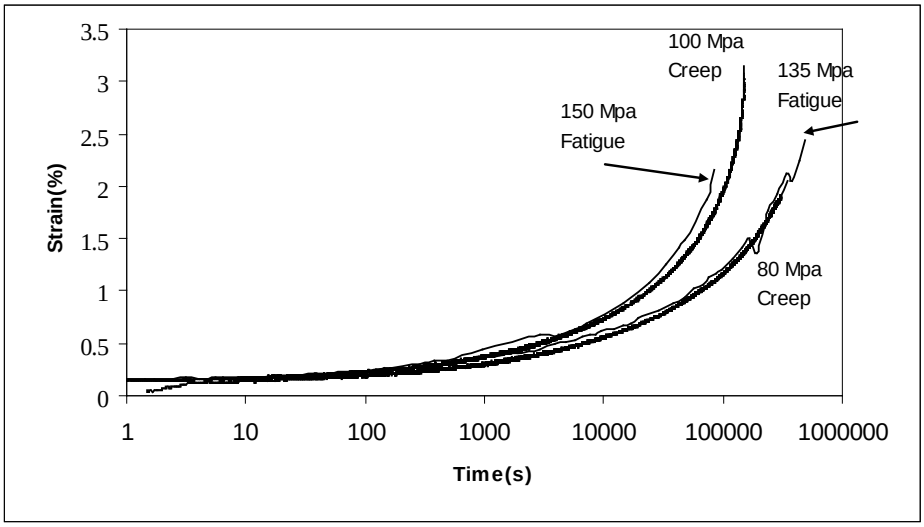


**Figure 46. Mean Creep Strain versus Time**

Figure 46 suggests that the135 MPa fatigue specimen and the 80 MPa creep specimen have very similar strain rate as the strain versus time graph virtually overlaps. The 150 MPa fatigue and 100 MPa creep specimens also overlap but not as closely after 10,000 seconds. In both cases a 33 to 40 % reduction in stress is required to transition from fatigue stress to creep stress while maintaining a similar strain rate profile. The failure of the 150 MPa specimen before the 100 MPa creep specimen suggests that there is another failure mechanism occurring during fatigue loading for this specimen besides creep.

Figure 47 shows the strain versus time for 152.5 MPa fatigue specimen initially falls between that of the 120 and 110 MPa creep specimens until 1000 seconds after which the fatigue specimen is able to maintain and accelerate its strain rate much longer before failing.

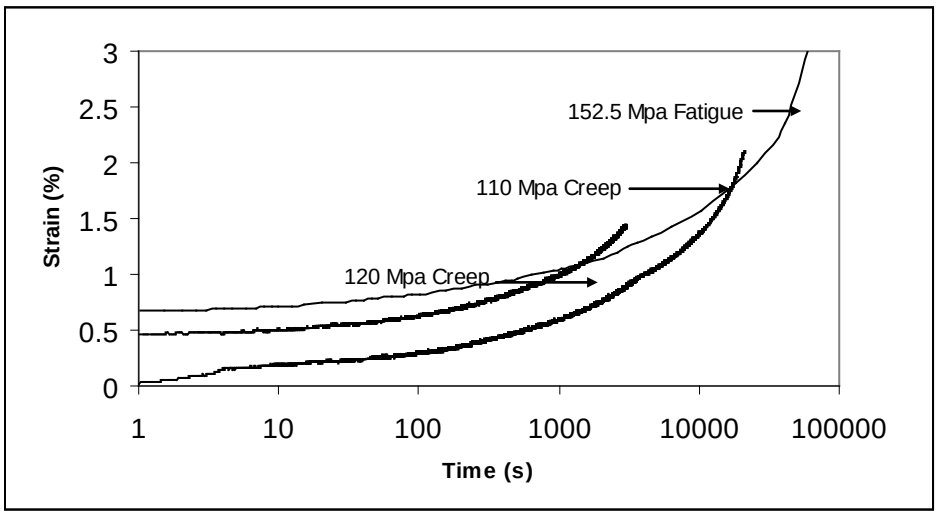


**Figure 47. Mean Strain versus Time**

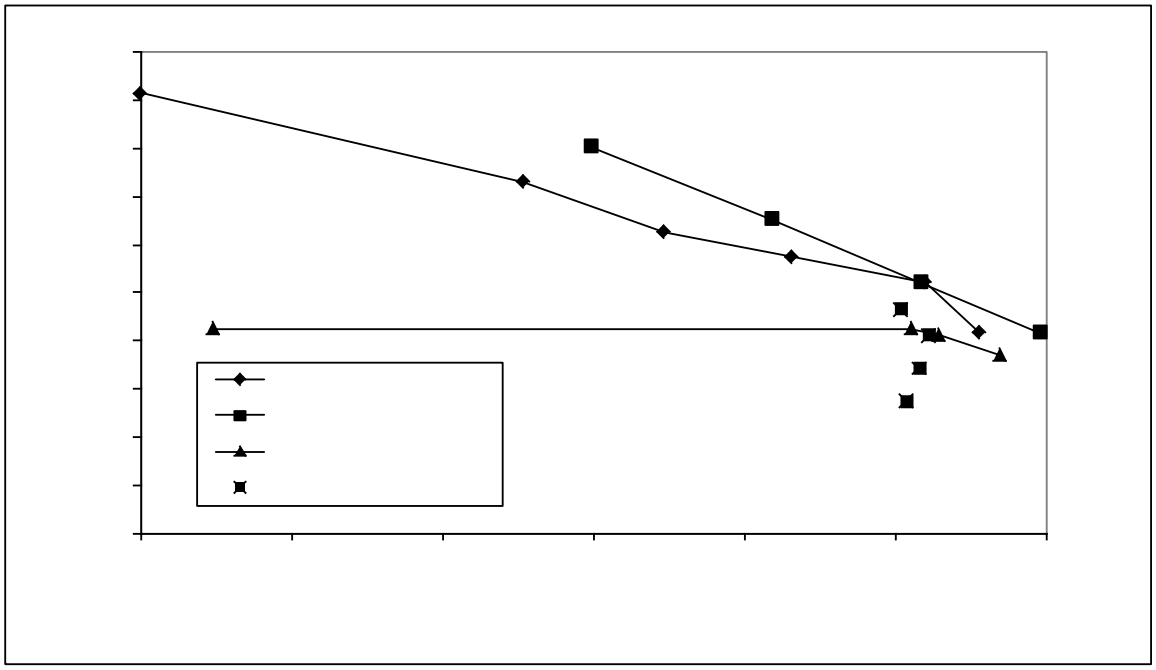

**Figure 48. Mean Stress versus Time to Failure**

In addition to plotting mean strain versus time, mean stress versus time was plotted in Figure 48.Mean stress versus time to failure shows fatigue life to be particularly sensitive to double edge notch geometry. The double edge notch fatigue life is flat until mean stress is reduced to less than 41% UTS after which the slope is similar to unnotched specimens. The creep data also suggests that the double notch specimens are experiencing stress concentrations at all stress levels which are greater than their unnotched counterparts except for a mean stress at 52% at which the double edge notched and unnotched specimens are very similar. In short, mean stress must be reduced by approximate 15% for double edge notch creep specimens and greater than approximately 25% for fatigue specimens in order to achieve similar life spans.

## 4.7 Microstructural Analysis

After all creep and fatigue testing was completed, the N720/A specimens were examined via optical and SEM microscopes. The optical microscope was used to analyze side views of the specimen in order to verify location of failure and determine any macro-material behavior that contributed to specimen failure. The SEM was used to obtain higher magnification end views to determine fiber, matrix, or fiber/matrix interaction behavior which contributed to failure.

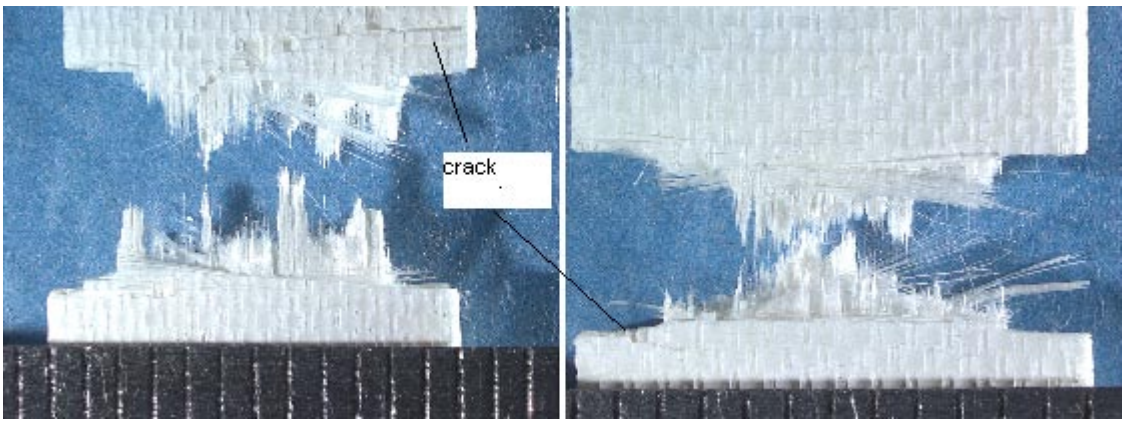


**Figure 49. 80 MPa (left) and 100 MPa (right) Creep**

Note: (Ruler = mm)

Both creep specimens in Figure 49 show marked fiber pullout as well as some surface cracks near the edge notches. Crack growth occurred along the edge notches on both specimens. Note that the 80 MPa specimen did not break during creep loading as it survived the programmed MTS machine limit of 100 hours. This photo was taken after monotonic testing to check retained strength.

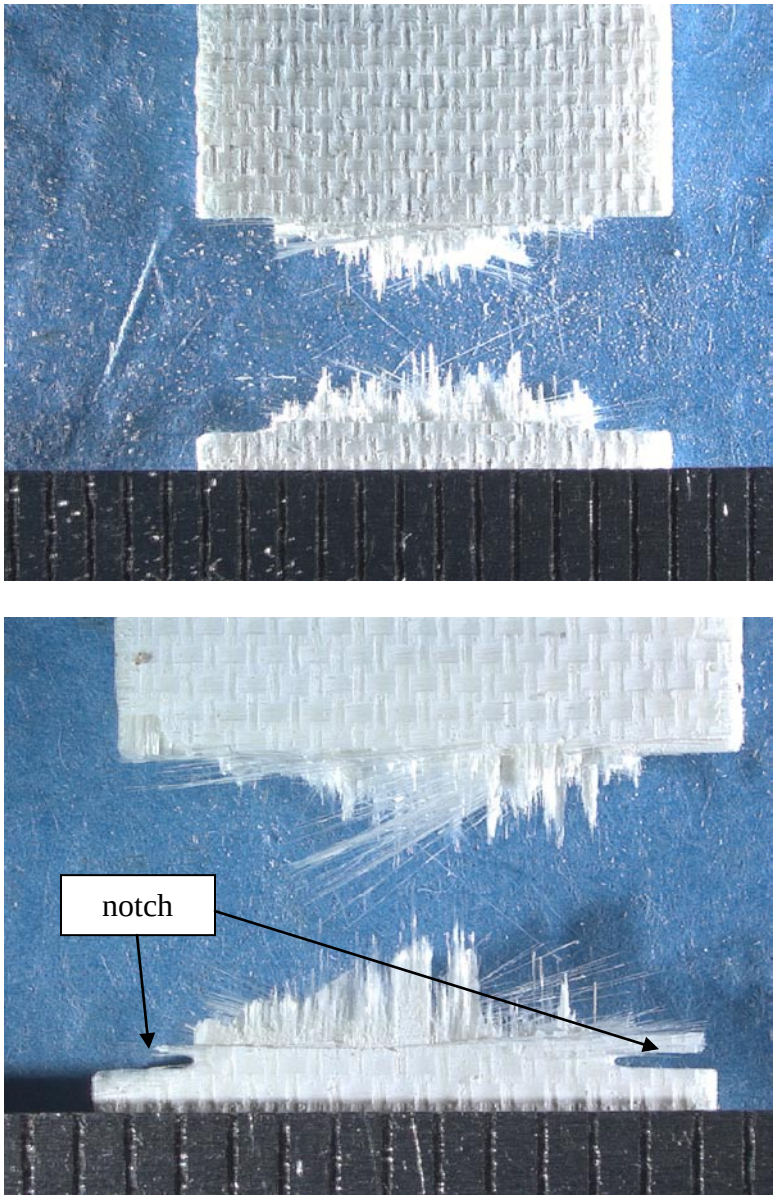


**Figure 50. 110 MPa (top) and 120 MPa (bottom) Creep, (scale in mm)**

The 110 and 120 MPa creep specimens in Figure 50 both show a pyramid fracture shape where the primary fiber pullout is at the center of the specimen. On the 120 MPa creep specimen the fracture plane is on top of the notch on both sides. This suggests that the crack propagated up the 0° fibers from the notch edge before moving across the 90° fibers.

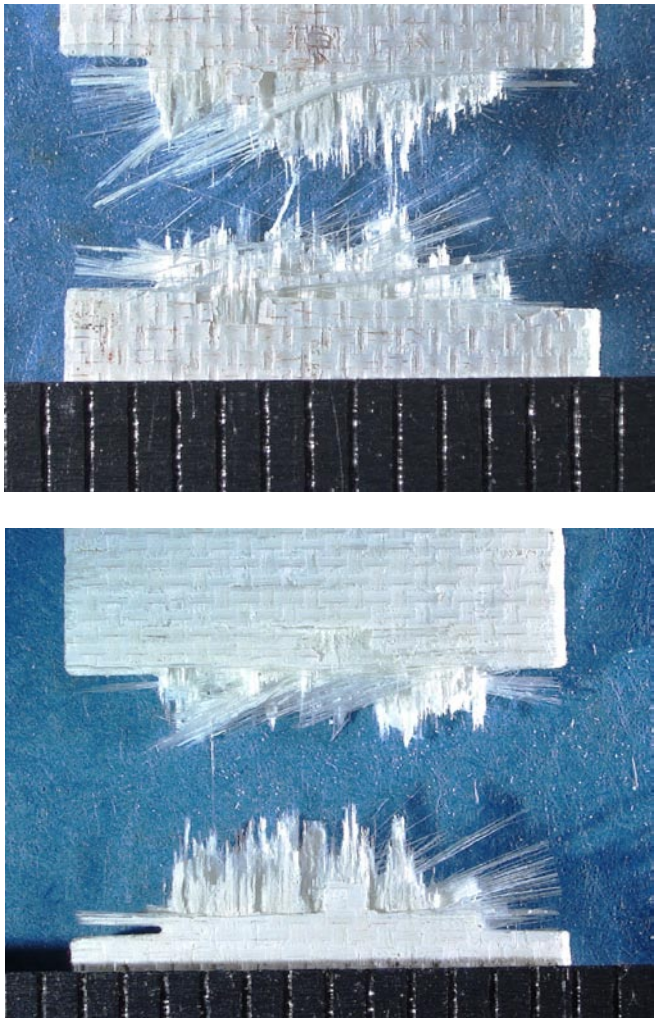

**Figure 51. 140 MPa (top) and 175 MPa (bottom) Creep, (scale in mm)**

The highest creep strain specimens in Figure 51 show similar macro behavior as the lower stressed specimens. The 175 MPa specimen shows crack propagation along the 0° fibers from the notch edge before moving across the 90° fibers similar to the 120 MPa specimen in Figure 50. Because the 175 MPa creep specimen failed instantaneously, it also represents monotonic failure like the photo of the 80 MPa creep specimen in Figure 9. However, no discernable visible difference can be inferred from failure under a monotonic or creep loading condition.

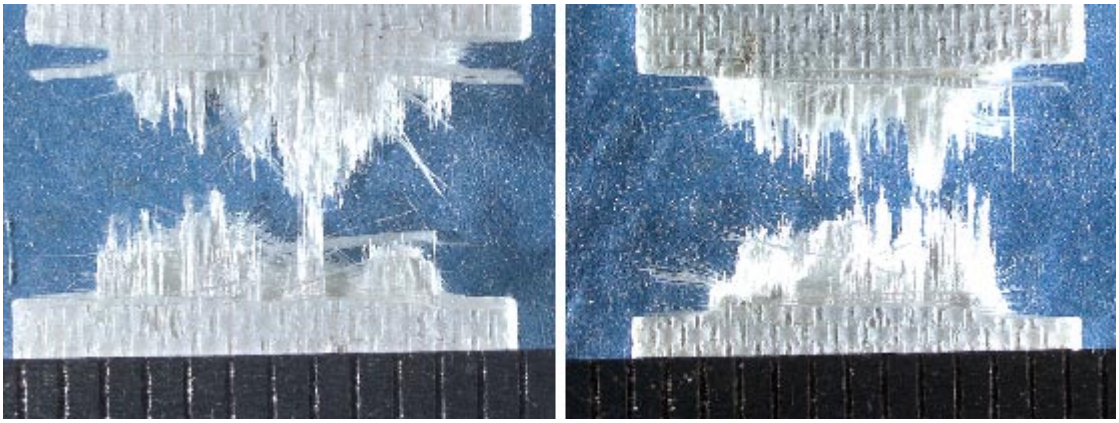

**Figure 52. 135 MPa (left) and 150 MPa (right) Fatigue**

Note: (ruler = mm)

The 135 and 150 MPa fatigue specimens display similar fracture behavior as the previous creep specimens. Most fiber pullout is located in the center of each specimen. Some of the 90° tows fanned out during failure – especially the tows near the apex of the edge notches.

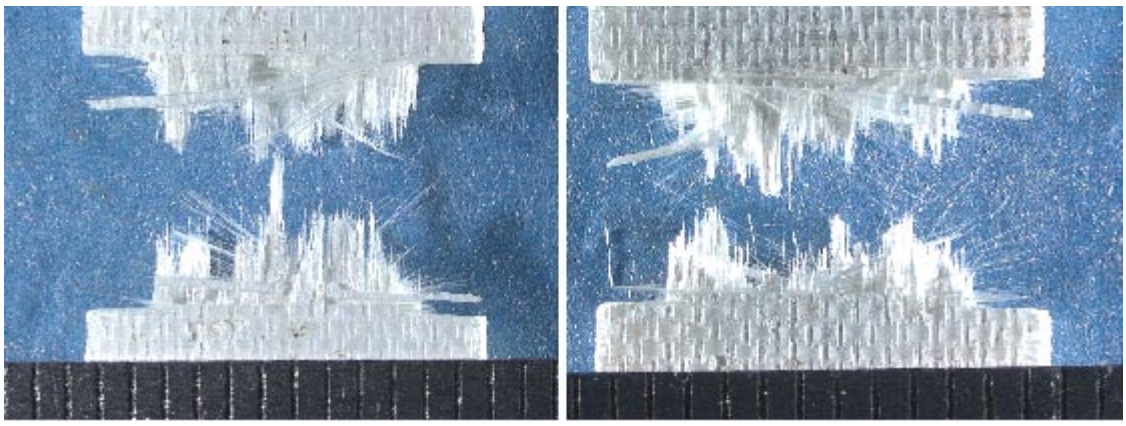

**Figure 53. 152.5 MPa (left) and 155 MPa (right) Fatigue**

Note: (ruler = mm)

The 152.5 MPa specimen shows similar behavior as previous specimens; however, the 155 MPa specimen has less fiber pullout in the center. This is probably due to the rapid onset of failure once the outside fibers had pulled out and fractured.

Higher magnification end views of all specimens were made utilizing the SEM after gold coating the fracture surfaces. The methodology employed in SEM examination utilized progressively higher magnifications of three fracture surface regions (i.e. right, middle and center). This was done to follow the crack growth propagation path from the notch edge until final fracture at the specimen center. Figure 54 represents the three regions of interest. Note, subsequent figure captions reference approximate location of SEM micrographs.

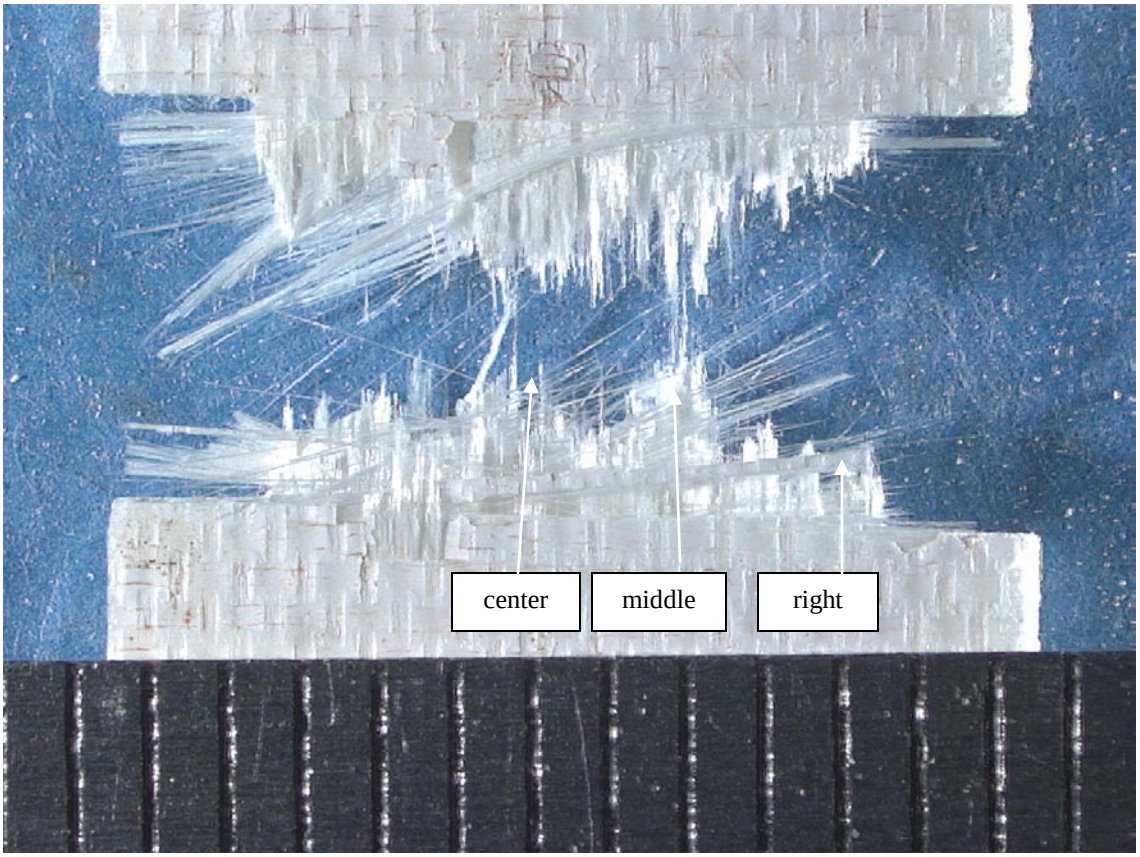


**Figure 54. Three Regions of Interest for SEM Micrographs**

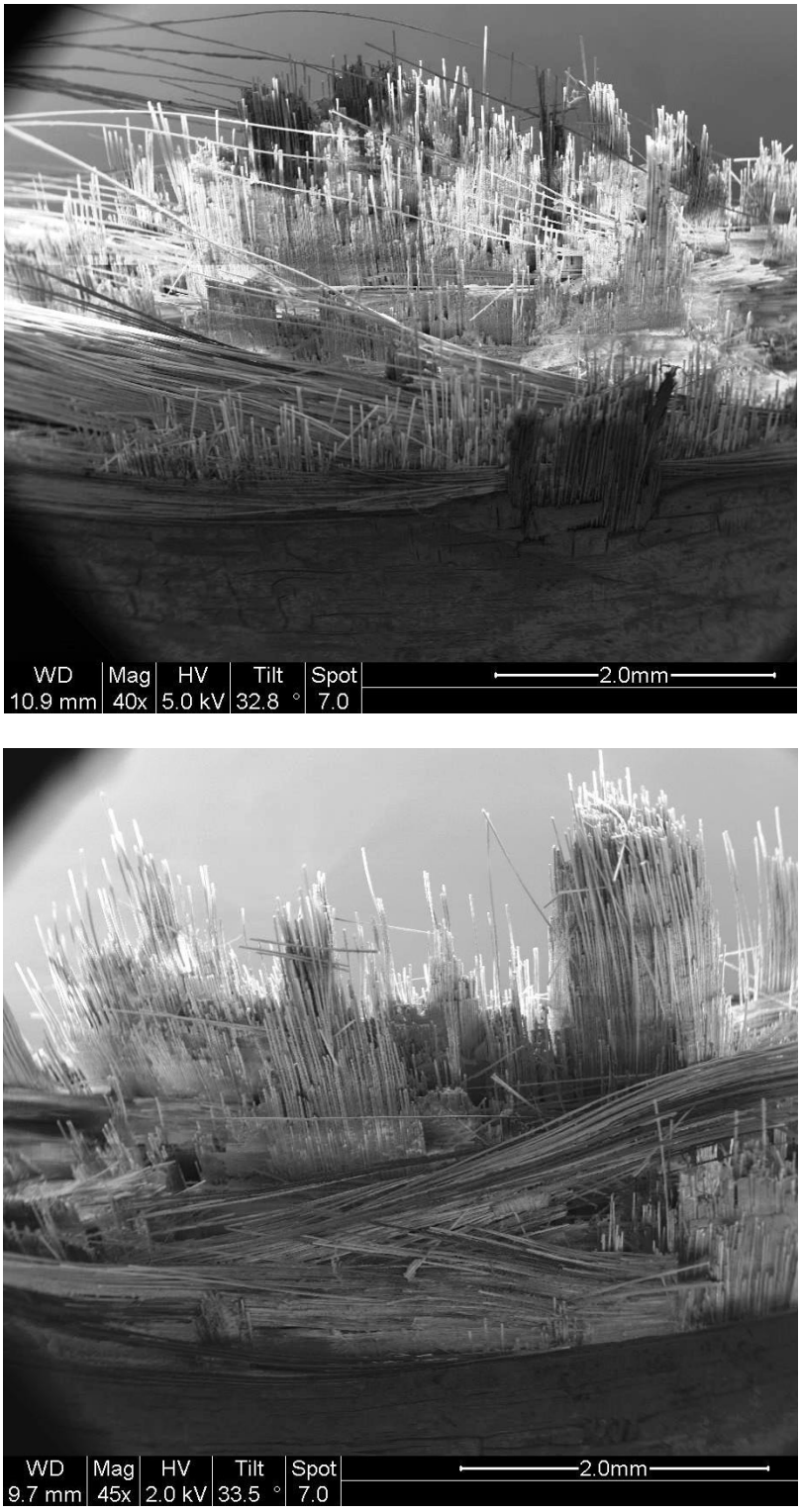


**Figure 55. 140 MPa Creep (top) and 150 MPa Fatigue (bottom)**

Note: both micrographs taken at center of specimens.

The end views of all SEM images were similar as represented by Figure 55. Past research by Sullivan indicated that there is no visible impact on the appearance of fractured specimens when loading method is changed from monotonic, to creep and to fatigue. The one notable exception is that the fracture plane was always on or adjacent to the edge notches where the cross-sectional area was the smallest. Figure 56 shows where the edge notch meets the crack propagation plane. The fiber pullout is generally much shorter near the notches but gets longer as the crack propagates toward the center of the specimen.

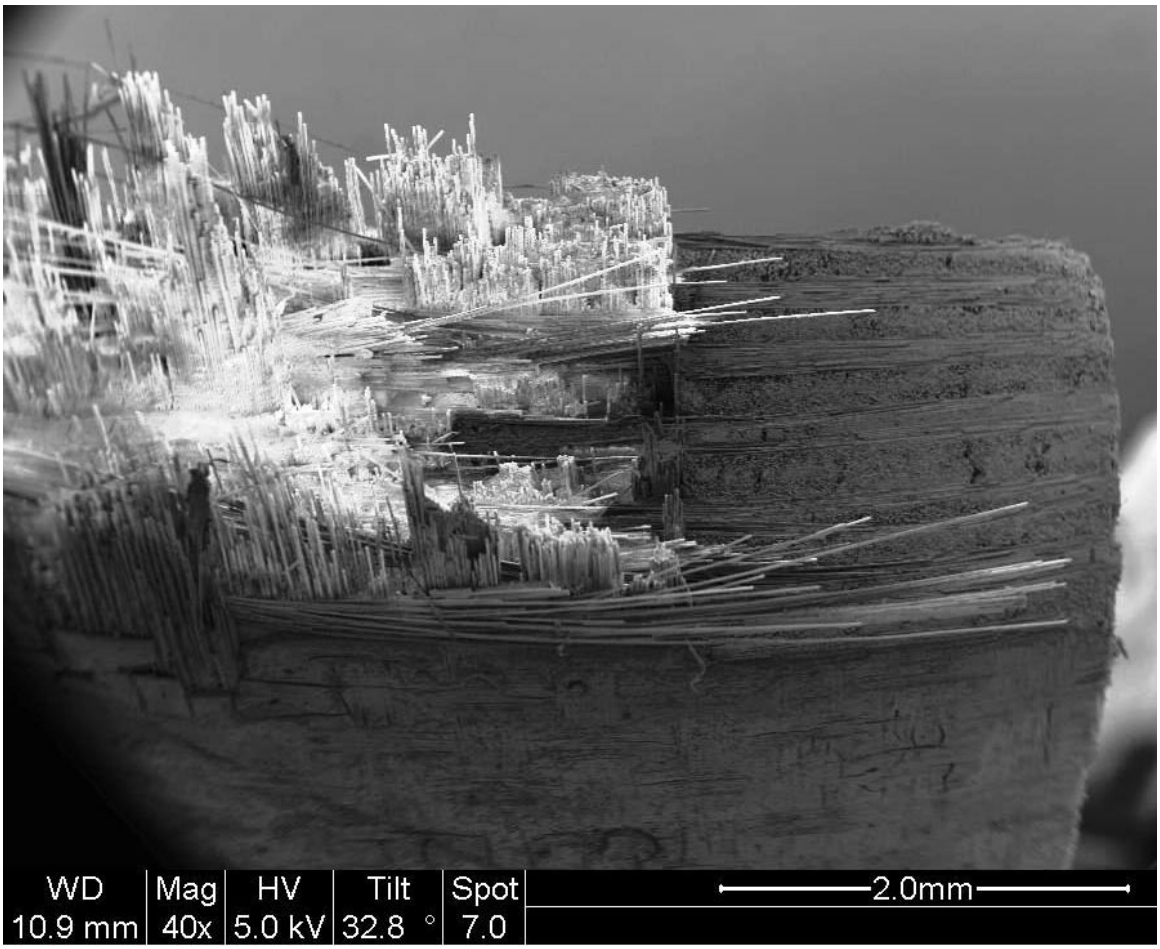


**Figure 56. 140 MPa Creep (right edge notch)**

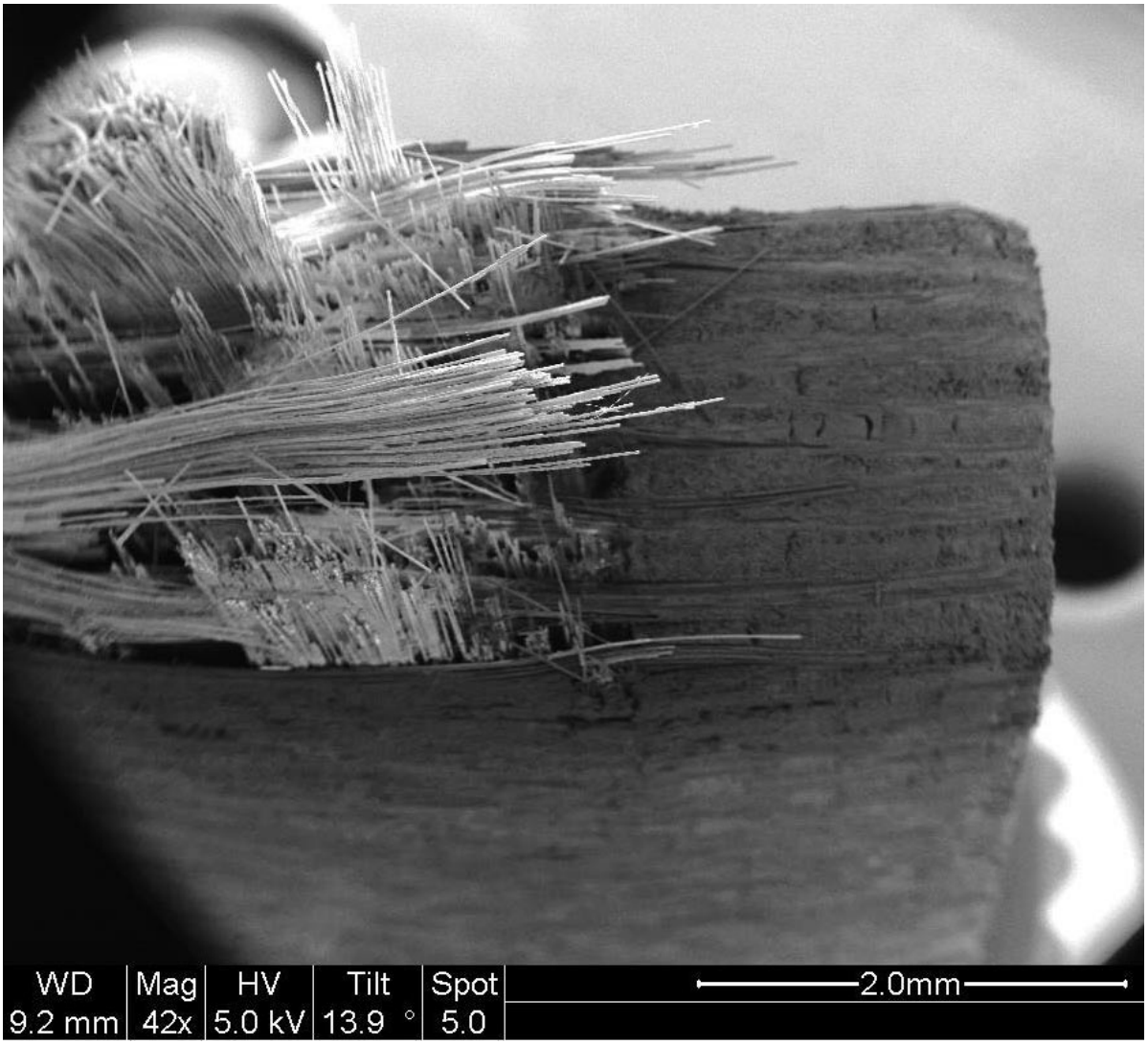


**Figure 57. 150 MPa Fatigue (right edge notch)**

Figure 57 shows the right edge notch of a fatigue specimen. Similar to the creep specimen in Figure 56, the crack propagation plane starts at the notch and the fiber pullout length increases moving from the notch to the center of the specimen.

Besides the notch acting as a starting point for fracture plane propagation, the inherent porosity and small cracks of the matrix act as crack growth facilitators. This behavior can lead to offset crack planes (i.e. non-planar crack growth) in high stress regions. Figure 58 highlights offset planes in both creep and fatigue loading.

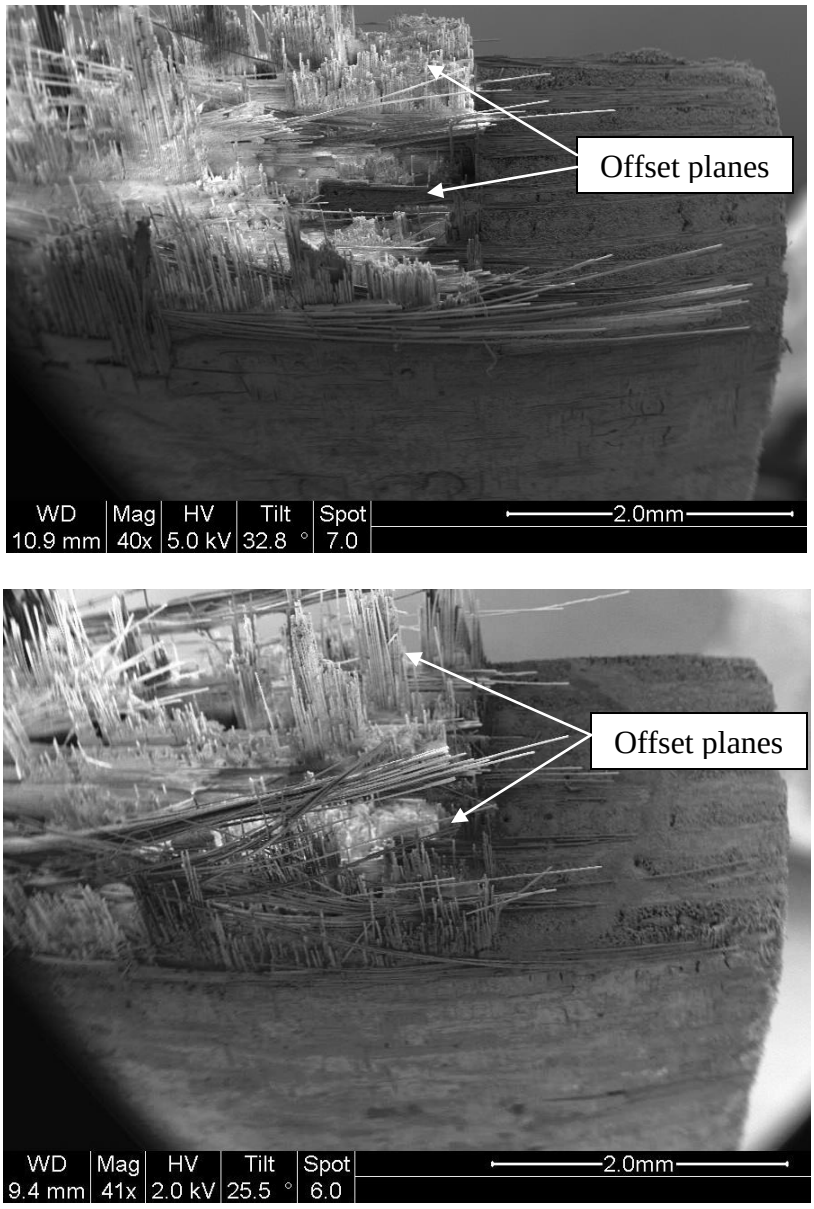


**Figure 58. Offset Crack Planes**

Top: 140 MPa Creep (right side),
Bottom: 155 MPa Fatigue (middle)

Stress dissipation was caused by the 0° fibers deflecting stress into the 90° fibers. This was facilitated by the matrix porosity and allowed for some crack bridging to occur. In areas where greater matrix cracking was observed, more individual fiber pullout was also observed. However, when the matrix remained tightly bonded, this prevented individual 0° fibers from pulling out singly but instead pulling out as bundles (see Figures 59 and 60). This pulled-out bundle then would fracture across the transverse plane. Level areas of planar fracture could also be seen in regions where the 0° fibers did not develop any microcracking (see Figure 61).

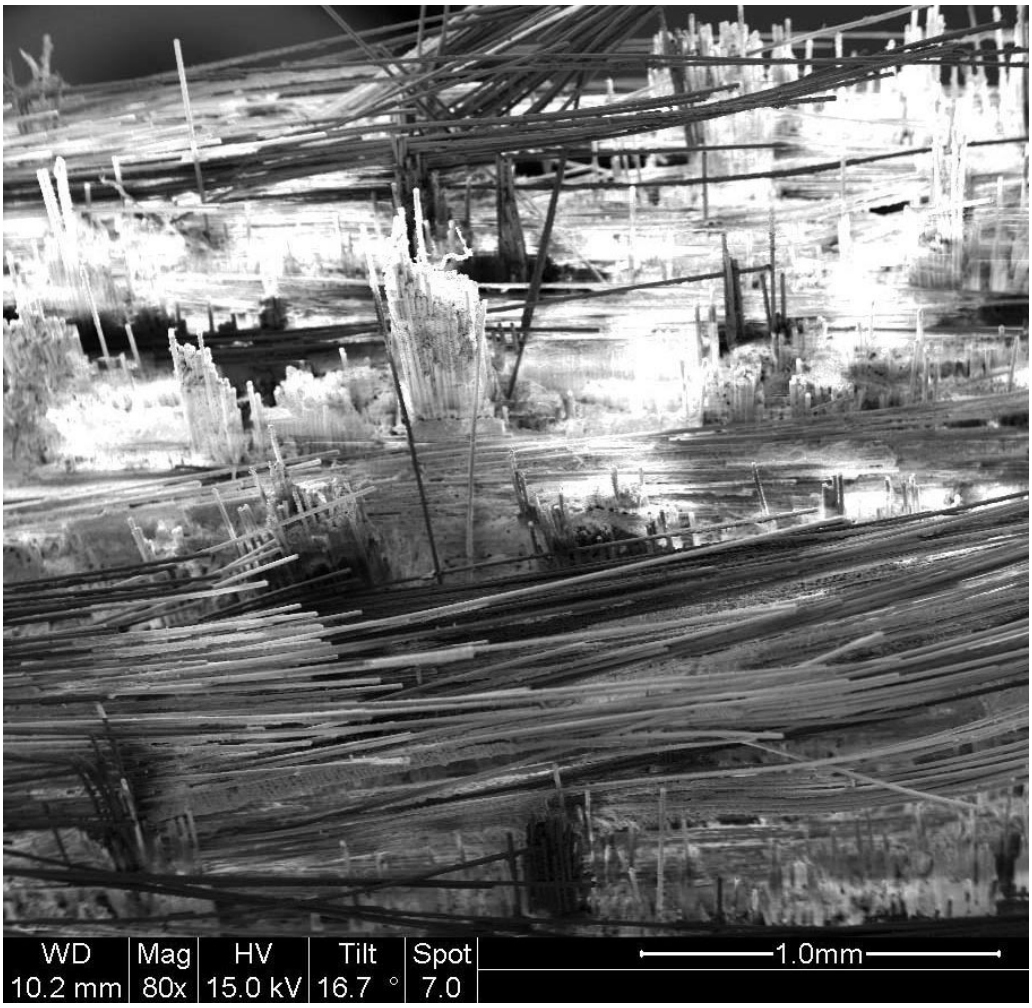


**Figure 59. Individual and Bundle Fiber Pullout, 175 MPa Creep (middle)**

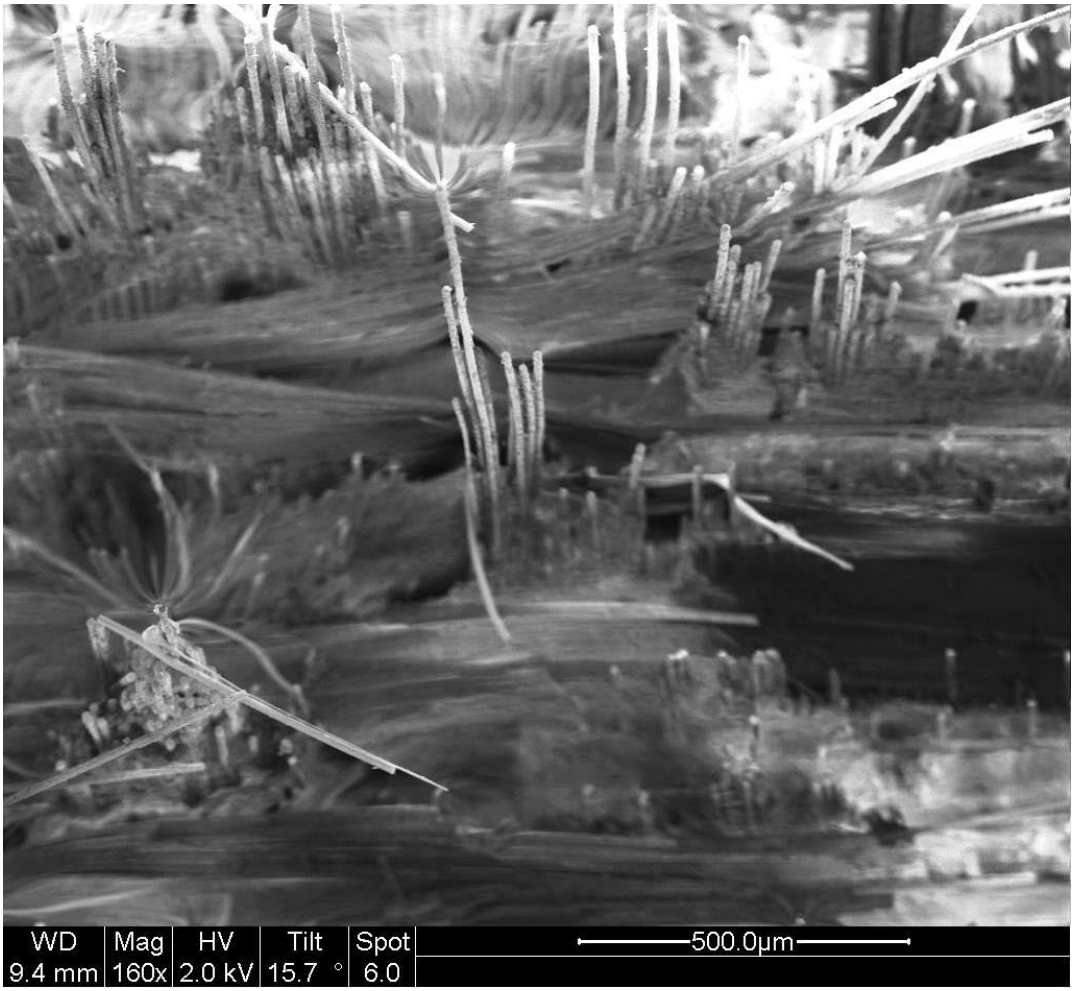


**Figure 60. Individual and Bundle Fiber Pullout, 155 MPa Fatigue (center)**

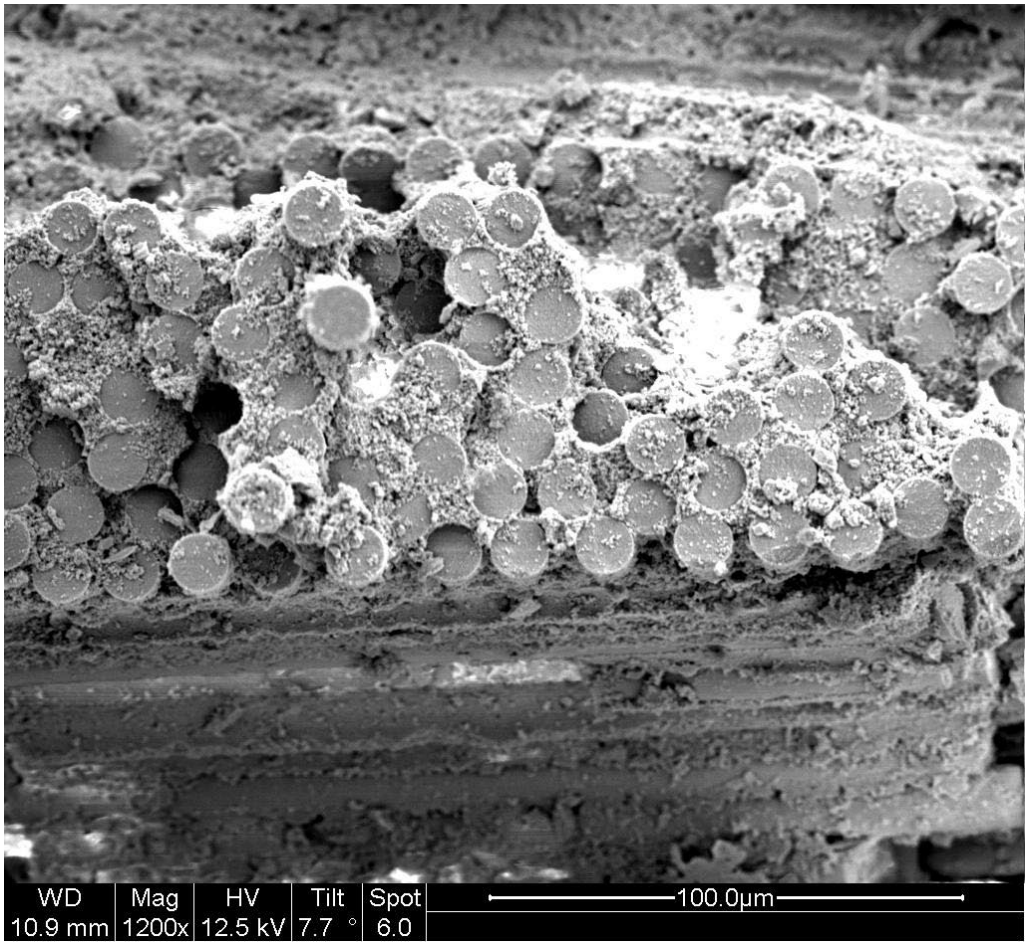


**Figure 61. Planar Fracture of 0° Fibers (120 MPa Creep)**

A comparison of similar creep and fatigue surfaces show little differentiation between the loading conditions and the visible failure. Figures 62-65 compare representative regions of creep and fatigue, namely, the notch region, fiber bundle, and individual fibers. Figure 62 shows a representative notch region for a creep or fatigue specimen.

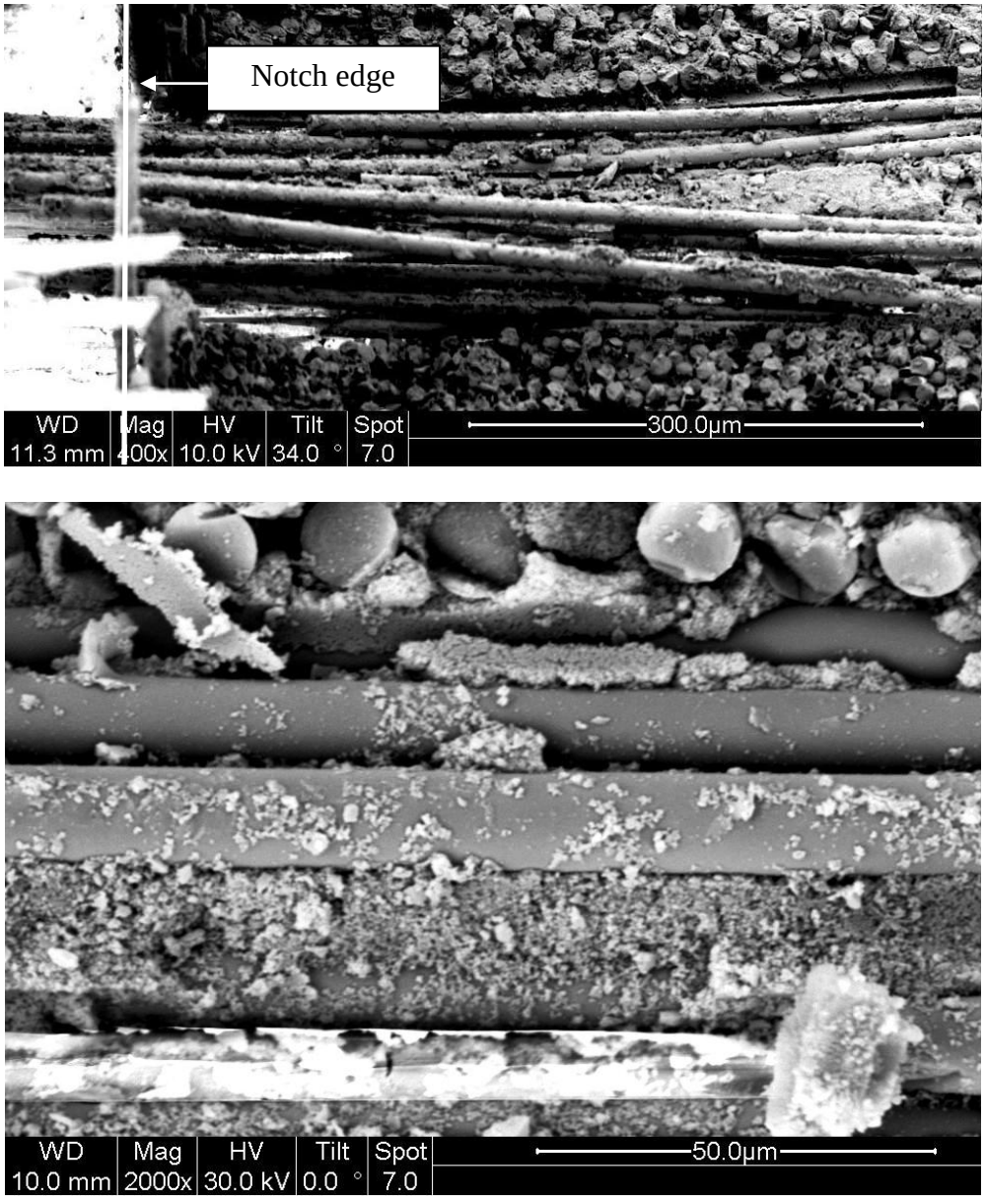


**Figure 62. Representative Notch Regions, Top (400x), Bottom (2000x)**

Figure 63 shows representative fiber bundles for creep and fatigue specimens. Again, there is little visible difference between creep and fatigue micrographs.

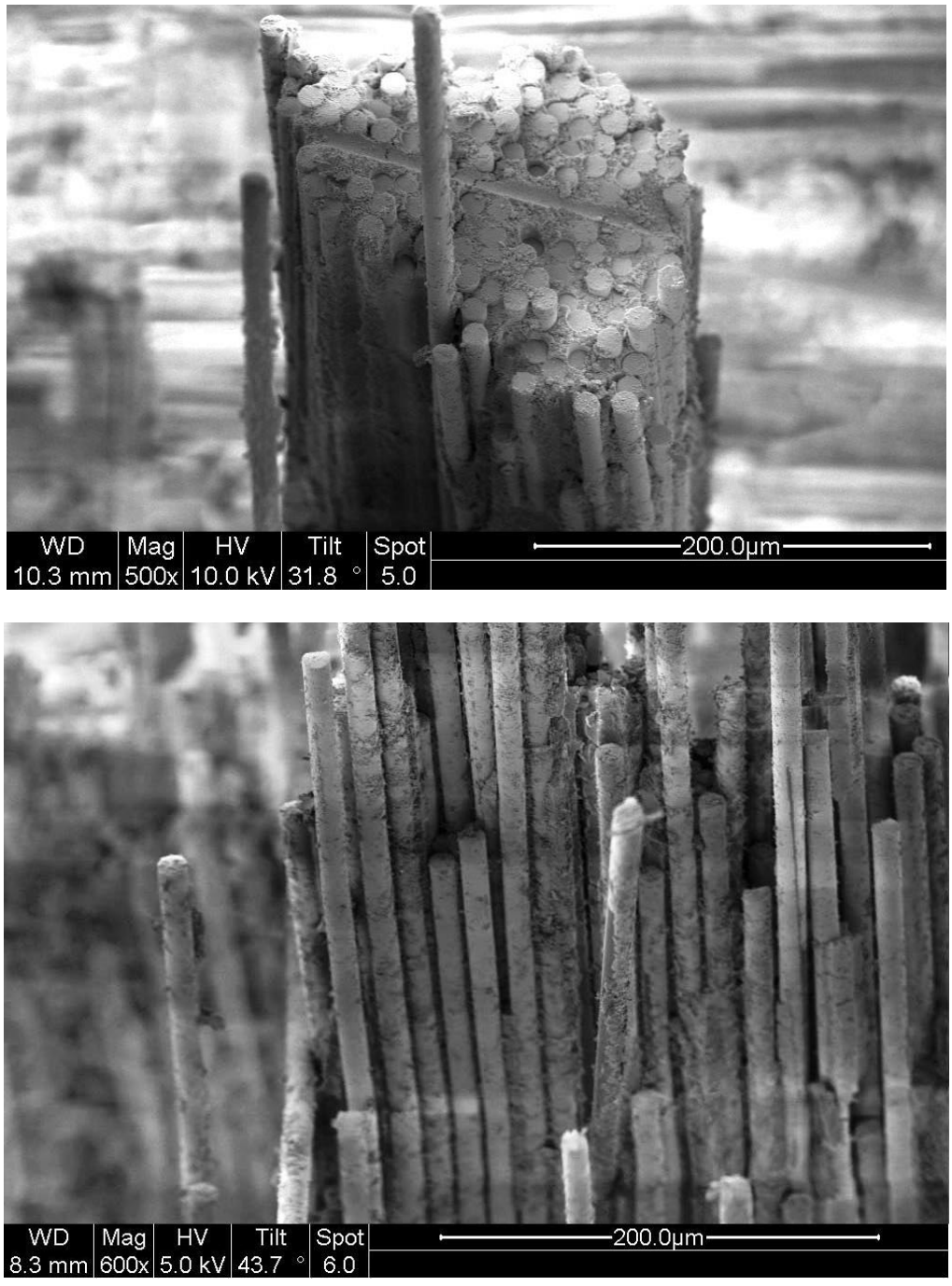


**Figure 63. 0° Bundles**

Top: 100 MPa Creep (center)
Bottom: 152.5 MPa Fatigue, (center)

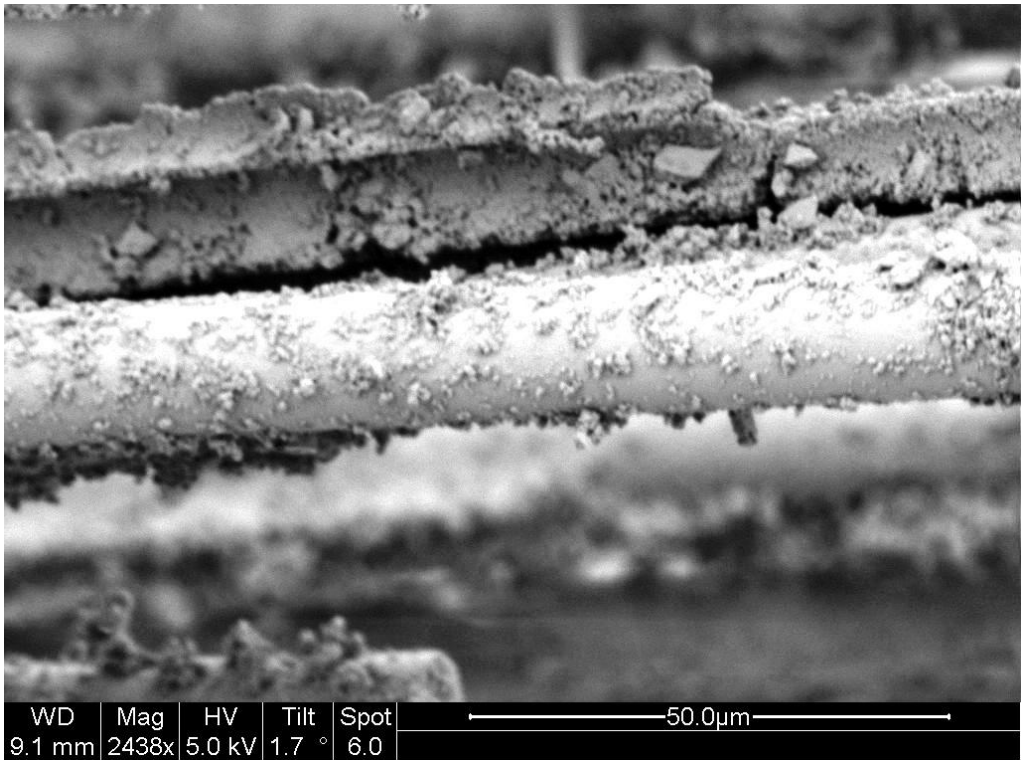


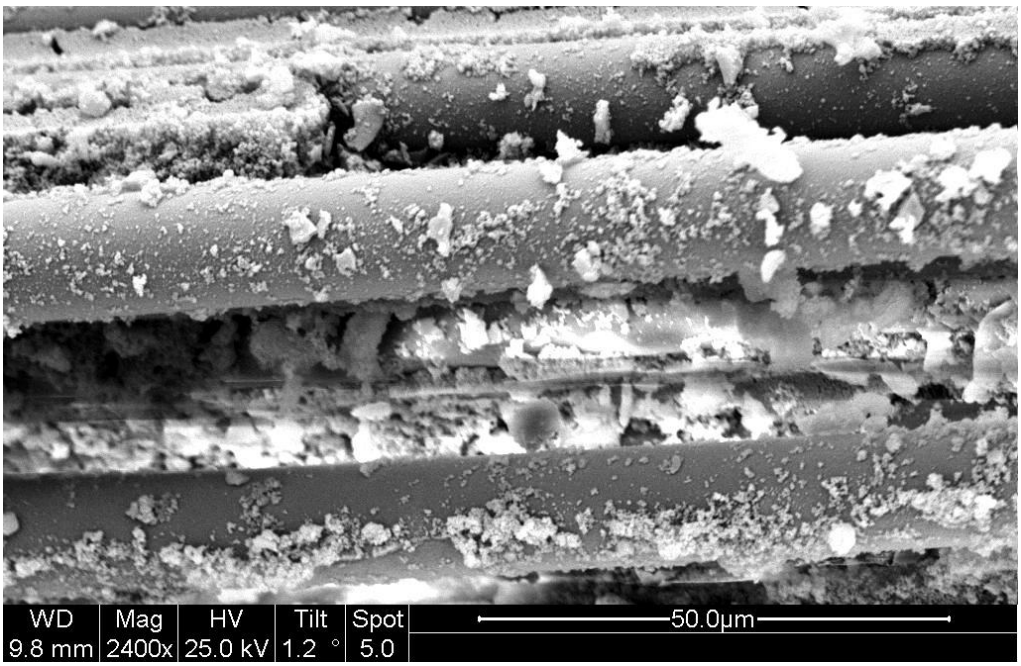


**Figure 64. 90° Fibers**

Top: 150 MPa Fatigue Fiber/Matrix (middle)
Bottom: 175 MPa Creep (middle)

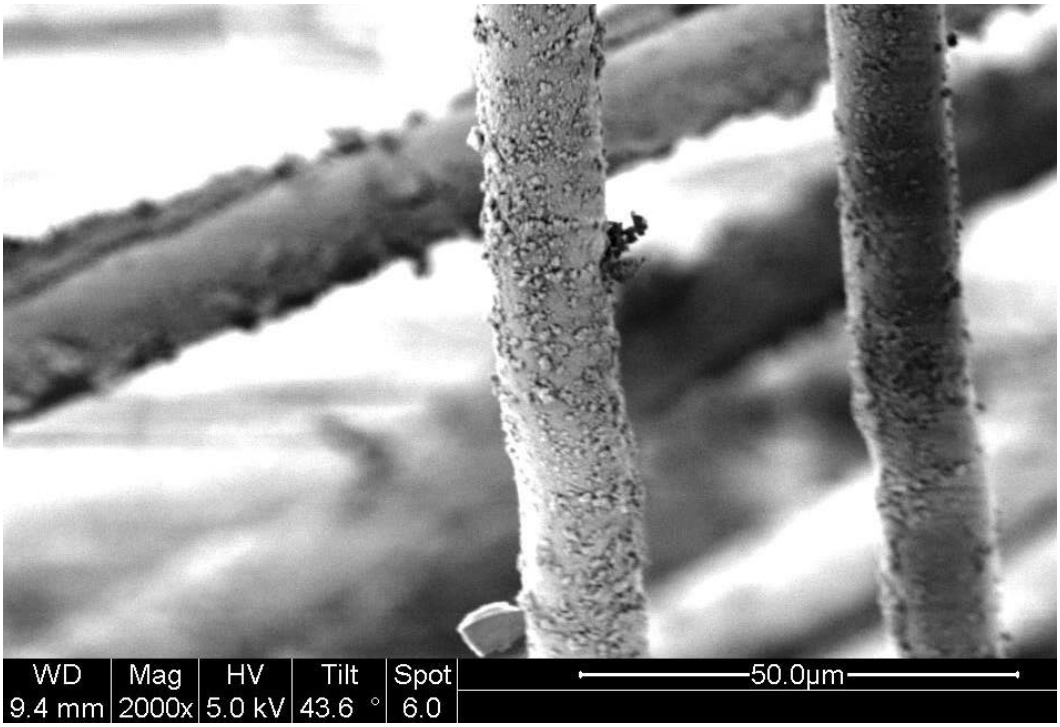


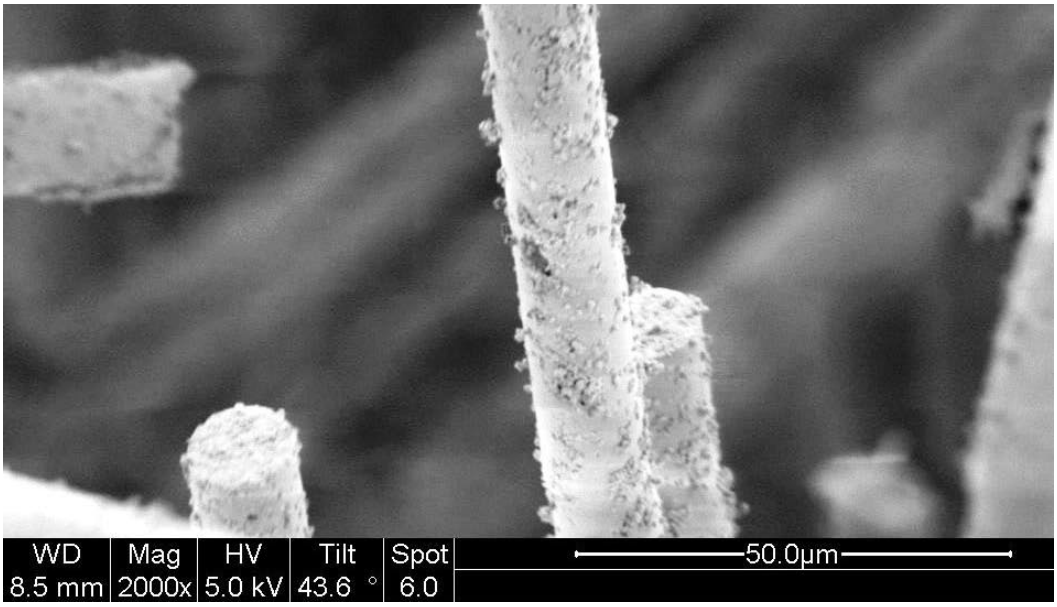


**Figure 65. 0° Individual Fibers**

Top: 110 MPa Creep (center)
Bottom: 152.5 MPa Fatigue (middle)

## 4.8 Summary

The double edge notch specimens showed notch sensitivities during all tests performed in this study. The 175 MPa creep test was essentially a monotonic test as rupture occurred within 1 second of reaching the desired load. If this is taken as a monotonic test, then UTS is reduced by 9% just by introducing the double edge notch geometry.

Creep data also suggests sensitivity to the double edge notch geometry. Creep life tests imply that specimens would need to be loaded at 10% less normalized creep load compared to unnotched specimens for similar creep life. Most double edge notch creep specimens displayed primary and secondary creep and two specimens also showed tertiary creep. The 175 MPa creep specimen only showed primary creep but it is likely that this is more representative of monotonic loading rather than creep loading as the specimen failed immediately. Creep rates of the double edge notch specimen are on the order of 2 to 6 times that of unnotched specimens. The only specimen which lasted the machine programmed 100 hour runout was the 80 MPa specimen (or 42% UTS). This specimen achieved monotonic tensile strength of 166 MPa or 86% of original UTS for retrained strength.

Fatigue data was also sensitive to the double edge notch geometry. The data in this study were in contrast to data presented by Eber who found good fatigue response of unnotched N720/A in 1200°C of air. The only sample which met the fatigue limit of 500,000 cycles was the 135 MPa specimen (70% UTS). Under monotonic testing, this specimen failed at 161 MPa or 84% of original UTS for retained strength. When net

section stress of fatigue specimens was plotted versus cycles, it was found that the double edge notch time to failure is very sensitive to stress. Specifically, the trend line slope for this graph is nearly flat, implying that a slight increases in stress leads to a disproportionately reduced fatigue life. Hysteresis data was examined for each fatigue specimen. The narrow and mostly linear behavior allowed the calculation of stiffness versus cycles. It was found that material stiffness was decreasing with progressing cycles. The damage mechanism involved both fatigue and creep when loaded under fatigue conditions.

A comparison of creep and fatigue loading versus specimen life was conducted. First, strain was plotted versus logarithmic time to failure. The 150 MPa fatigue specimen displayed a nearly identical strain rate as the 100 MPa creep specimen; however, the creep specimen lasted longer. Conversely, the 135 MPa fatigue and 80 MPa creep specimens showed nearly identical strain rates but this time the creep specimen had a longer life. Next, a plot was made of mean net section stress versus time to failure. In all cases, the fatigue net section stress was lower than that of creep. This suggests that there is another damage agent present in the fatigue specimens besides creep.

One dilemma that occurred during the data collection of all tests was the unusually high failure strains achieved. After conducting a test on an aluminum alloy dog bone specimen, the MTS machine and extensometer was verified as working correctly. The author's opinion is that the high failure strains are due to the notch opening more than than actual strains of failed material. This is likely due to the fact that the extensometer

measures the extension on the same edge where the notch is located. Therefore, any notch opening would give an exaggerated reading by the extensometer.

Microstructural analysis showed the creep and fatigue specimens to be indistinguishable. In all specimens, the fracture occurred along the notch plane. In the high stress area at the notch tip, there was shorter fiber pullout indicating the 0° fibers failed near their monotonic limit. However, the drop in stress away from the notch tip allowed more matrix cracking vice fiber fracture. This facilitated fiber pullout which was evidenced primarily in the center of the specimens. When matrix cracking was not present, the fibers either failed in a level plane or whole bundles of fibers were pulled out and then fractured. By introducing double notch geometry to the N720/A specimen, monotonic UTS strength was reduced by 9%.

## V. Conclusions and Recommendations

The presence of double edge notches with notch ratio (2a/w) of .33 has substantial effects on the N720/A CMC at 1200°C air. Creep stress must be reduced by 10% of unnotched UTS and fatigue stress must be reduced by >15% of unnotched in order to achieve the same material life. The fatigue specimens are particularly sensitive to mean stress under fatigue loading. The samples in this test were tension-tension loaded under a sinusoidal regime where the stress ratio, $\frac{\sigma_{\min}}{\sigma_{\max}}$, was only 5%. If the stress ratio and thereby the mean stress were higher, fatigue life could be greatly reduced. Mean net section stress for this data suggests that samples need to be at <40% UTS before fatigue life will increase with decreasing loads.

Micrograph pictures conformed to previous research. Specifically, creep and fatigue specimens were largely indistinguishable from on another. Fiber pullout was a dominant feature of all specimens.

Possible areas for future research include notch performance with variable fiber orientation or variable notch ratios (2a/w). Additionally, the author would suggest using mini strain gauges both near the notch apex as well as the specimen center to obtain the most accurate strain measurements possible

## Appendix: Additional SEM Micrographs

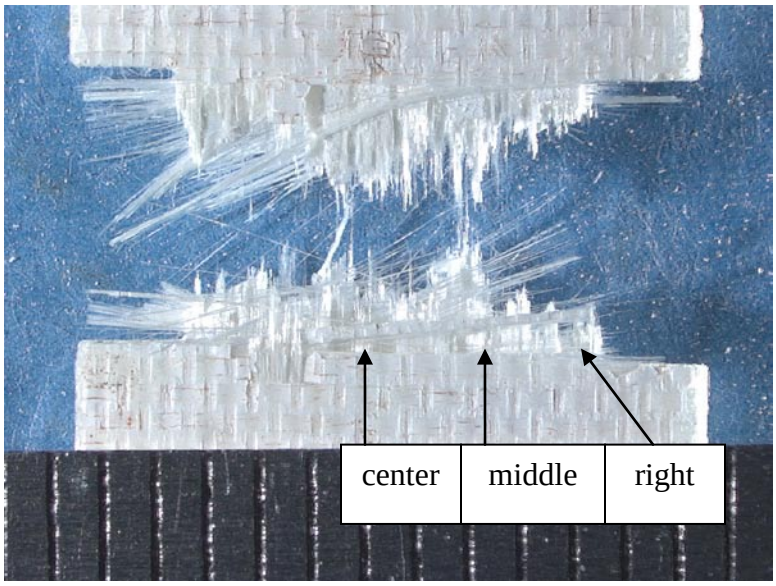


**Figure 66. Center, Middle and Right Regions Explored under SEM**

Note that Figure 61 highlights the regions of focus under the SEM – *center*, *middle* and *right*. These will be referred to in the following micrographs.

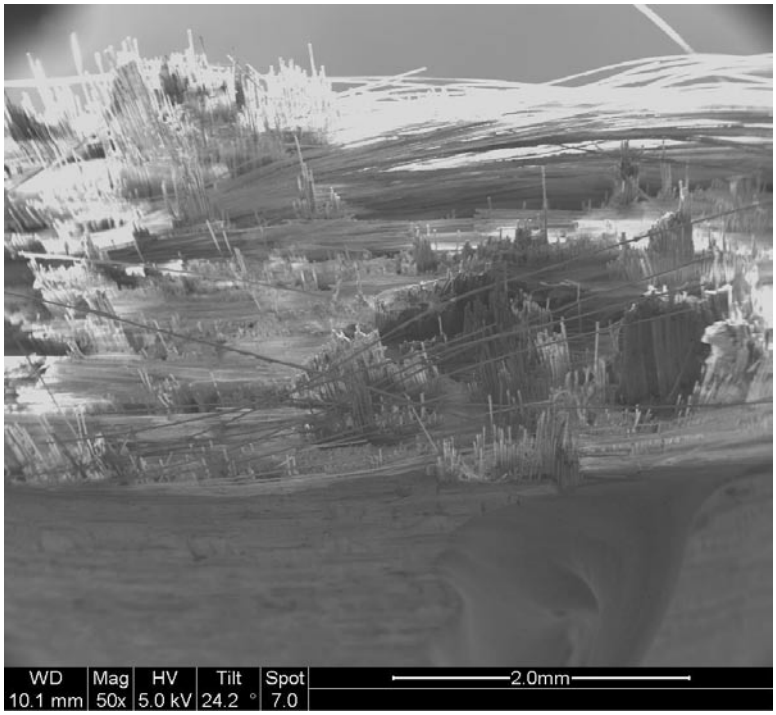


**Figure 67. 80 MPa Creep (center)**

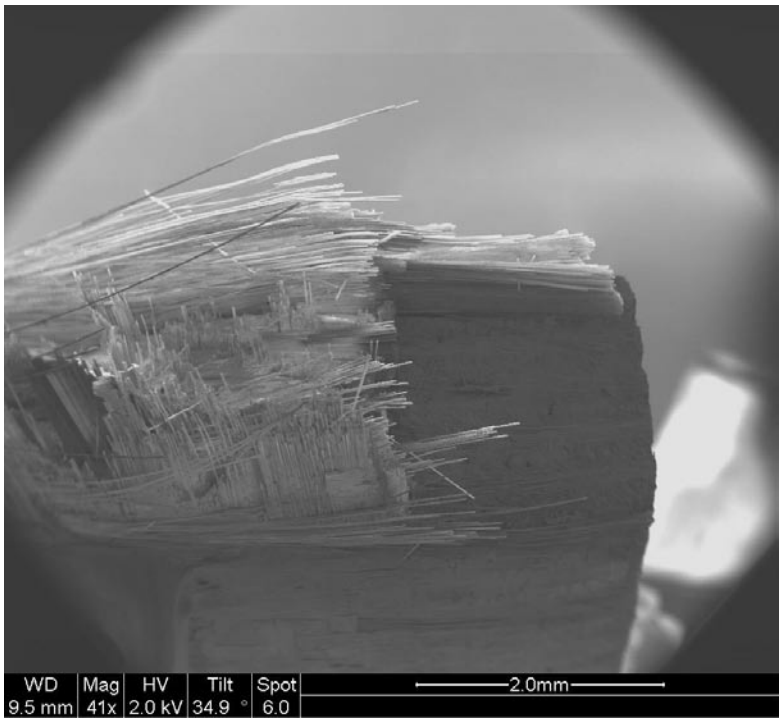


**Figure 68. 80 MPa Creep (right notch)**

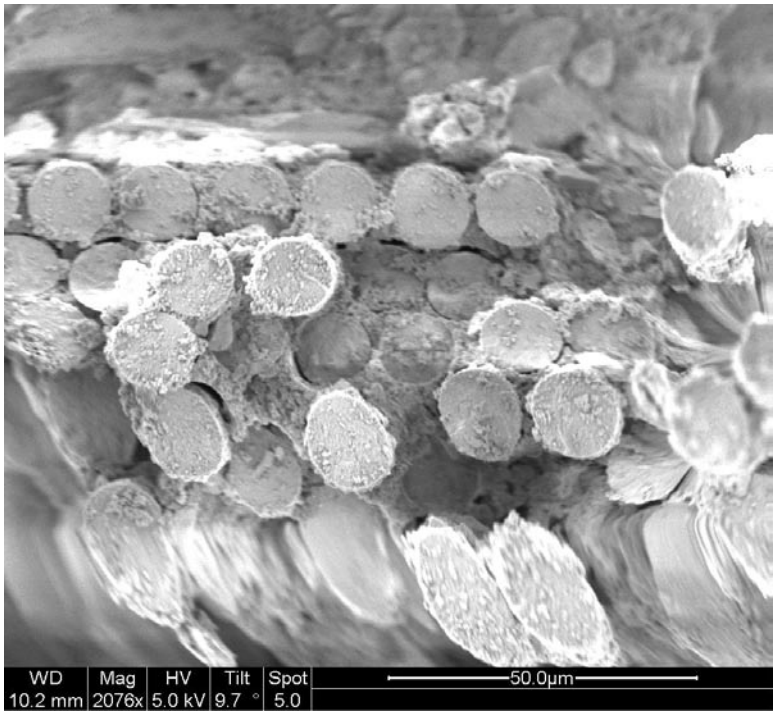


**Figure 69. 100 MPa Creep (center)**

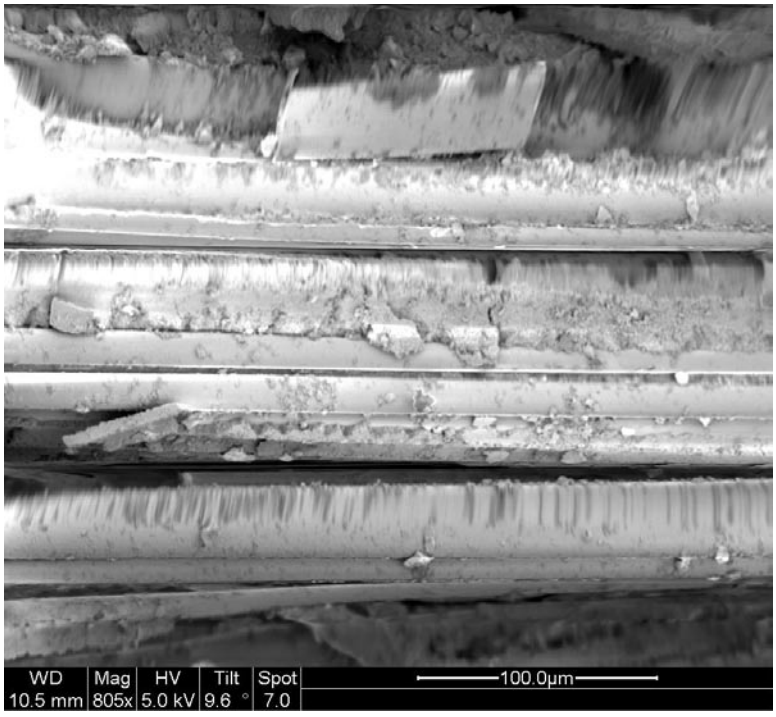


**Figure 70. 100 MPa Creep (right)**


**Figure 71. 100 MPa Creep (center)**

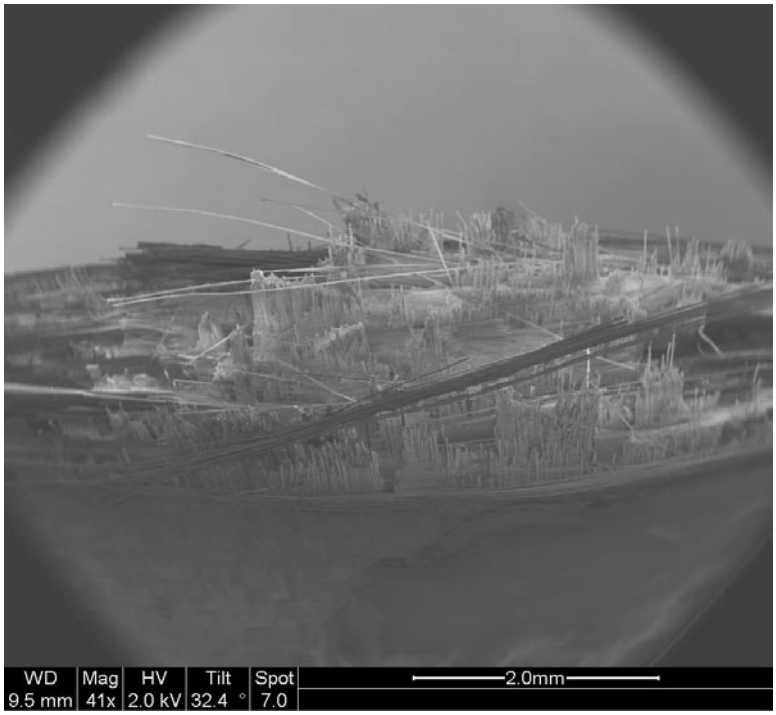


**Figure 72. 110 MPa Creep (center)**

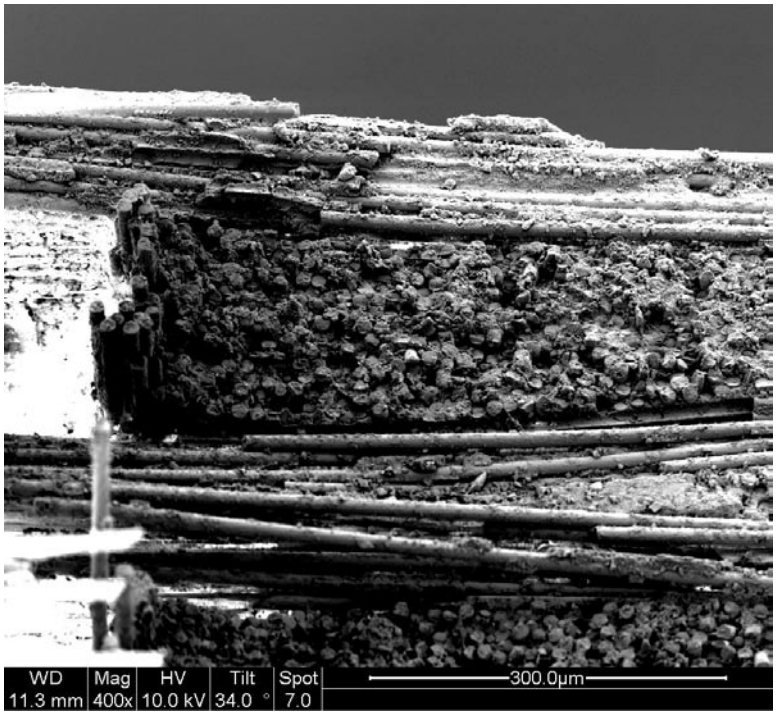


**Figure 73. 110 MPa Creep (right notch)**


**Figure 74. 110 MPa Creep (right side)**


**Figure 75. 120 MPa Creep (center)**

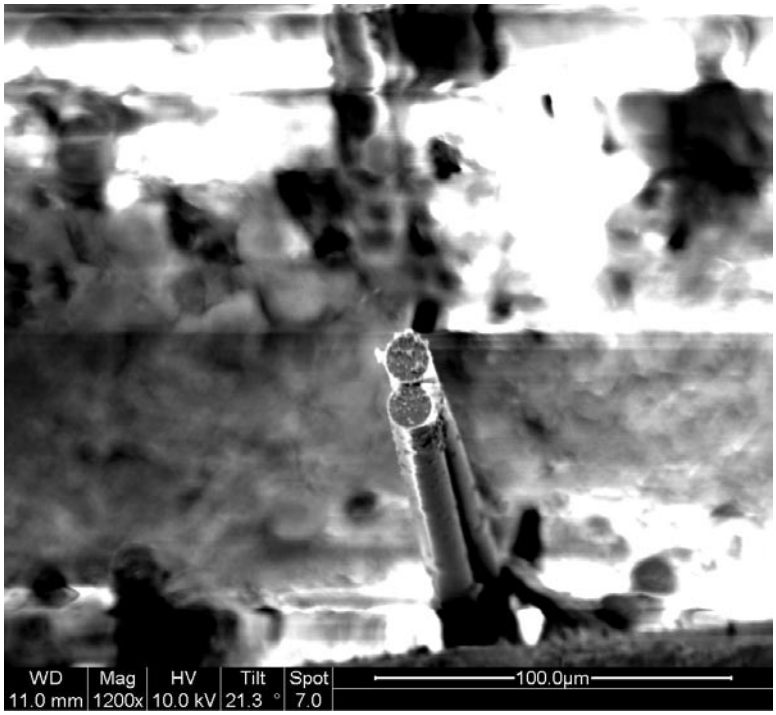


**Figure 76. 120 MPa Creep (center)**

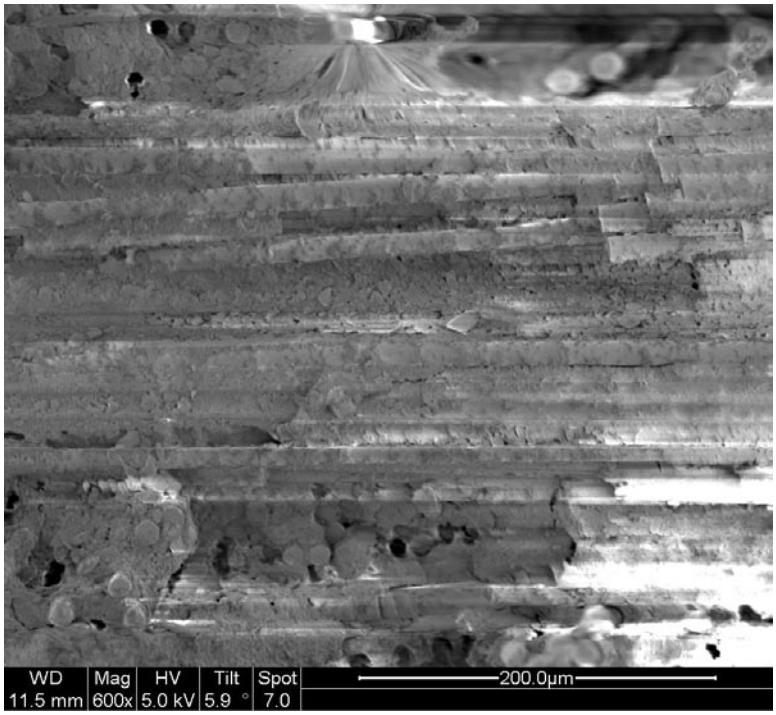


**Figure 77. 120 MPa Creep (right middle)**


**Figure 78. 120 MPa Creep (right)**

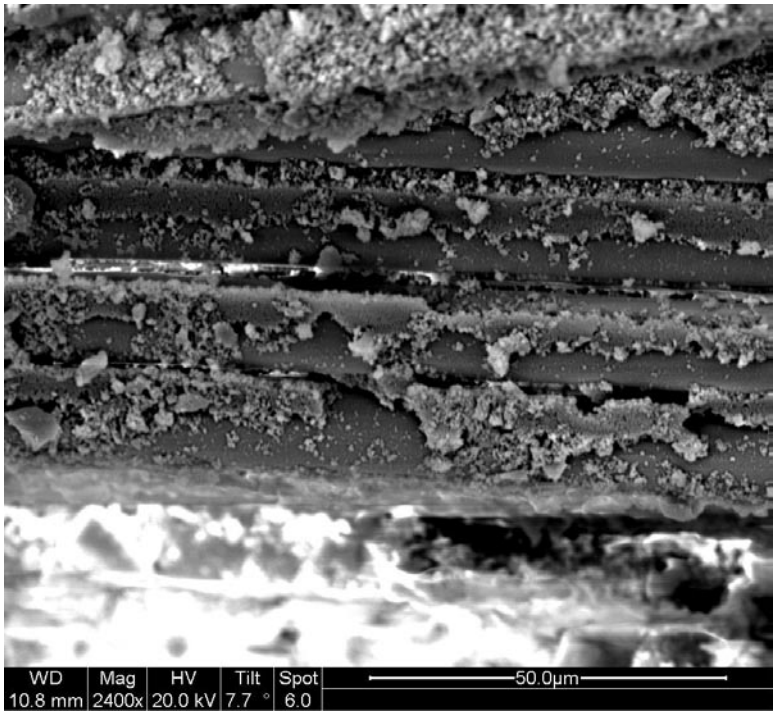


**Figure 79. 120 MPa Creep (right)**

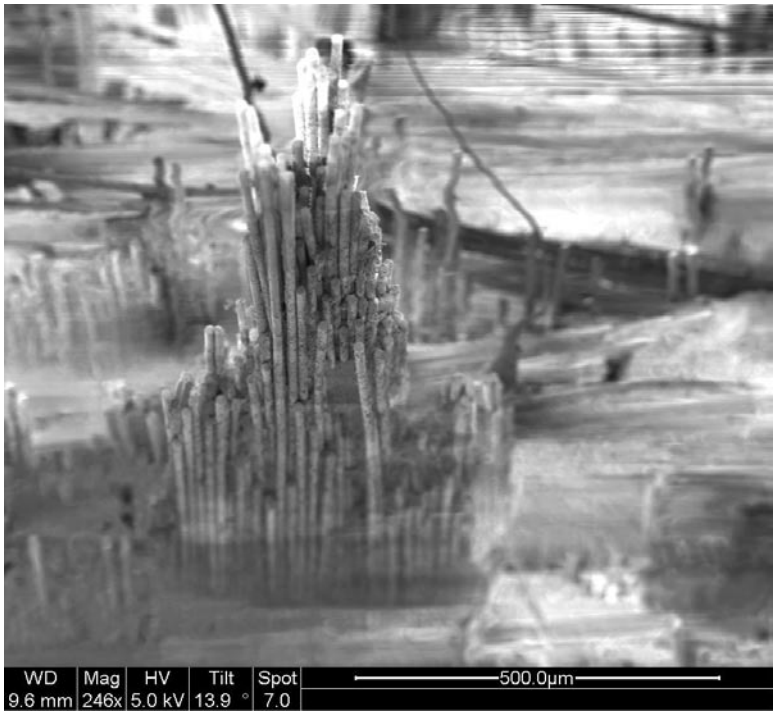


**Figure 80. 140 MPa Creep (center)**

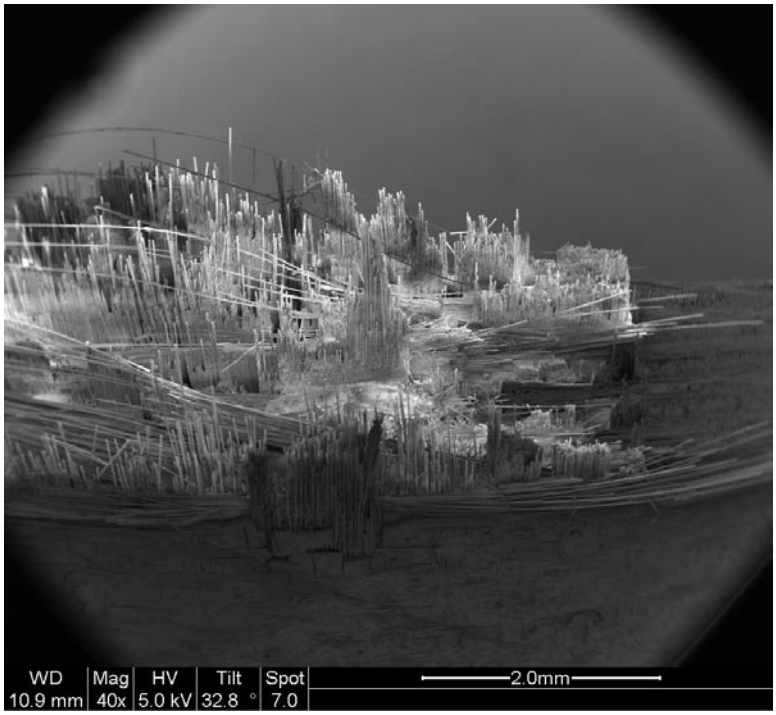


**Figure 81. 140 MPa Creep (middle)**

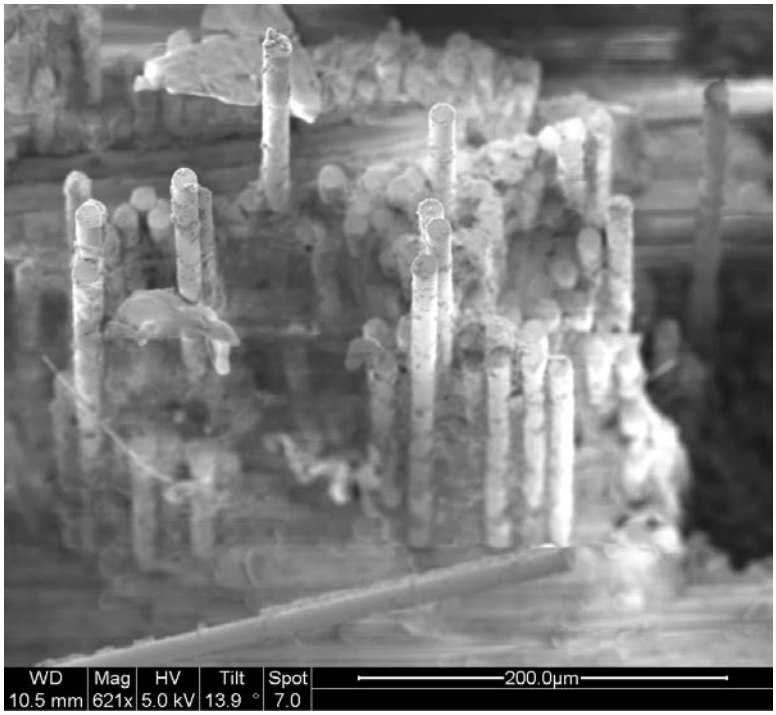


**Figure 82. 140 MPa Creep (middle)**

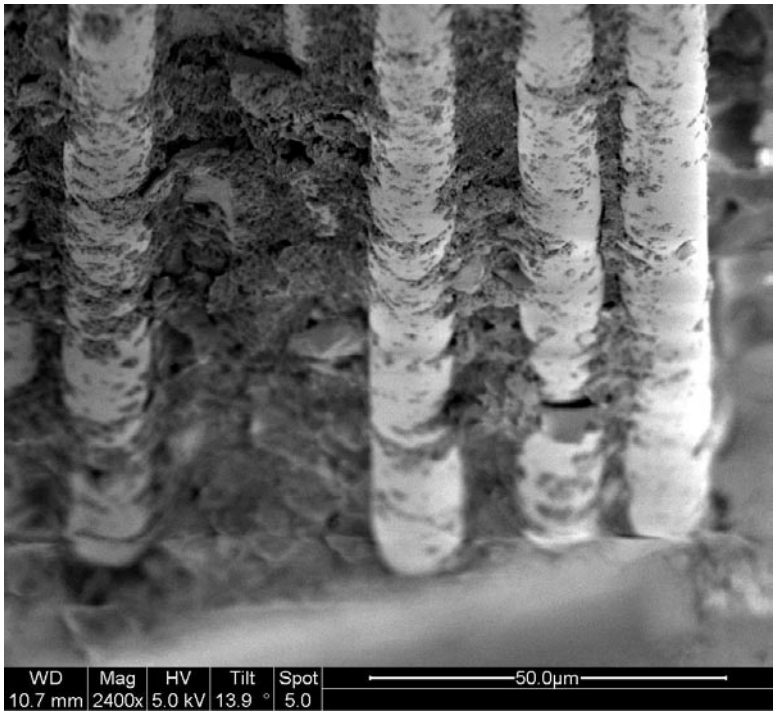


**Figure 83. 140 MPa Creep (right)**

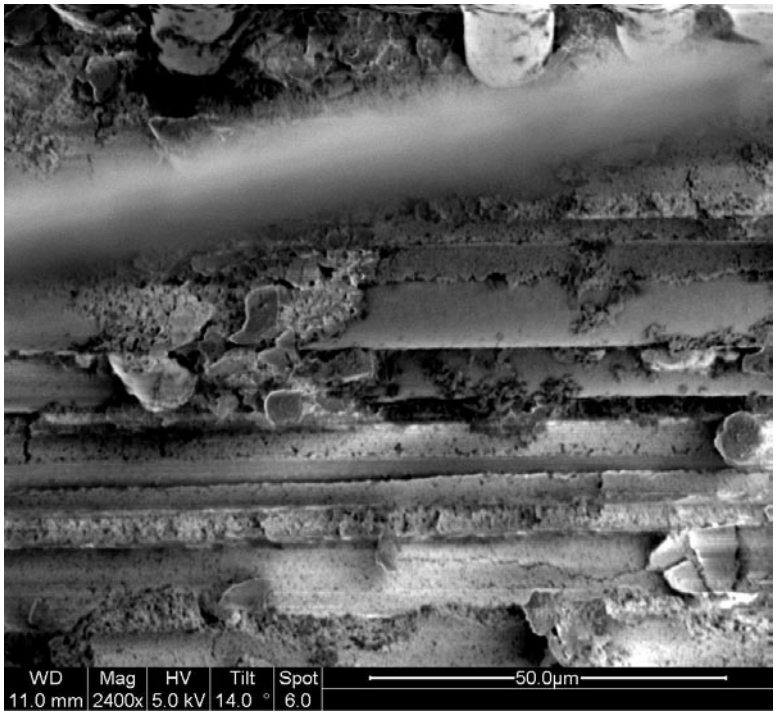


**Figure 84. 140 MPa Creep (right)**

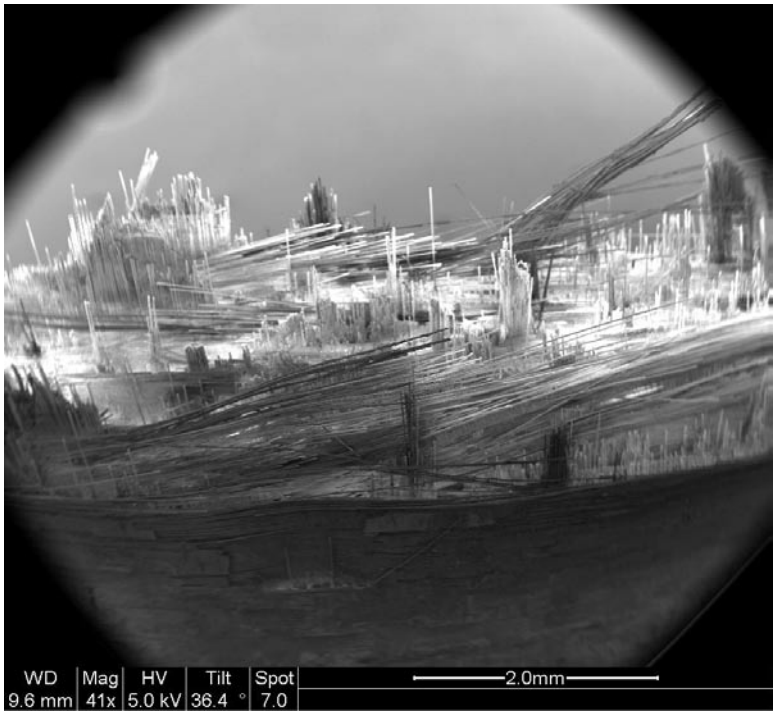


**Figure 85. 175 MPa Creep (center)**

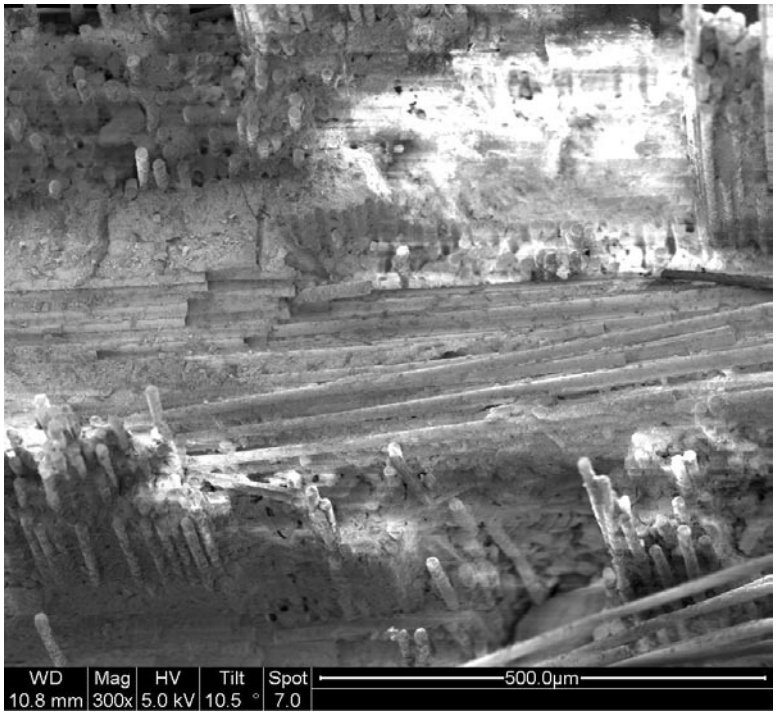


**Figure 86. 175 MPa Creep (center)**

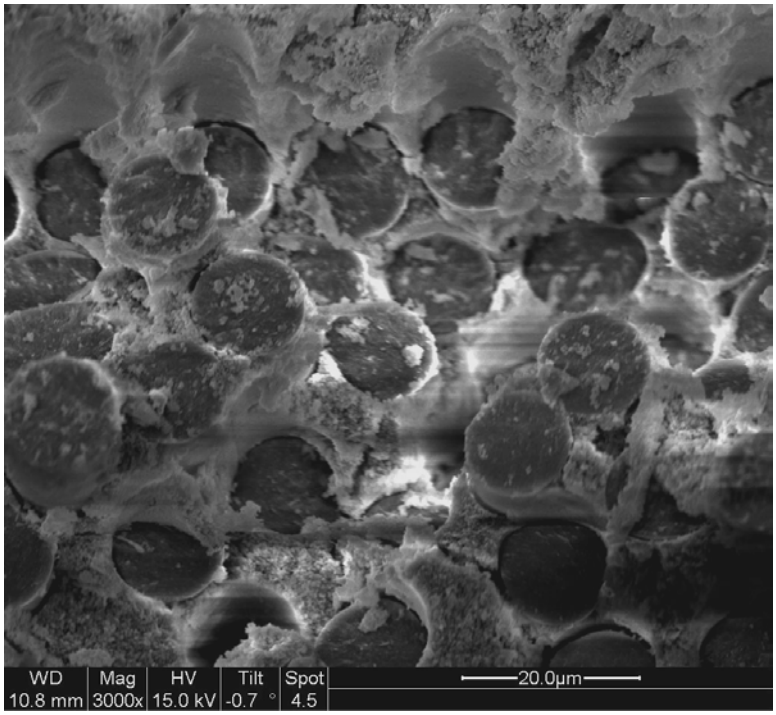


**Figure 87. 175 MPa Creep (center)**

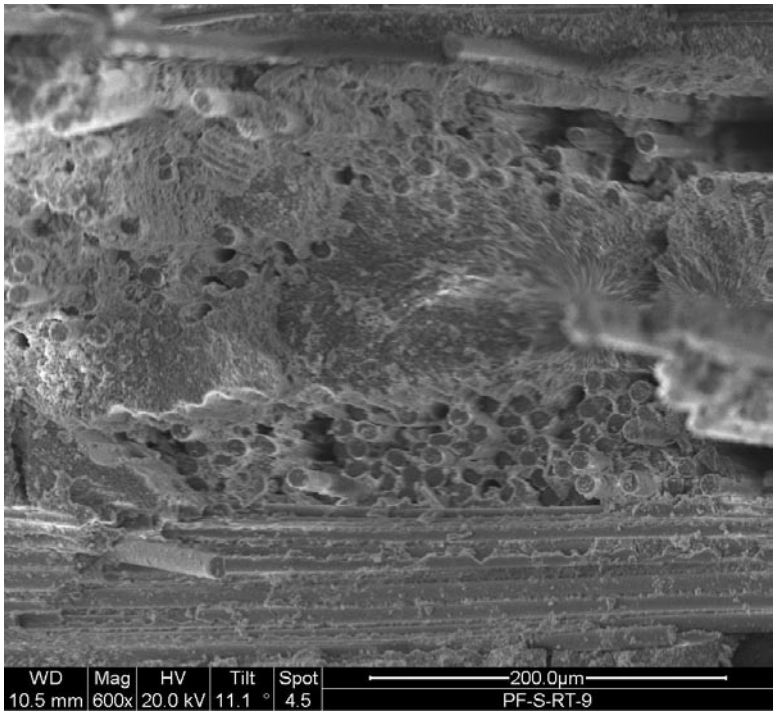


**Figure 88. 175 MPa Creep (middle)**

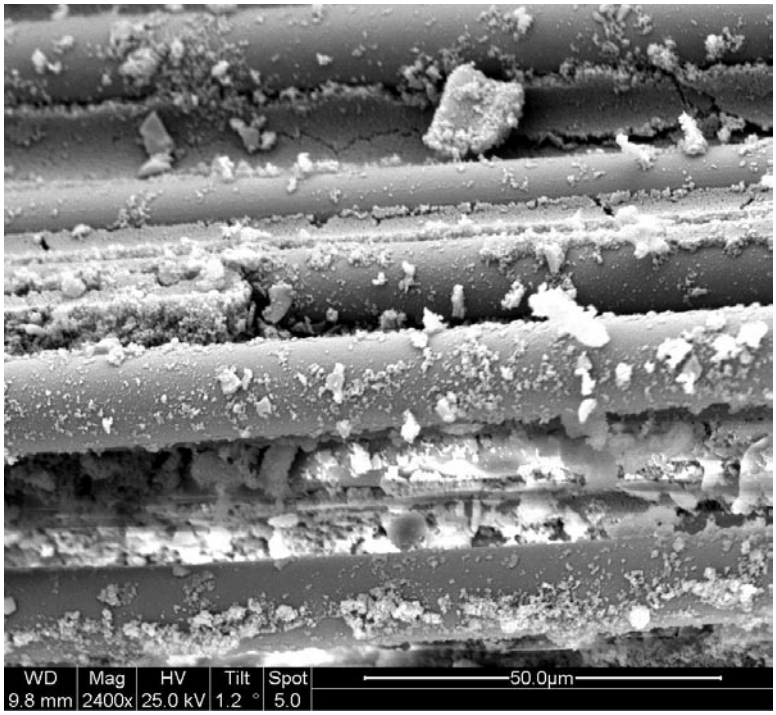


**Figure 89. 175 MPa Creep (middle)**

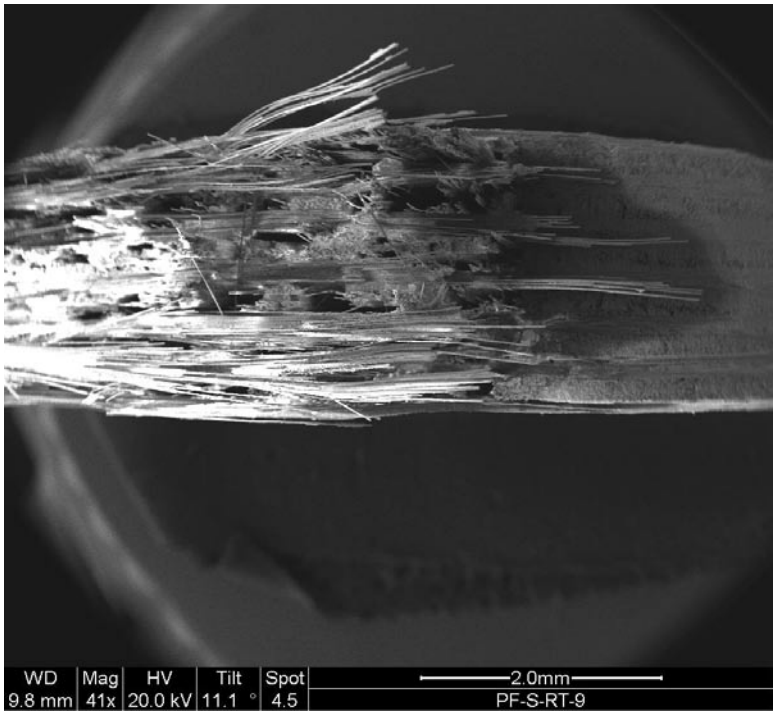


**Figure 90. 175 MPa Creep (right)**

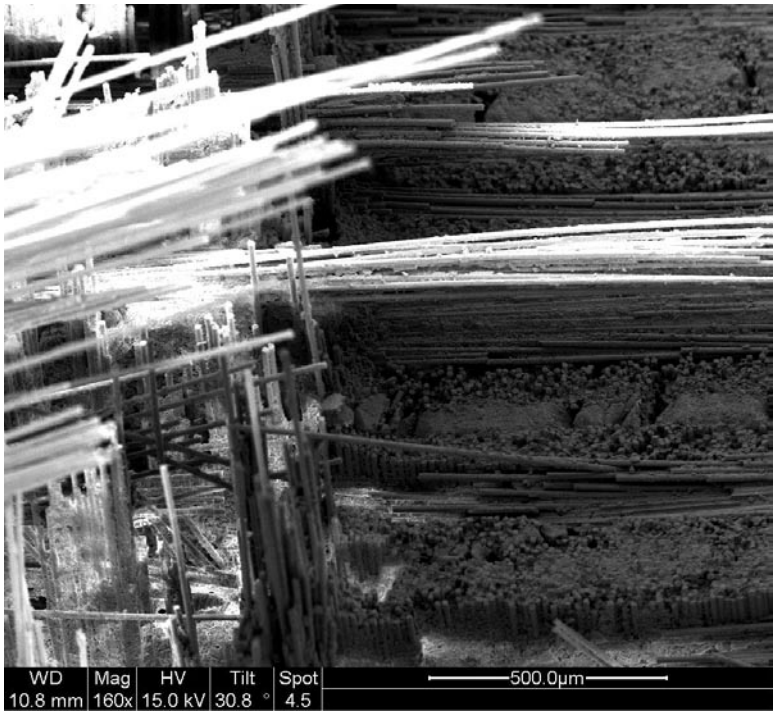


**Figure 91. 175 MPa Creep (right)**

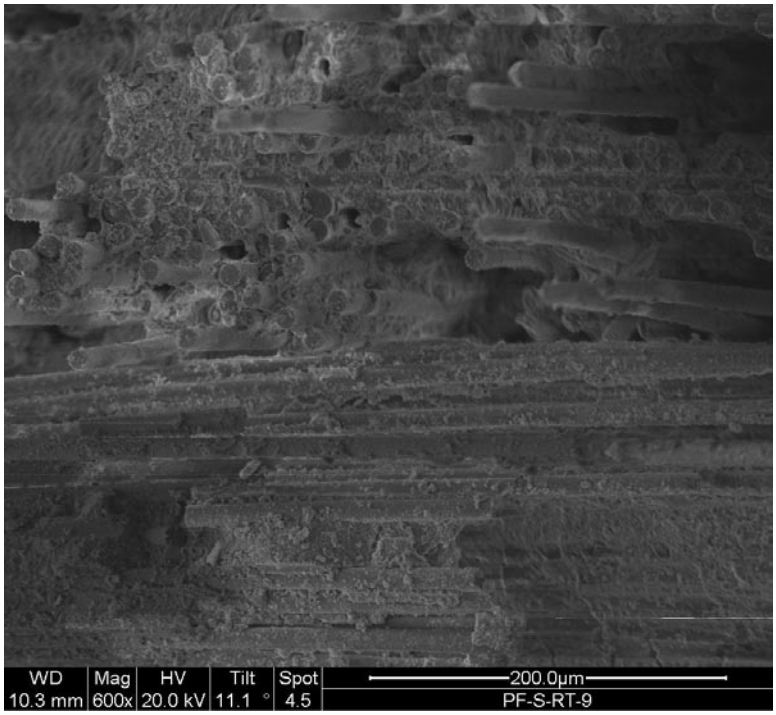


**Figure 92. 175 MPa Creep (right)**

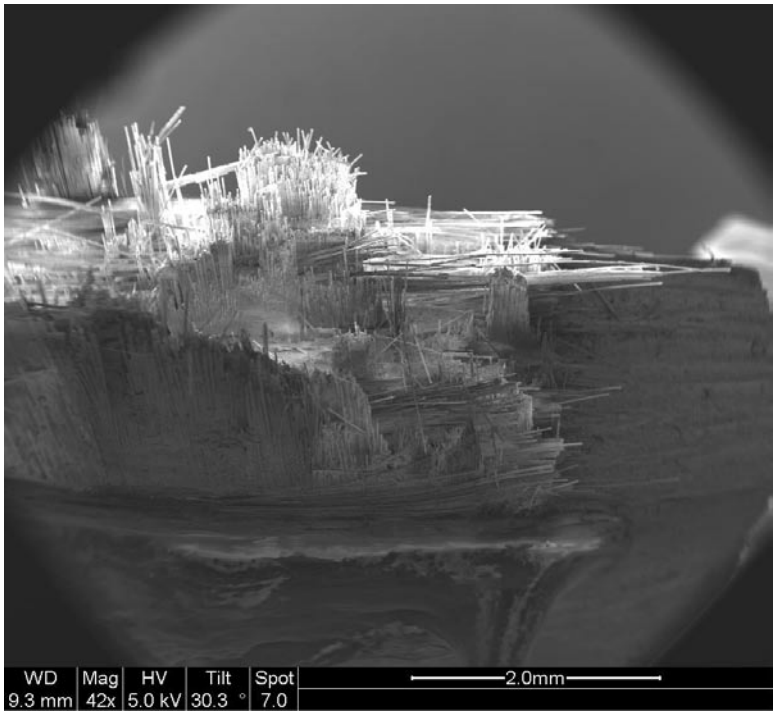


**Figure 93. 135 MPa Fatigue (middle)**

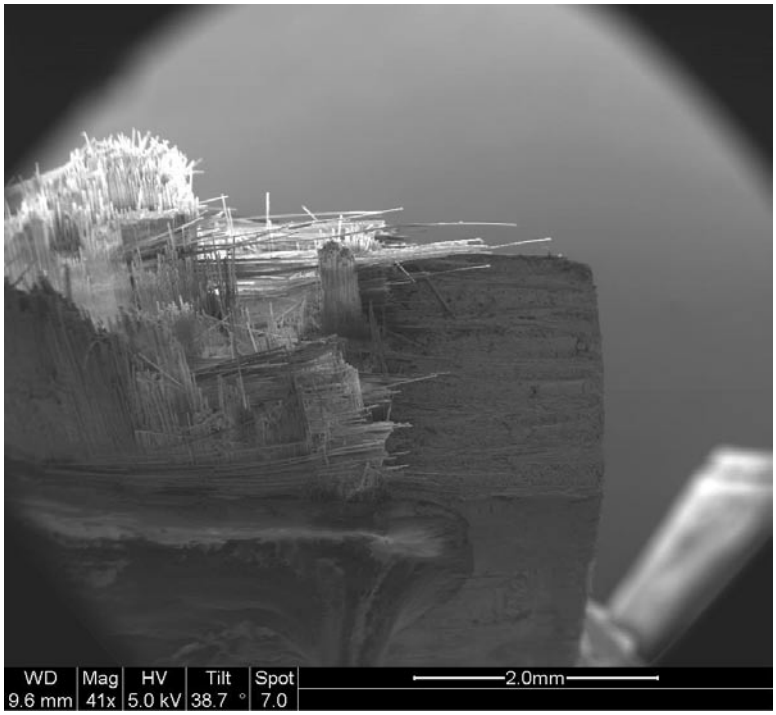


**Figure 94. 135 MPa Fatigue (right)**

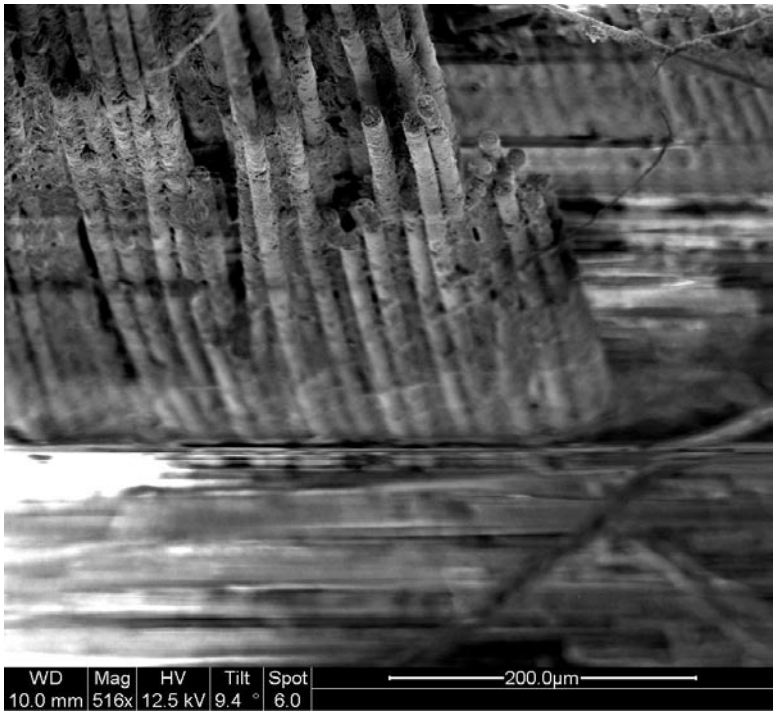


**Figure 95. 150 MPa Fatigue (middle)**

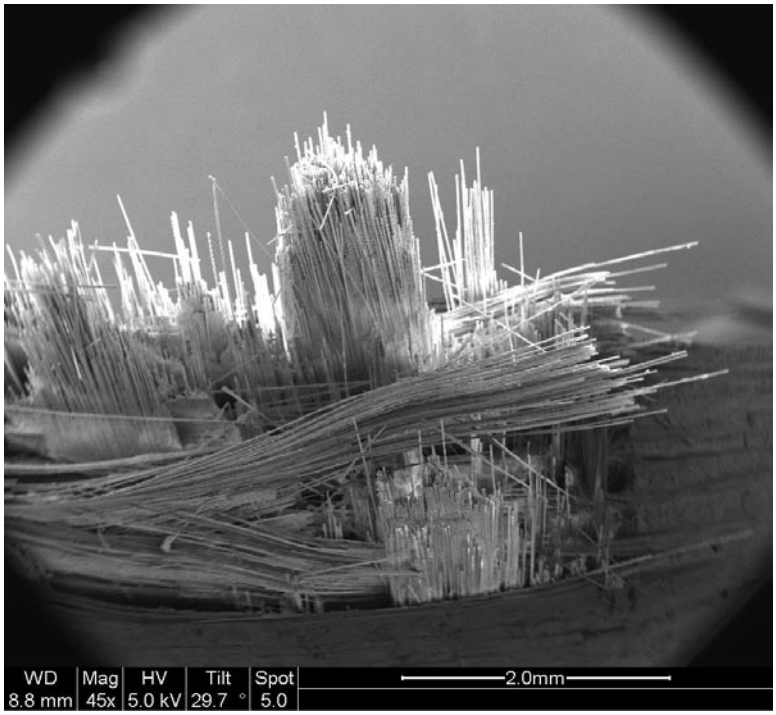


**Figure 96. 150 MPa Fatigue (middle)**

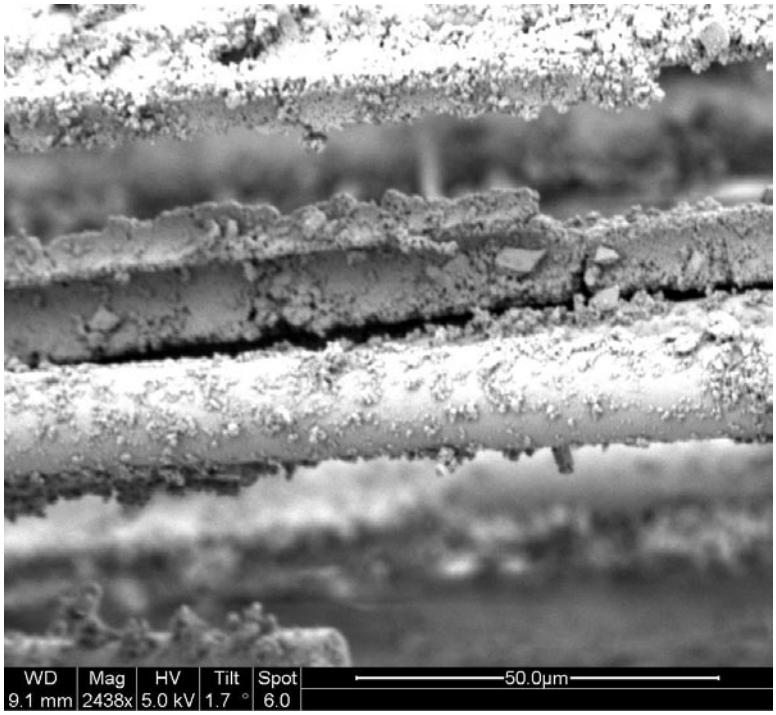


**Figure 97. 150 MPa Fatigue (middle)**

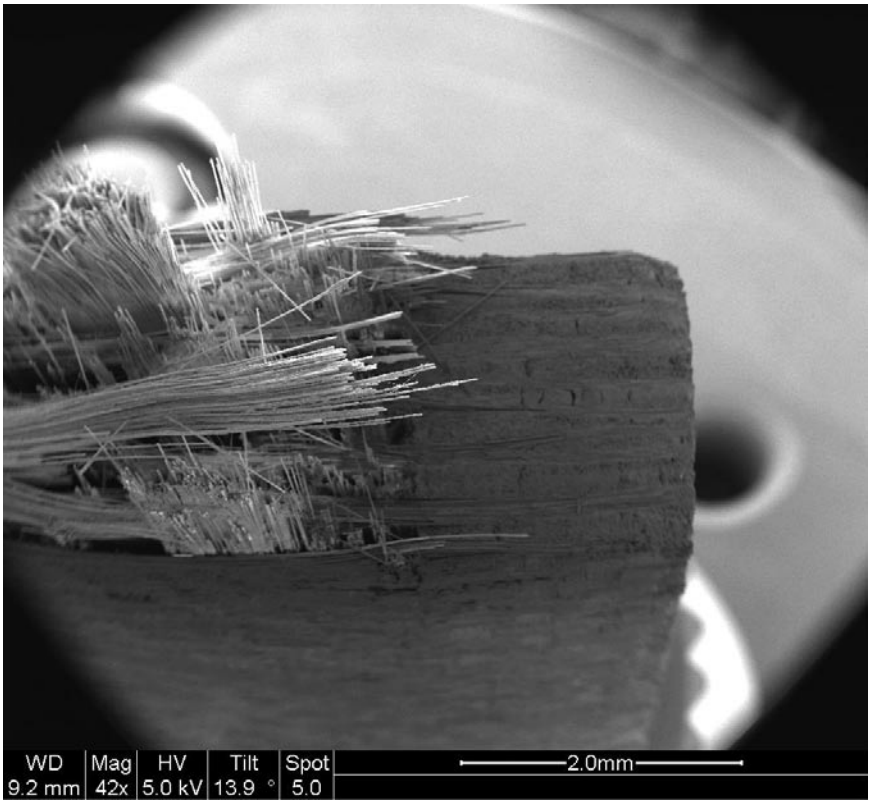


**Figure 98. 150 MPa Fatigue (right)**

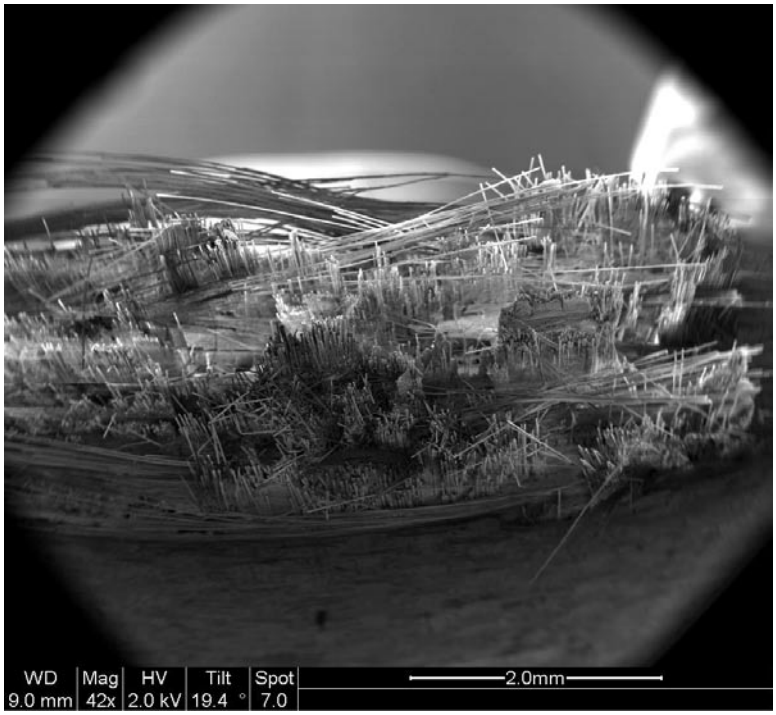


**Figure 99. 152.5 MPa Fatigue (center)**

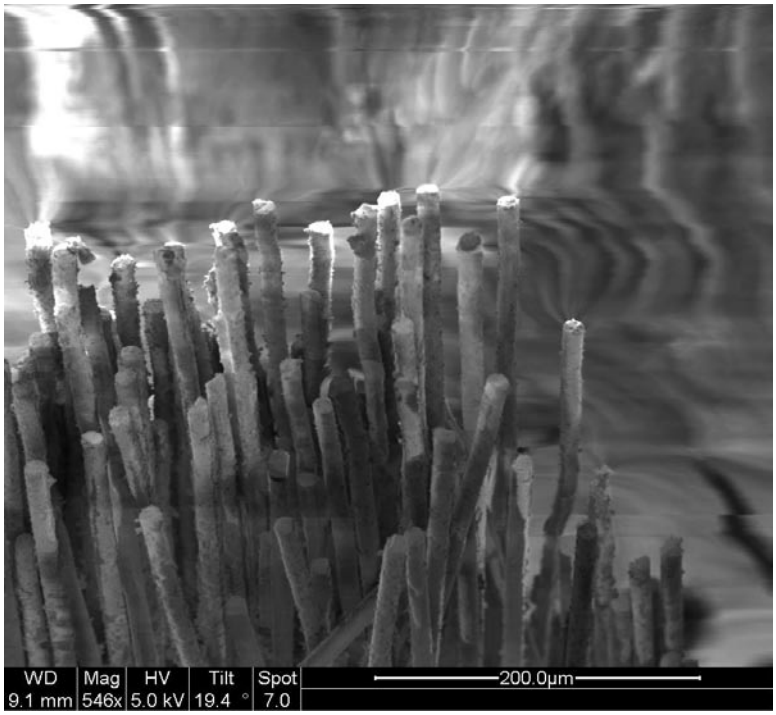


**Figure 100. 152.5 MPa Fatigue (center)**

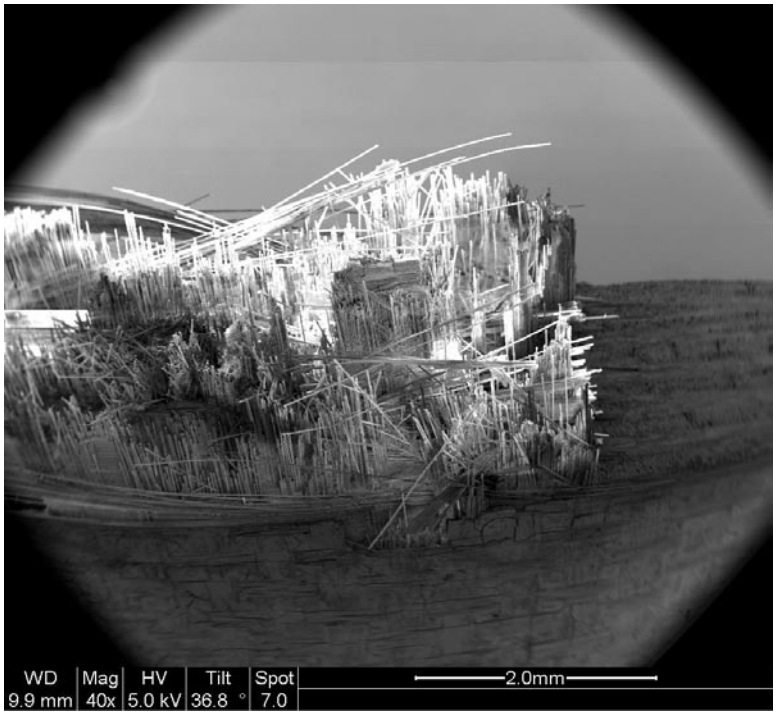


**Figure 101. 152.5 MPa Fatigue (middle)**

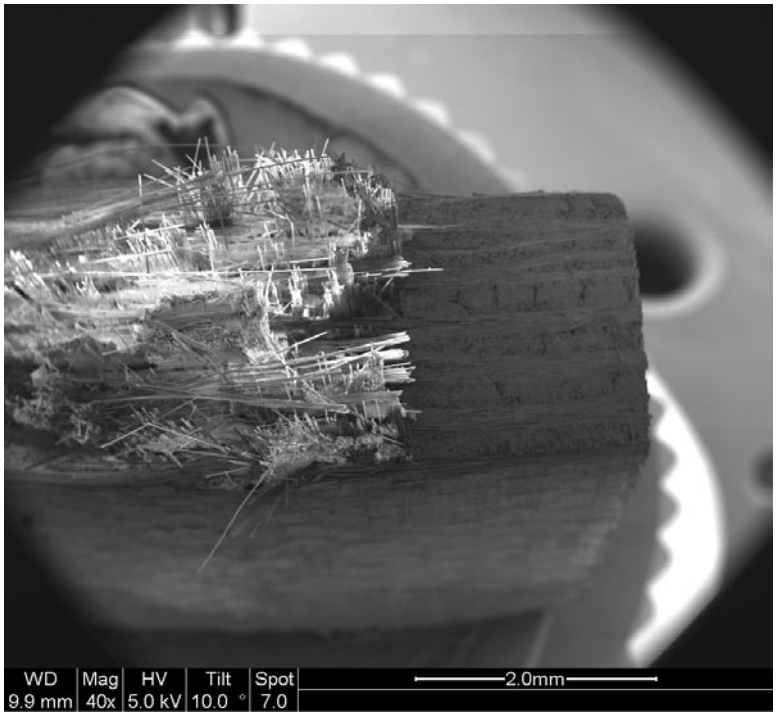


**Figure 102. 152.5 MPa Fatigue (right)**

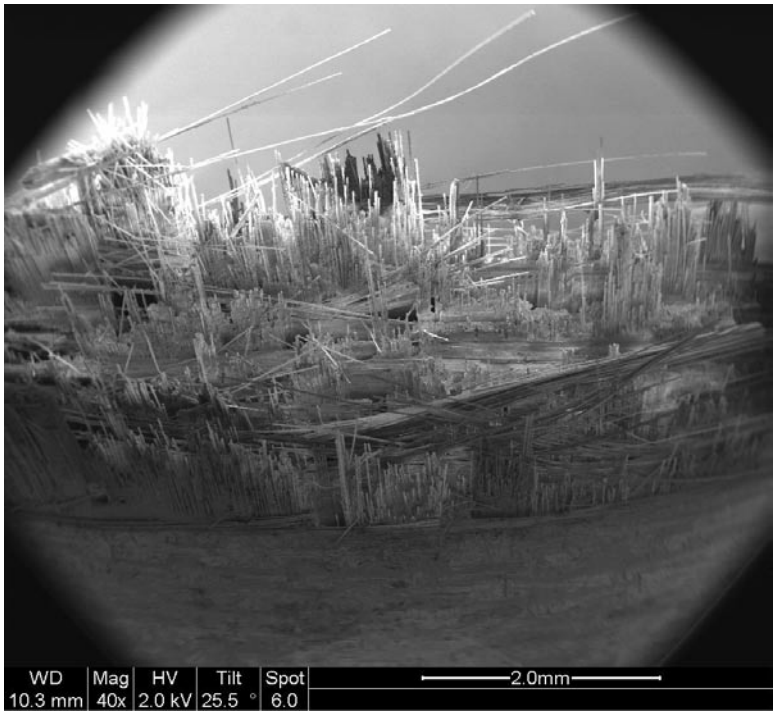


**Figure 103. 155 MPa Fatigue (center)**

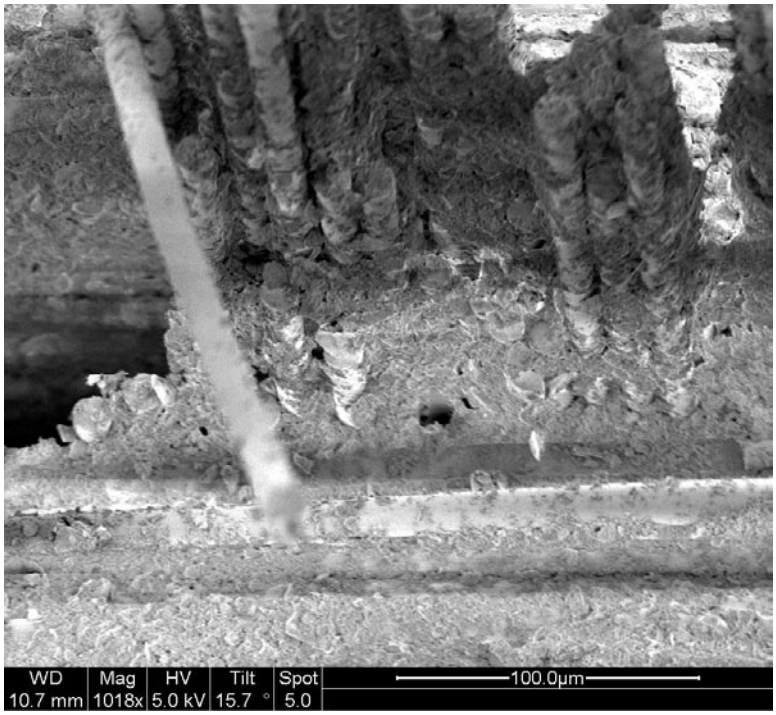


**Figure 104. 155 MPa Fatigue (center)**

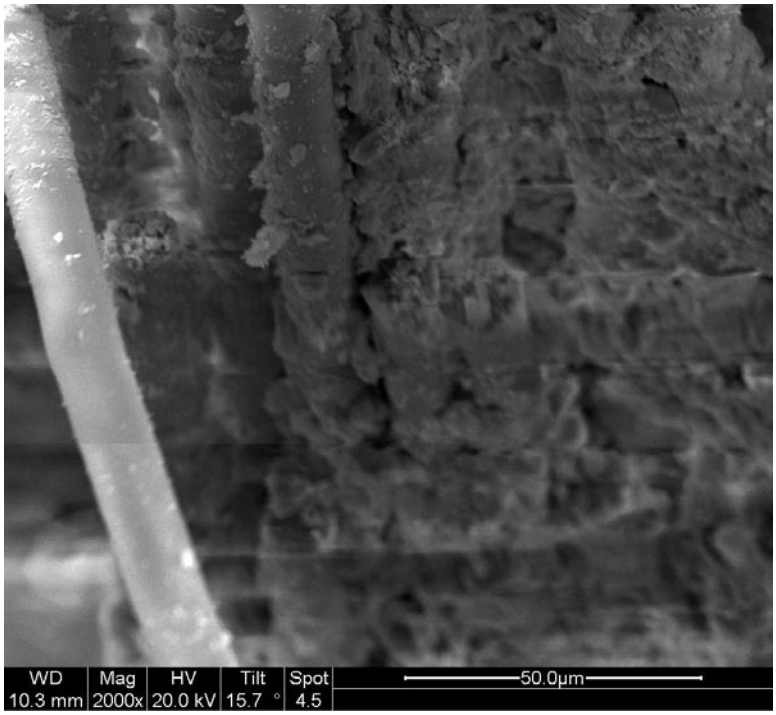


**Figure 105. 155 MPa Fatigue (center)**

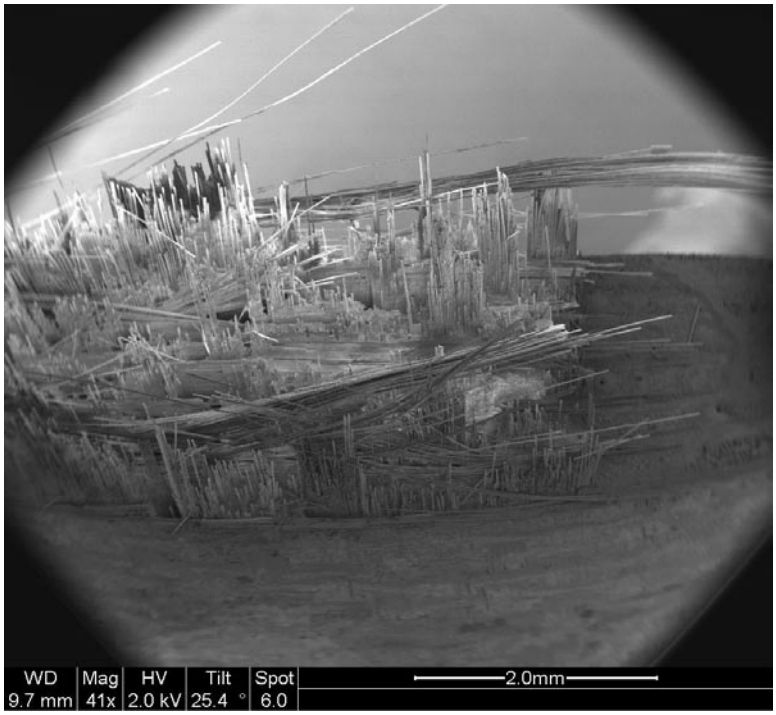


**Figure 106. 155 MPa Fatigue (middle)**


**Figure 107. 155 MPa Fatigue (right)**

## Bibliography


1. "3M Ceramic Fiber Typical Properties," Nextel™ Ceramic Textiles Technical Notebook. Product Brochure. St. Paul MN: 3M Corporation, no date.

2. Antti, M-L. and Edgar Lara-Curzio. "Effect of Notches, Specimen Size, and Fiber Orientation on the Monotonic Tensile Behavior of Composites at Ambient and Elevated Temperatures," *Ceramic Engineering and Science Proceedings*, 22[3], 643-650 (2001).

3. Antti, M-L., E. Lara Curzio and R. Warren. " Thermal degradation of an oxide fibre (Nextel 720)/aluminosilicate composite,"*Journal of the European Ceramic Society*, 24: 565-578 (2004).

4. Baker, A., Dutton, S., Kelly, D. *Composite Materials for Aircraft Structures* (Second Edition). Virginia: AIAA, 2004.

5. Barnard, P., M. B. Henderson and N Rhodes. "CMC Integration and Demonstration for Gas Turbine Engines," Applied Thermal Engineering, 24[11-12]: 1755-1764 (2004).

6. Buchanan, Dennis J., Reji John and Larry P. Zawada. "Notched Fracture Behavior of Oxide/Oxide Nextel™720/AS Composite," *Ceramic Engineering and Science Proceedings*, 21[3], 581-588 (2000).

7. Cantor, B., F.P.E Dunne, I.C. Stone, eds. *Metals and Ceramic Matrix Composites*. Philadelphia: Institute of Physics Publishing, 2004.

8. Chawla, K.K. *Ceramic Matrix Composites*, London: Chapman and Hall, 1993.

9. Composite Optics Inc. Ceramics. "Oxide-Oxide Overview." Unpublished article. n. pag. http://www.coiceramics.com/cmcdevelopment.htm. 10 May 2005.

10. Daniel, Isaac M. and Ori Ishai. *Engineering Mechanics of Composite Materials* (Second Edition). New York: Oxford UP, 2006.

11. Dowling, Norman E. *Mechanical Behavior of Materials: Engineering Methods for Deformation, Fracture, and Fatigue* (Second Edition). New Jersey: Prentice Hall, 1999.

12. Eber, Chalene A. *Effect of Temperature and Steam Environment on Fatigue Behavior of an Oxide-Oxide Continuous Fiber Ceramic*. MS thesis, AFIT/GA/ENY/05-M09. School of Engineering and Management, Air Force Institute of Technology (AU), Wright-Patterson AFB OH, March 2005.

13. Gdoutos, E.E. *Fracture Mechanics* (Second Edition), MA: Springer, 2005.

14. Harlan, Lee B. *Creep-Rupture Behavior of an Oxide/Oxide Ceramic Matrix Composite at Elevated Temperature in Air and Steam Environments*. MS thesis, AFIT/GA/ENY/05-M05. School of Engineering and Management, Air Force Institute of Technology (AU), Wright-Patterson AFB OH, March 2005.

15. Heredia, Fernando E., et al. "Notch Effects in Carbon Matrix Composites," *Journal of the American Ceramic Society*, 77[11], 2817-2827 (1994).

16. John, Reji, Dennis J. Buchanan, Victoria A. Kramb and Larry P. Zawada. "Creep-Rupture Behavior of Oxide/Oxide Nextel™720/AS and MI SiC/SiC Composites with Effusion Holes," *Ceramic Engineering and Science Proceedings*, 23[3], 617-628 (2002).

17. Jurf, R. A. and Butner, S. C. "Advances in Oxide-Oxide CMC," *Journal of Engineering for Gas Turbines and Engine Power*, 122: 202-205 (April 2000).

18. Kaya, C., Butler, E.G., Selcuk, A., Boccaccini, A.R., and Lewis, M.H. "Mullite (Nextel™ 720) fibre-reinforced mullite matrix composites exhibiting favourable thermomechanical properties," Journal of the European Ceramic Society, 22: 2333-2342 (2002).

19. Kramb, Victoria A., Reji John and David A. Stubbs. "A study of the damage progression from notches in an oxide/oxide ceramic-matrix composite using ultrasonic C-scans," *Composites Science and Technology*, 61[11], 1561-1570 (2001).

20. Kramb, Victoria A., Reji John and Larry P. Zawada. "Notched Fracture Behavior of an Oxide/Oxide Ceramic-Matrix Composite, "*Journal of the American Ceramic Society*, 82[11], 3087-96 (1999).

21. Lewinsohn, C. A., C.H. Henager Jr. and R.H. Jones. "Fibers to Bridged Cracks," *Journal of the American Ceramic Society*, 21[3], 415-422 (2000).

22. Mackin, Thomas J., et al. "Notch Sensitivity and Stress Redistribution in Three Ceramic-Matrix Composites," *Journal of the American Ceramic Society*, 78[7], 1719-1728 (1995).

23. Mattingly, Jack D., William H. Heirser and David T. Pratt. *Aircraft Engine Design* (Second Edition). Reston VA: American Institute of Aeronautics and Astronautics, 2002.

24. Merhman, J. M. *Effect of Hold Times on Fatigue Behavior of Nextel™720/Alumina Ceramic Matrix Composite at 1200°C in Air and in Steam Environments*. MS thesis, AFIT/GA/ENY/06-M23. School of Engineering and Management, Air Force Institute of Technology (AU), Wright-Patterson AFB OH, March 2006.

25. Musil, Sean S. *Creep Behavior of an Oxide/Oxide Composite with Monazite Coating at Elevated Temperatures*. MS thesis, AFIT/GA/ENY/05-M14. School of Engineering and Management, Air Force Institute of Technology (AU), Wright-Patterson AFB OH, March 2005.

26. Oates, Gordon C. *Aerothermodynamics of Gas Turbine and Rocket Propulsion* (Third Edition). Reston VA: American Institute of Aeronautics and Astronautics, 1997.

27. Steel, Steven G. *Monotonic and Fatigue Loading Behavior of an Oxide/Oxide Ceramic Matrix Composite*. MS thesis, AFIT/GA/ENY/00-M02. School of Engineering and Management, Air Force Institute of Technology (AU), Wright-Patterson AFB OH, March 2000.

28. Stephen, Ralph, et al. *Metal Fatigue in Engineering* (Second Edition). New York: Wiley and Sons, 2001.

29. Sullivan, Mark A., *Creep-Rupture and Fatigue Behaviors of Notched Oxide/Oxide Ceramic Matrix Composite at Elevated Temperature*. MS thesis, AFIT/GA/ENY/06-M30. School of Engineering and Management, Air Force Institute of Technology (AU), Wright-Patterson AFB OH, March 2006.

30. Veitch, Lisa C. and William S. Hong. "Will Pigs Fly Before Ceramics Do?" *Ceramic Engineering and Science Proceedings*, 22[3], 31-42 (2001).

31. Wilson, D. M., S. L. Lieder and D. C. Lueneburg. "Microstructure and High Temperature Properties of Nextel 720 Fibers," *Ceramic Engineering and Science Proceedings*, 16[5], 1005-1014 (1995).

32. Zok, W. and Carlos G. Levi. "Mechanical Properties of Porous-Matrix Ceramic Composites," *Advanced Engineering Materials*, 3[1-2]: 15-23 (2001).

# REPORT DOCUMENTATION PAGE

*Form Approved*
*OMB No. 074-0188*



| 1. REPORT DATE *(DD-MM-YYYY)* | 2. REPORT TYPE | 3. DATES COVERED *(From – To)* |
|---|---|---|
| 19-06-2008 | **Master's Thesis** | August 2006 – June 2008 |

**4. TITLE AND SUBTITLE**

Creep-Rupture And Fatigue Behavior Of A Notched Oxide/Oxide Ceramic Matrix Composite At Elevated Temperature

**5a. CONTRACT NUMBER**

**5b. GRANT NUMBER**

**5c. PROGRAM ELEMENT NUMBER**

**6. AUTHOR(S)**

Boyer, Barth, H., Lieutenant Commander, USN

**5d. PROJECT NUMBER**

**5e. TASK NUMBER**

**5f. WORK UNIT NUMBER**

**7. PERFORMING ORGANIZATION NAMES(S) AND ADDRESS(S)**
Air Force Institute of Technology
Graduate School of Engineering and Management (AFIT/EN)
2950 Hobson Way, Building 641
WPAFB OH 45433-7765

**8. PERFORMING ORGANIZATION REPORT NUMBER**

AFIT/GAE/ENY/08-J01

**9. SPONSORING/MONITORING AGENCY NAME(S) AND ADDRESS(ES)**
N/A

**10. SPONSOR/MONITOR'S ACRONYM(S)**

**11. SPONSOR/MONITOR'S REPORT NUMBER(S)**

**12. DISTRIBUTION/AVAILABILITY STATEMENT**

APPROVED FOR PUBLIC RELEASE; DISTRIBUTION UNLIMITED.

**13. SUPPLEMENTARY NOTES**

**14. ABSTRACT**

The inherent resistance to oxidation of oxide/oxide ceramic matrix composites makes them ideal for aerospace applications that require high temperature and long life under corrosive environments. The ceramic matrix composite (CMC) of interest in the study is the Nextel™720/Alumina (N720/A) which is comprised of an 8-harness satin weave of Nextel™ fibers embedded in an alumina matrix.

One of the top applications for N720/A is in the combustion section of a turbine engine. This will require mounting and shaping the material with rivets and possibly sharp edges thereby introducing geometry based stress concentration factors. Sullivan's research concentrated on the effects of central circular notches with a notch to width ratio (2a/w) of 0.33. This study expands upon his research to include the creep and fatigue response to double edge notch geometry with the same notch to width ratio of 0.33. In short, 12.0 mm wide rectangular specimens with two edge notches of 2 mm depth and 0.15 mm width were subjected to creep and fatigue loading conditions in 1200°C of air. All fracture surfaces were examined by an optical microscope and a scanning electron microscope.

Sullivan's research concluded that specimens with a central circular notch were insensitive to creep but slightly more sensitive to fatigue than unnotched specimens. In contrast, this study showed significant creep and fatigue life reductions for double edge notch specimens.

**15. SUBJECT TERMS**

Creep, Fatigue, Ceramic Matrix Composites, N720/A, Notch

| 16. SECURITY CLASSIFICATION OF: | | | 17. LIMITATION OF ABSTRACT | 18. NUMBER OF PAGES | 19a. NAME OF RESPONSIBLE PERSON |
|---|---|---|---|---|---|
| REPORT | ABSTRACT | c. THIS PAGE | | | Dr. S. Mall (ENY) |
| U | U | U | UU | 116 | **19b. TELEPHONE NUMBER** *(Include area code)* (937) 255-3636, e-mail: Shankar.Mall@afit.edu |